

University of Colorado
Department of Aerospace Engineering Sciences
Senior Projects - ASEN 4028

Nano-Stratospheric Aerosol Measurement
(NanoSAM)
Project Final Report

Monday 4th May, 2020

1. Information

1.1. Project Customers

Name: Jim Baer Address: 1600 Commerce St, Boulder, CO 80301 Email: jbaer@ball.com Phone: 303-939-6297
--

1.2. Project Advisor

Name: Zoltan Sternovsky Affiliation: Laboratory for Atmospheric and Space Physics (LASP) Email: Zoltan.Sternovsky@colorado.edu Phone: 303-735-6272 (LASP)
--

1.3. Group Members

Project Manager: Hui Min Tang Email: huta9063@colorado.edu Phone: 720-401-9621	Chief Systems Engineer: Jacob Romero Email: jacob.romero@colorado.edu Phone: 720-384-8158
Electronics Lead: Jared Cantilina Email: Jared.Cantilina@colorado.edu Phone: 850-502-0347	Structures Lead: Jessica Harris Email: jessica.harris-1@colorado.edu Phone: 719-373-9936
Financial Lead: Josh Horst Email: joshua.horst@colorado.edu Phone: 503-616-1707	Materials Lead: Quinn LaBarge Email: michael.labarge@colorado.edu Phone: 720-746-8779
Optics Lead: Conner McLeod Email: conner.mcleod@colorado.edu Phone: 907-350-3378	Manufacturing Lead: Aanshi Panchal Email: aanshi.panchal@colorado.edu Phone: 630-965-5002
Optics Lead: Sara Reitz Email: sara.reitz@colorado.edu Phone: 720-378-1573	Software Lead: Matt Weber Email: matthew.c.weber@colorado.edu Phone: 303-241-5804
Safety & Testing Lead: Jaykob Velasquez Email: jaykob.velasquez@colorado.edu Phone: 719-281-9849	

Contents

1	Information	1
1.1	Project Customers	1
1.2	Project Advisor	1
1.3	Group Members	1
2	Project Purpose	12
3	Project Objectives & Functional Requirements	12
3.1	Specific Objectives	13
3.2	CONOPS	14
3.3	Project Deliverables	15
3.4	Functional Block Diagram	16
3.5	Functional Requirements	17
4	Design Process & Outcome	18
4.1	Summary of Alternative Designs and Trade Studies	18
4.1.1	Electronics Subsystem	18
4.1.2	Optics Subsystem	19
4.2	Requirements Flow-down	20
4.3	Resulting Design	25
4.3.1	Optics Baseline Design Overview	25
4.3.2	Optics Detailed Design	25
4.3.3	Electronics Baseline Design Overview	35
4.3.4	Electronics Detailed Design	35
4.3.5	Structural Baseline Design Overview	42
4.3.6	Structural Detailed Design	43
4.3.7	Software Baseline Design Overview	43
4.3.8	Software Detailed Design	43
4.4	Critical Project Elements	43
5	Manufacturing	44
5.1	Structural Manufacturing	44
5.1.1	Structural Parts Manufactured	44
5.1.2	Structural Parts Purchased	45
5.2	Optics Manufacturing	45
5.2.1	Optical Parts Made	45
5.2.2	Optical Parts Purchased	48
5.3	Electronics Manufacturing	48
5.4	Software Manufacturing	49
5.5	Integration of Parts	49
5.5.1	Opto-Mechanical Integration	49
5.5.2	Electronics Integration	50
6	Verification & Validation	50
6.1	Optics Verification & Validation	51
6.1.1	Optics Component Integration Verification	51
6.1.2	Optics System Alignment Verification and Validation	52
6.2	Electronics Verification & Validation	63

6.2.1	Component Tests	63
6.2.2	System Tests	64
6.3	Mechanical Verification & Validation	66
6.4	Integration Verification and Validation	67
7	Risk Assessment & Mitigation	68
8	Project Planning	70
8.1	Organizational Chart	70
8.2	Work Breakdown Structure	72
8.3	Work Plan	74
8.4	Cost Plan	77
8.4.1	Uncertainty	79
8.4.2	Industrial Cost Breakdown	79
8.5	Test Plan	80
8.6	Design Validation	83
9	Lessons Learned	84
9.1	Optics	84
9.2	Manufacturing	85
9.3	Electronics	85
9.4	Software	85
9.5	Systems Engineering	85
9.6	Project Management	86
10	Individual Report Contributions	87
11	Appendix A: Alternate Designs Considered & Trade Studies	88
11.1	Alternate Designs Considered	88
11.1.1	Electronics System	88
11.1.2	Optics Designs Considered	94
11.2	Trade Studies	101
11.2.1	Photodiode Selection	101
11.2.2	ADC Selection	102
11.2.3	On-Board Controller Selection	104
11.2.4	External Memory Selection	106
11.2.5	Reflector Telescope Type Selection	108
11.2.6	Mirror Substrate Selection	110
11.2.7	Mirror Surface Coating Selection	112
11.2.8	Filter Selection	113
11.3	Metric Score Justification	115
11.3.1	Photodiode Selection	115
11.3.2	ADC Selection	116
11.3.3	On-Board Controller Selection	117
11.3.4	External Memory Selection	119
11.3.5	Optics System	120
11.3.6	Reflector Telescope Type Selection	120
11.3.7	Mirror Substrate Selection	123
11.3.8	Mirror Surface Coating Type Selection	123
11.3.9	Filter Selection	124

12 Appendix B: Drawings	126
12.1 Optical Bench Part Drawings	126
12.2 Enclosure Drawings	128
12.3 Electronics	130
12.3.1 Schematic	130
12.3.2 Layout	135
12.4 Signal-to-Noise Ratio Calculation Code	136
13 Appendix C: Project Management	139
14 References	142

List of Figures

1	Project Elements Table	13
2	NanoSAM Full Mission CONOPS	14
3	NanoSAM Demonstration CONOPS	15
4	Functional Block Diagram	17
5	Vertical Resolution Diagram	21
6	MTF Requirement Development	22
7	Requirements Flow Down Part 1	23
8	Requirements Flow Down Part 2	24
9	Optics Baseline Design Overview	25
10	NanoSAM Optics System Zemax Model	26
11	Pinwheel Diagram - High MTF	26
12	Pinwheel Diagram - Low MTF	26
13	Diffraction-Limited MTF Comparison (SAM II and NanoSAM)	27
14	Sun Image on Pinhole with Dimensions	27
15	Spectral Performance of the Filter Assembly near the 1.03 μ CLW	28
16	+ focus, + out-of-plane, and in-plane Displacements	29
17	System Shift Due to Thermal Expansion of Steel Washers	30
18	Optical Bench Design	30
19	Bench Base Plate	31
20	SolidWorks and Zemax Model Integration	31
21	Aperture Plate	32
22	Photodiode Block - Exploded View	32
23	Photodiode Block - W/ Reflective Half Sphere	32
24	Light Ray Footprint on Active Area	33
25	Focus Shims	33
26	In-plane Shims	33
27	Out-of-plane Shims	33
28	Tooling Plate and Screw	34
29	Mounting Hardware	35
30	Electronics Block Diagram	35
31	Analog electronics schematic	36
32	Digital electronics schematic	37
33	Power electronics schematic	39
34	Power usage by component	39
35	Analog and digital ground planes. Star connection point not shown.	40
36	Series termination on a SPI bus	40
37	Suggested vs implemented dual power supply layout	41
38	Suggested vs implemented 3.3V power supply layout	41
39	Summary: Contributions to Noise	42
40	NanoSAM Plate Module System	43
41	NanoSAM Enclosure	43
42	Enclosure Tube with Plates	45
43	Plate Module Assembly	45
44	Plate Module Assembly within Enclosure	45
45	Manufactured Diode Block	46
46	Optical Bench Phase 1	47
47	Optical Bench Phase 2	47

48	Optical Bench Phase 3	47
49	Manufactured Aperture Stop	47
50	Manufactured Optical Shims	47
51	Manufactured Tooling Plate View 1	48
52	Manufactured Tooling Plate View 2	48
53	Manufactured Sighting Tabs	48
54	Optical Bench View 1	49
55	Optical Bench View 2	49
56	Optical Bench View 3	49
57	Optical Bench View 4	49
58	Optical Bench System	50
59	Plate Module Assembly w/ Optical Bench	50
60	Aperture Stop and Filter Alignment View	50
61	Fully Integrated Software & Electronics PCB	50
62	Electronics PCB Mechanical Integration	50
63	ZYGO DynaFiz Interferometer (left) and Example Software Output (right)	52
64	Wyant Zernike Term Expansion and Wavefront Pattern	53
65	Zernike Coefficient (Z3-Z7) Response vs. In-plane Tilt, Out-of-plane Tilt, and Focus Displacement	53
66	Interferometer Return Sphere	54
67	NBK-7 Convex Half Sphere Lens	54
68	Conceptual Diagram for Mirror to Interferometer Alignment	55
69	Optical Bench Position Constraint	55
70	Mirror to Interferometer Alignment Configuration	55
71	Aluminum OAP WFE	56
72	Aluminum OAP WFE with Aperture Mask	56
73	Aluminum OAP MTF with Aperture Mask	57
74	Aligned Sighting Tab Cross-hair Projection	57
75	Conceptual Diagram for Diode Block Alignment Derivation	58
76	Chrome Half Sphere WFE and Zernike Coeff.	58
77	Chrome Half Sphere Surface	58
78	Diode Block in Starting Shim Derivation Physical Configuration	59
79	Pinhole Surface Return Conceptual Diagram	60
80	Pinhole False Interferogram	61
81	Maximum Radial Offset	62
82	Expected results from stability and noise test	65
83	Stability test set up	66
84	Places in the Enclosure Where Inspection will take place	67
85	Langley Plot Simulation Result	67
86	FMEA of NanoSAM	68
87	FMEA of NanoSAM with Mitigation Methods and New Ratings	69
88	Organizational Chart of NanoSAM	71
89	Part 1 out of 4 of NanoSAM Gantt chart	75
90	Part 2 out of 4 of NanoSAM Gantt chart	75
91	Part 3 out of 4 of NanoSAM Gantt chart	75
92	Part 4 out of 4 of NanoSAM Gantt chart	75
93	Gantt Chart with Critical Path.	76
94	NanoSAM Projected Budget: \$3755	77
95	NanoSAM Final Cost Sheet 1	78
96	NanoSAM Final Cost Sheet 2	78

97	NanoSAM Actual vs. Predicted Budget	79
98	Industrial Cost Breakdown	80
99	Test Plan Part 1	81
100	Test Plan Part 2	82
101	Example Langley Plot [3]	83
102	Airmass Determination Method	84
103	A cross section of a typical PIN photodiode, showing the P layer, the Intrinsic layer, and the N layer.	88
104	A typical cross section view of the heterojunction PIN photodiode	89
105	Flash ADC	90
106	Successive Approximation ADC Block Diagram	91
107	Sigma-Delta ADC Block Diagram	91
108	Cassegrain Reflector	95
109	Newtonian Reflector	96
110	OAP Reflector	96
111	Prime Focus (On-Axis Telescope)	97
112	Optical Bench Drawing	126
113	Aperture Stop Drawing	126
114	Diode Block Drawing	127
115	Tooling Plate Drawing	127
116	Tooling Plate Drawing	128
117	Enclosure Tube Drawing	128
118	Enclosure Bottom Drawing	129
119	Enclosure Top Drawing	129
120	Enclosure Handle Drawing	130
121	PCB Layout	135
122	Part 1 of 4 of task list	139
123	Part 2 of 4 of task list	140
124	Part 3 of 4 of task list	140
125	Part 4 of 4 of task list	141

List of Tables

2	MTF Budget for Feasible Alignment Configuration of NanoSAM Optics System	29
3	Manufactured and Purchased Structural Parts	44
4	Manufactured and Purchased Optics Parts	45
5	Zernike Coefficient Description and Ordering	53
6	Zernike Coefficients for Aligned OAP-Interferometer	56
7	Zernike Coefficients Reference for Aligned Half Sphere Position on 3-axis Stage	59
8	Micrometer Displacements for Initial Shim Stack Thickness Derivation	60
9	Zernike Coefficients for Aligned Diode Block	60
10	MTF Degradation Budget Actual Versus Feasible Alignment	63
11	Component Test Results	64
12	System Test Results	64
13	Test Plan Overview	83
15	Summary: Pros and Cons of Silicon Photodiodes	88
16	Summary: Pros and Cons of InGaAs Photodiodes	89
17	Summary: Pros and Cons of Germanium Photodiodes	89
18	Summary: Pros and Cons of Flash ADCs	90
19	Summary: Pros and Cons of SAR ADCs	91
20	Summary: Pros and Cons of Sigma-Delta ADCs	92
21	Summary: Pros and Cons of FPGA Controller	92
22	Summary: Pros and Cons of Micro-Controller	92
23	Summary: Pros and Cons of Micro-Controller	93
24	Summary: Pros and Cons of SSDs	93
25	Summary: Pros and Cons of Micro-SDs	93
26	Summary: Pros and Cons of USBs	93
27	Summary: Pros and Cons of NAND Flash	94
28	Summary: Pros and Cons of Cassegrain Telescope	95
29	Summary: Pros and Cons of Newtonian Telescope	96
30	Summary: Pros and Cons of OAP Reflector	96
31	Summary: Pros and Cons of Prime Focus (On-Axis) Telescope	97
32	Summary: Pros and Cons of Aluminum 6061-T6	97
33	Summary: Pros and Cons of Floated Borosilicate	98
34	Summary: Pros and Cons of Borosilicate	98
35	Summary: Pros and Cons of Fused Silica	98
36	Summary: Pros and Cons of Protected Aluminum	99
37	Summary: Pros and Cons of Enhanced Aluminum	99
38	Summary: Pros and Cons of Protected Silver	99
39	Summary: Pros and Cons of Protected Gold	99
40	Summary: Pros and Cons of Linear Variable Bandpass Filtering	100
41	Summary: Pros and Cons of Traditional Coating	100
42	Summary: Pros and Cons of Hard Coating	100
43	Summary: Pros and Cons of Custom Coating	101
45	Photodiode Trade Study Metrics and Weighting	101
46	Photodiode Metric Score Categorization. Note that the numbers in the responsivity section is the range where the photodiode is able to measure.	102
47	Photodiode Trade Study Scoring	102
49	Analog-to-Digital Converter Trade Study Metrics and Weighting	103
50	Analog to Digital Converter Metric Score Categorization	104

51	Analog to Digital Converter Trade Study Scoring	104
53	On-Board Controller Trade Study Metrics and Weighting	105
54	On-Board Controller Metric Score Categorization	106
55	On-Board Controller Trade Study Scoring	106
57	External Memory Trade Study Metrics and Weighting	107
58	External Memory Metric Score Categorization	108
59	External Memory Trade Study Scoring	108
61	Telescope Type Metric Score Categorization	109
62	Telescope Type Trade Study Metrics and Weighting	110
63	Telescope Type Trade Study Scoring	110
65	Mirror Substrate Trade Study Metrics and Weighting	111
66	Mirror Substrate Metric Score Categorization	112
67	Mirror Substrate Trade Study Scoring	112
69	Mirror Surface Coating Trade Study Metrics and Weighting	112
70	Mirror Surface Coating Metric Score Categorization	113
71	Mirror Surface Coating Trade Study Scoring	113
73	Filter Trade Study Metrics and Weighting	114
74	Filter Metric Score Categorization	115
75	Filter Trade Study Scoring	115

Acronyms

ADC	:	Analog-to-Digital Converter
ADCS	:	Attitude Determination Control System
AIAA	:	American Institute of Aeronautics and Astronautics
ASTP	:	Apollo Soyuz Test Project
BW	:	Bandwidth
CONOPS	:	Concept of Operations
COTS	:	Consumer Off-the-Shelf
CU Boulder	:	University of Colorado Boulder
CTE	:	Coefficient of Thermal Expansion
CWL	:	Center Wavelength
DET	:	Detection
EFL	:	Effective Focal Length
EM	:	Electromagnetic
FBD	:	Functional Block Diagram
FMEA	:	Failure Mode & Effects Analysis
FOV	:	Field-of-View
FWHM	:	Full Width at Half Maximum
IDE	:	Integrated Development Environment
IR	:	Infrared
ISS	:	International Space Station
MTF	:	Modulation Transfer Function
NanoSAM	:	Nano-Stratospheric Aerosol Measurement
NIR	:	Near Infrared
OAP	:	Off-Axis Parabolic Mirror
OCC	:	Occurrence
PAB	:	Project Advisory Board
PF	:	Prime Focus
RMS	:	Root Mean Squared
RPN	:	Risk Priority Number
RQMT	:	Requirement
RVM	:	Requirement Verification Matrix
SAM	:	Stratospheric Aerosol Measurement Mission
SAGE-II	:	Stratospheric Aerosol and Gas Experiment II
SEV	:	Severity
SNR	:	Signal-to-Noise Ratio
SSD	:	Solid State Drive
STK	:	Systems Tool Kit
SPI	:	Serial Peripheral Interface
USB	:	Universal Serial Bus
VDC	:	Volts Direct Current
WFE	:	Wavefront Error

Nomenclature

A_{ap}	=	Aperture area, m^2
α	=	Coefficient of Thermal Expansion
BW	=	Filter bandwidth, nm
c	=	Speed of light in vacuum, m/s
D	=	Aperture diameter
E_{photon}	=	Energy of photon, J
e	=	Elementary charge, C
ϵ	=	Normal Strain
f	=	Frequency of light, Hz
f_{DC}	=	Worst-case transimpedance amplifier signal frequency, Hz
FOV	=	Instrument field-of-view, $arcmin^2$
I	=	Solar irradiance
I_{dark}	=	Dark current from photodiode, A
$I_{max,in}$	=	maximum noise current from transimpedance amplifier, A/\sqrt{Hz}
I_o	=	Direct solar irradiance
I_{PS}	=	Noise current from power supply, A
I_{tran}	=	Noise current from transimpedance amplifier, A
L	=	Thickness
λ	=	Wavelength
LSB	=	ADC least significant bit, e^-/s
M	=	ADC margin
m	=	Airmass
N	=	Number of measurements per sample
NA	=	Numerical aperture
N_{dark}	=	Dark current noise term, e^-/s
N_{shot}	=	Shot noise term, e^-/s
N_{PS}	=	Power supply noise term, e^-/s
N_{tran}	=	Transimpedance amplifier noise term, e^-/s
n	=	ADC bits
P	=	Power through aperture to mirror, W
Φ	=	Solar spectral irradiance, $Wm^{-2}nm^{-1}$
PRR_{op-amp}	=	Power rejection ratio for op-amp
Ψ	=	Photon rate reflected off mirror, e^-/s
Q	=	Quantum efficiency of photodiode
R	=	Responsivity of photodiode, A/W
$R_{feedback}$	=	Value of feedback resistor connected to op-amp, Ω
R_{mirror}	=	Mirror reflectivity
S	=	Signal from photodiode, e^-/s
τ	=	Optical depth (Slope of Langley plot)
θ	=	Angular resolution
θ_{sd}	=	Solar disk diameter expressed as angle, $arcmin$
V	=	Volt
V_{PS}	=	Voltage noise from power supply, A
ν	=	Spatial/Angular frequency
ν_c	=	Cutoff frequency
ν_n	=	Normalized frequency

2. Project Purpose

Jacob Romero, Hui Min Tang

To aid in the scientific understanding of aerosol concentrations and their associated influences Earth-observing instruments are needed to collect long-term measurements in the Earth's stratosphere. Stratospheric aerosols are a suspension of fine solid or liquid particles that exist in the stratosphere region of Earth's atmosphere. The particles are approximately 0.1 to 1.0 micrometers in diameter that mostly originate from sulphur-rich volcanic eruptions [30]. Since these particles impact many elements of human life ranging from avionics to the planet's climate, several techniques have been developed for the measurement of aerosol concentrations, including the Stratospheric Aerosol Measurement (SAM) experiment for the Apollo Soyuz Test Project (ASTP), which is the predecessor of NanoSAM. The major disadvantage of SAM and other systems is the low data density capacity. For example, the current SAM instrument, SAGE-III, is mounted on the ISS and can only capture approximately 30 aerosol measurements per day, based on the orbital period of the ISS. In addition, previous projects have also been expensive and complex. Therefore, the NanoSAM team will design, construct, and test a functioning radiometric measurement system that is smaller, lighter, cheaper, and able to provide a higher data density.

Through NanoSAM's CubeSat-sized radiometric measurement system, a constellation of NanoSAM radiometers can be deployed to significantly increase the number of aerosol measurements taken each day. The increase in data frequency will greatly improve the overall data density and data resolution of aerosol concentrations, allowing climatologists more data with better quality for research.

The long-term NanoSAM mission will utilize the same process for obtaining aerosol concentrations as the SAGE-III, the solar occultation method. SAGE-III and other solar occultation instruments self-calibrate at the top of the stratosphere to acquire a baseline solar irradiance measurement. As the orbit progresses, the instrument will scan through discrete layers of stratosphere to obtain attenuated solar irradiance measurements. By referencing the baseline measurement, the attenuation and the aerosol concentration can be determined. A successful NanoSAM mission will prove the feasibility of a flight-capable CubeSat that can be deployed in a constellation to improve aerosol concentration data. However, due to time and financial constraints, this year's NanoSAM team will only prove that the radiometric measurement system can be resized to a volume of 10x10x15cm or smaller while achieving better data resolution than past instruments. The terminology used to describe the payload's volume throughout the document is "Units" or just "U", the standard sizing terminology for CubeSats. 1U corresponds to 10x10x10 cm, 1.5U to 10x10x15 cm and so on.

The purpose of this year's NanoSAM project is to design, build, and test an optical instrument that will be capable of measuring solar irradiance such that aerosol concentrations data in the stratosphere can be obtained in the future through the solar occultation method. A senior design projects team from the Ann H.J. Smead Aerospace Engineering Department of the University of Colorado Boulder will collaborate with engineers at Ball Aerospace Corporation to construct a functioning optics system that is able to measure solar irradiance in a narrow spectral band centered at 1.02 μm . An accompanying electronics system capable of collecting and packetizing the irradiance data for download will also be produced. These systems will be compatible with a 1U CubeSat bus footprint and the corresponding architecture. With the time and budget allotted, the deliverables will only include the optics system, electronics system, and any accompanying software.

3. Project Objectives & Functional Requirements

Jacob Romero, Hui Min Tang

Based on the purpose of the NanoSAM project, the team must construct a radiometric measurement instrument payload with its accompanying software and electronics. The performance of the payload must be an improvement from the SAM missions to meet the goals and motivation behind NanoSAM.

3.1. Specific Objectives

Three levels of success were determined for the NanoSAM project to satisfy the design problems. These were determined by the team together with the customer. Level 1 corresponds to the absolute minimum standard for success while level 3 correlates to the goals that NanoSAM aims to achieve. Table 1 below shows the specific objectives for NanoSAM project. The level 3 specific objectives are then used to create functional requirements and its flow down matrix, which can be found in Section 4. The specific objectives of the project are tasks or specifications that the payload must meet for the proper system to be built. If any one of these objectives are not met, the system will fail to achieve the customer’s desires and will be classified as a failure. To limit the possibility of failure, the levels of success have been developed to ensure that if only the elements in level 1 are achieved, the project will still be able to collect radiometric data.

If the level 3 goals are not achieved, the project will not meet customer requirements but the final product will still be functioning. For example, the level 3 goal for the instrument’s SNR of 3500 will surpass SAM-II’s SNR. Level 1 and level 2 values were obtained from 80% and 90% of the level 3 value. The resulting instrument will still be able to obtain valid irradiance data.

Throughout the two semesters of developing and manufacturing NanoSAM, level 2 of data capture and level 3 of payload instrumentation size and mechanical structure has been accomplished. Due to circumstances, a complete test of each subsystem as well as the full integration of the project was not implemented. Therefore, the levels at which the other project elements have met, such as solar irradiance, instrument SNR, and vertical resolution, could not be identified.

Project Elements	Level 1	Level 2	Level 3
Solar Irradiance	The solar irradiance data collected is stable with minimal fluctuations.	The solar irradiance data is stable with minimal fluctuations and repeatable.	The solar irradiance data is stable with minimal fluctuations and repeatable. Data exhibits approximately linear trends that are independent of temperature variation.
Instrument SNR	The optical instrument has a SNR of 2800 or greater.	The optical instrument has a SNR of 3150 or greater.	The optical instrument has a SNR of 3500 or greater.
Vertical Resolution	The optical instrument's FOV facilitates a vertical resolution that produces accurate scientific data.	Same as level 1	The optical instrument's FOV facilitates a vertical resolution profile of 1 km or less.
Data Capture	The ADC converts the light signal measured by a photodetector into electrical current that can be read by supporting electronics.	Supporting electronics and software acquires, digitizes, packetizes, and downloads raw data from a photodetector to a computer.	Supporting electronics and software acquires, digitizes, packetizes, and downloads raw data from a photodetector to a computer without drawing more than 4.5W of power over 30 measurements.
Payload Instrumentation Size	The payload consisting of a radiometer and supporting electronics can be extrapolated to a CubeSat greater than 2U.	The payload consisting of a radiometer and supporting electronics can be extrapolated to a 2U CubeSat.	The payload consisting of a radiometer and supporting electronics can be extrapolated to a flight ready 1.5U CubeSat.
Mechanical Structure	The radiometer will be arranged on a lab bench for demonstration purposes.	The payload will be able to fit inside a 2U enclosure. Radiometer and supporting electronics does not need to be secured to the enclosure to verify that the selected CubeSat size can house all components.	The payload will be able to fit inside a 1.5U enclosure. Radiometer and supporting electronics will be secured to the enclosure to verify that the selected CubeSat size can house all components.

Specific Objectives

Figure 1. Project Elements Table

3.2. CONOPS

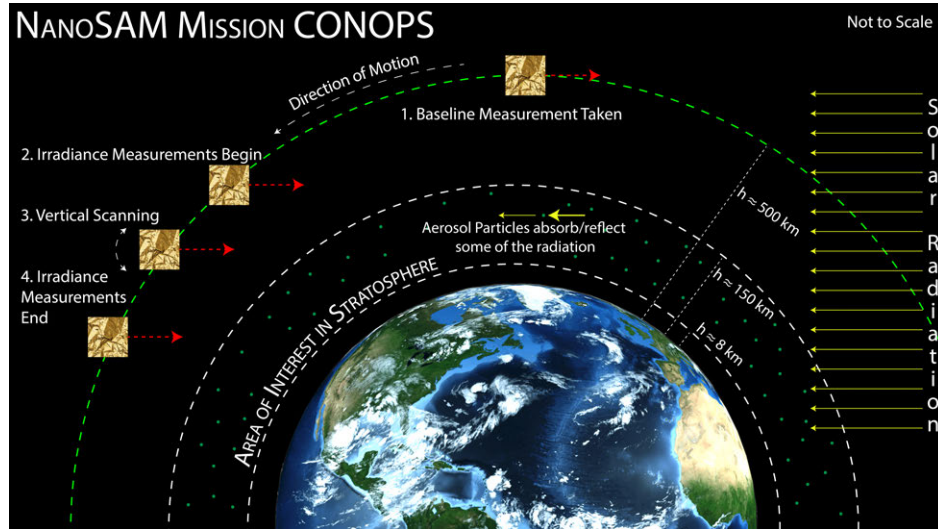


Figure 2. NanoSAM Full Mission CONOPS

The NanoSAM mission CONOPS, shown above, illustrates the solar occultation method and how a flight capable NanoSAM system would work on orbit. Stage 1 shows the baseline irradiance measurement being taken at the top of the orbit where the NanoSAM field-of-view is unimpeded by Earth's stratosphere. As the orbit progresses along the direction of motion to stage 2, the irradiance measurements begin when the field-of-view (FOV) captures the area of interest in the stratosphere. Vertical scanning, stage 3, will allow the instrument to discretize layers of the stratosphere in 1km altitude increments. Once the Sun is no longer visible and the measured solar irradiance drops below a specified value, the measurements end, shown in stage 4. Note that this CONOPS describes a sunset event for an on-orbit operation only. During orbit, there will also be sunrise events. The major difference between the sunset and sunrise events is when the baseline measurement is taken. For the sunrise event, the baseline measurement is taken after the irradiance measurements.

This mission CONOPS shows the functions that needs to be replicated or simulated in the NanoSAM project to prove that a CubeSat-sized mission will be able to collect the required irradiance data. This year's NanoSAM team will use the following demonstration CONOPS to simulate an on-orbit system and ensure the ground system is capable of collecting the necessary data at the required precision.

The demonstration CONOPS in Fig. 3 illustrates the full system integration test that would have been performed in April 2020, had testing not been halted due to the global pandemic. Initially, the optical system and accompanying support equipment, consisting of a power supply, solar tracker, tripod, and external computer, would be set up on an open field with a clear line of sight to the solar path during the day. The power supply and external computer would be attached to the appropriate ports of the payload. The payload would then be secured to the solar tracker, which would in turn be attached to the tripod. The solar tracker that the NanoSAM team selected contains a built-in solar tracking feature performed by its camera. To align NanoSAM to a higher precision, minor adjustments can be made utilizing the joystick on the solar tracker. The attached pointing tabs on the NanoSAM enclosure are aligned to the optical system's optimal pointing direction; hence any misalignment can be remedied with the joystick controls.

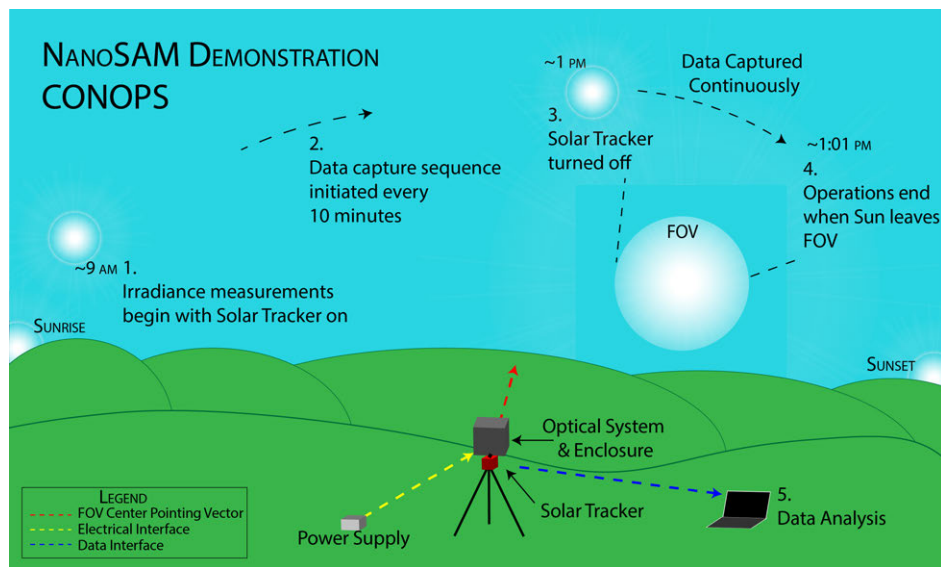


Figure 3. NanoSAM Demonstration CONOPS

At this point, the irradiance measurements begin via a user-input software command, as shown in step 1 of the figure. A data capture sequence is initiated by the user every ten minutes, and data is captured for five minutes (step 2). This frequency and duration of data capture generates the amount of radiometric data captured in one day of on-orbit use. The measurements must be taken until solar noon is reached, which is why the data is periodically captured until approximately 1pm. The exact time of solar noon depends on the location and time of the year. At step 3, the solar tracker is turned off and data starts to be captured continuously. As the Earth rotates, the sun slowly leaves the field-of-view of the optical system, as illustrated by the FOV bubble in step 4. This process takes approximately one minute based on the pin-hole field stop size of the optical instrument. Once the sun has moved sufficiently far away from the center of the field-of-view, the measured irradiance will drop below a threshold value. At this point, the system stops collecting data, and the field test operations end.

After the field test has been completed, the team will offload the collected data to an external source, which, in this case, is a laptop computer. The team will then inspect the data to make sure the anticipated amount has been collected. Next, the data captured during the test will be used to extrapolate to an unattenuated solar light source. The extrapolated value will represent the baseline measurement against which all other measurements are referenced. Since previous systems have captured the same data for an unattenuated solar light source, comparisons between the two sets of data can be made to analyze the accuracy of NanoSAM. This demonstration will provide verified solar irradiance data that eventual end users at LASP and other atmospheric research centers can utilize to determine aerosol concentrations.

3.3. Project Deliverables

At the end of the spring semester 2020, the NanoSAM team will provide the customers at Ball Aerospace Corporation with the NanoSAM measurement device, the accompanying software package, any purchased testing equipment, and the necessary documentation and resources that will aid in the continuation of the project. The measurement device will consist of a radiometric measurement system, an electronics system, and a mechanical structure to house and secure the aforementioned systems. The software package will be provided such that future users can command the system and process the collected data. Since most testing will require future teams of the NanoSAM project to perform, the purchased hardware will be provided along with the NanoSAM system. The accompanying documentation and archives is vital for future University of Colorado Boulder senior projects teams to continue the work of the current team. Therefore, the all documents are uploaded into a Google Drive folder owned by the university for ease of access by future teams. Since modifications to the NanoSAM system is essential for the system to be flight-capable,

providing future teams with all the design work and considerations will allow them to pick up where NanoSAM left off and work towards the NanoSAM mission goals.

The radiometric measurement system of the NanoSAM project consists of two major components — the optical system used to gather the desired image and the photodetector. The optical system is necessary to achieve the desired vertical profile, MTF, and signal strength. This optical system has been carefully designed with considerations of launch in mind; therefore the optical system should require little modifications to be used in a flight-capable system. A consumer off-the-shelf photodiode was also selected with considerations of an on-orbit operation. Apart from flight vibrational and thermal analyses, the team is confident that the delivered radiometric system will be capable of exceeding the performance of SAM on an eventual complete NanoSAM mission.

Next, the electronics system of the measurement device converts the analog irradiance data to a readable output file. The sets of collected data were planned to be a project deliverable, however due to the halt on testing no radiometric data from an integration test was collected. Similar to the optical system, the electronics components were selected with considerations for on-orbit conditions. However, not all components are radiation-hardened for space environment. The electronics system is housed on a printed circuit board (PCB) that can be easily removed and replaced, allowing future teams to replace electronics components with radiation-hardened ones suitable for spaceflight.

Furthermore, the mechanical structure that houses and secures the measurement device will be provided to verify the payload size requirements. Akin to the electronic components, the mechanical structure is not designed for spaceflight. They are provided only to prove that the payload can fit within the specifications for a standard CubeSat deployment module and to make transportation and testing of the system more convenient. The designed structure meets all the requirements for a CubeSat except for launch vibrational and thermal factors. Future teams will need to perform space environment testing on the designed structure to ensure the payload survive during and after launch.

Lastly, a software package that controls the measurement device and processes the collected data will be provided so that the customer and future users can continue to gather data and verify the functionality of the system before continuing to improve NanoSAM for launch. The software is created specifically for the ground tests that the team planned on performing in April 2020. Unfortunately, the software was not fully tested and integrated into the whole system so further testing is required. The software will only be useful for future teams in ensuring the consistency of the system's data output. In summary, all the deliverables mentioned above will allow future teams to continue the project from where it was left off easily.

3.4. Functional Block Diagram

In Fig. 4, the functional block diagram for NanoSAM is shown. In the FBD, the simulated bus architecture, electrical, optical, and software systems are all presented. The legend in the top right corner shows many important aspects of the FBD, including the type of signal (light, analog, or digital) and power distribution throughout the system (+5 VDC, -5VDC, or 12 VDC).

Initially, the signal is in the form of light from the sun. This light is filtered through two filters to isolate the desired wavelength. Once it passes through the optical system and is focused on the photodiode, the signal is converted to an analog electronic signal. This signal is then passed through an amplifier and low-pass filter to condition the signal and read measurements. The conditioned signal continues through an ADC where the output is a digital electronic signal. This digital signal is then stored and used to determine if the field-of-view is still on the solar disk. More detailed descriptions of how each of the systems work can be seen in section 4, "Design Process & Outcome".

The components of the FBD are a mixture of consumer off-the-shelf and team-designed hardware. The optical system is composed of COTS parts - filters, aperture, mirror, pinhole, and photodiode - that are assembled on a team-designed optical bench. The optical bench ensures the optical system is sufficiently aligned. Similarly the electrical system is a team-designed printed circuit board that incorporates COTS components. The software will be completely team-designed. Additionally the simulated bus architecture is comprised of COTS parts.

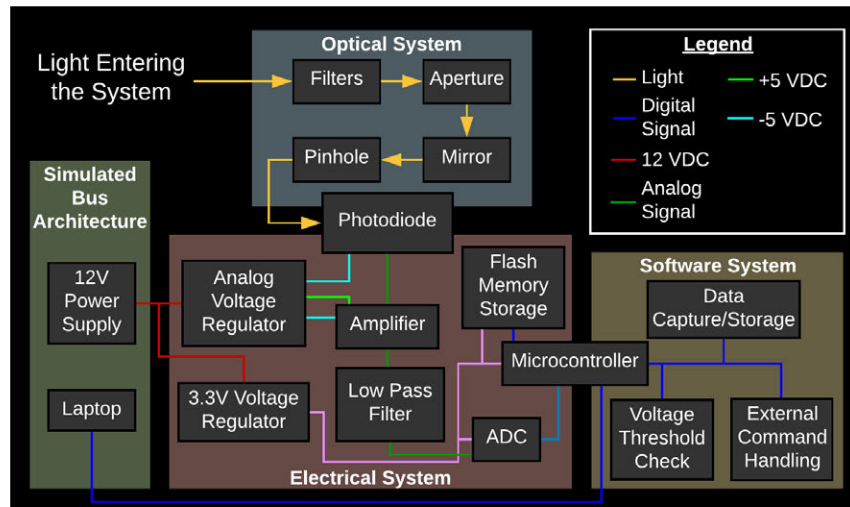


Figure 4. Functional Block Diagram

3.5. Functional Requirements

Using the NanoSAM mission CONOPS along with the demonstration CONOPS, three functional requirements were developed. These functional requirements describe the high-level functions that the NanoSAM system must perform to satisfy the customer's needs and be classified as successful.

- 1.0 The optical system of the payload shall be capable of collecting radiometry data.
- 2.0 The payload shall be able to be extrapolated to a flight ready 1.5U CubeSat.
- 3.0 The electronics system of the payload shall be capable of collecting, packetizing, and outputting radiometry data.

These are the functional requirements that are used to characterize the design of the system through the derivation of the design requirements. The first functional requirement describes the type of data the system must collect to solve for aerosol concentrations. It defines solar irradiance as the type of radiometric data that needs to be collected. The solar occultation method, outlined in Fig. 2, works by comparing solar irradiance measurements that have been collected from varying amounts of stratosphere to a baseline solar irradiance measurement that is obtained outside of the stratosphere. By calculating the attenuation between these two measurements, the aerosol concentrations can be determined. Without collecting the appropriate radiometric data, the NanoSAM system would not be able to provide data that can be used to solve for aerosol concentrations.

The second functional requirement defines the payload size to constrain the overall dimensions of the system. The motivation behind functional requirement 2.0 is to ensure the payload fits within a standard CubeSat deployment module, as requested by the customer. Usually, CubeSats contain internal power systems or an attitude determination and control system (ADCS), that takes up valuable space and mass. The main goals of this project is on the functionality of the payload so the power system and ADCS is not accounting for in the structure dimension requirements. With that said, the team anticipates that the internal power system and ADCS will take up an additional 0.5U. Therefore, the cross section that the NanoSAM payload needs to fulfil is a 10x10 cm square. Given this information, the team believes a flight-ready system will be able to fit within the specifications of a standard 1.5U CubeSat.

The final functional requirement describes the necessary capabilities of the electronics system. If the electronics system is unable to sufficiently collect, packetize, and output measurements, the irradiance data will not be properly collected, and the team will not be able to verify functionality of the payload. The electronics system needs to be able to properly collect the analog irradiance data and convert it to a digital signal. To output and ensure the data is

accurate, the electronics system needs to packetize the digital data. If the electronics system can adequately perform all of these tasks, the team will be able to verify that the measurement system functions properly.

These three functional requirements were used to develop baseline designs and to select components for trade studies. It was also used to create a detailed list of design requirements such that the design alternatives that were considered can be narrowed down to a final design. Details of the requirements flow-down can be found in section 4.2.

4. Design Process & Outcome

Quinn LaBarge, Jared Cantilina, Sara Reitz, Matt Weber, Aanshi Panchal, Jessica Harris, Conner McLeod, Jaykob Velasquez, Jacob Romero

Before choosing a design solution that meets all the specific objectives, critical project elements, and functional and design requirements, several trade studies were performed.

In the following sections, alternatives to the elected design solution are discussed based on the system it belongs in. Pros and cons of each component are compared and trade studies were performed to select the parts that fit best with the goals of NanoSAM. In the trade studies, each metric is given a weighting value before the components are assigned scores. The metrics used in the various trade studies are driven by the requirements flow-down in Section 4.2.

Finally, a baseline design devised from the trade studies is introduced. Detailed descriptions of each element can be found in Section 4.3.

To find the justifications for our considered alternate designs and trade studies, please refer to Appendix A.

4.1. Summary of Alternative Designs and Trade Studies

4.1.1. Electronics Subsystem

The electronics system must meet the requirements for Radiometry, Measurement Stability, Measurement Error, SNR, Dynamic Range, Data Collection, Data Storage, Data Output, and Average Power Draw. Although there are multiple ways of achieving these requirements, all of them require several same features: a photodiode to convert solar radiation into an electrical signal, a way to read the electrical signal, memory to store the data, and a controller to send the data.

Photodiode Selection

The three photodiodes considered were: Silicon, InGaAs, and Germanium. These photodiodes have different properties that offer pros and cons for this project. After conducting trade studies and providing weighting scores for the properties of the considered photodiodes, the final selection is the Silicon photodiode. This photodiode offers an acceptable bandwidth, low dark current, a sufficient active area, the highest responsivity at a wavelength of 1020 nm, and the lowest cost. These metrics of consideration were chosen for the photodiode trade study as they all impact mission success in varying degrees.

ADC Selection

The types of ADC considered were flash, successive approximation, and sigma-delta. The properties of the ADC types considered were weighted based on resolution, dynamic range, SNR, sampling rate, power consumption, and latency. After weighing the advantages and disadvantages of each ADC selection, the sigma-delta ADC was selected for the final design. This selection was made due to its high resolution, low SNR, moderately low power usage, and decent dynamic range. The sigma-delta ADC had one of the lowest sampling rates, but was still more than sufficient for the requirements of NanoSAM's data collection. The most important requirements for NanoSAM are low noise

and high resolution, which makes the sigma-delta ADC an excellent choice for the project.

On-Board Controller Selection

The on-board controllers considered were an FPGA, micro-controller, and a single board computer. The main consideration factors for these options were based on size, weight, hardware interfacing, ease of programming, processing power, power draw, and available software solutions. The hardware interfacing, ease of programming, and available software solutions were most heavily weighted in the trade study for the on-board controller because these factors are affected by both driving requirements of the project and available resources. The results of the trade study show that the micro-controller will be the best choice for NanoSAM's on-board controller as it has the lowest size, weight, power draw, as well as the highest ease of programming, and contains sufficient processing power.

External Memory Selection

The external memory options considered were a solid-state drive card, micro-SD card, flash drive (USB), and NAND flash chips. The trade studies weighed each of these options, taking into account the complexity of use, storage capacity, speed, reliability, size, and cost. The final design selection was the NAND flash chip. This selection was made due to the small size, low cost, and high reliability of the NAND flash chips. While the data storage per chip is relatively low compared to the other options, due to the low cost and small size, multiple chips may be used as required. The NAND flash chips are an excellent choice, as the reliability of the chip, as well as the ease of use, is critical for successful data collection.

4.1.2. Optics Subsystem

The NanoSAM optical system must meet the requirements for radiometry, including the vertical resolution, the field-of-view, the wavelength filtering, the MTF, and the optical alignment requirements. In addition, the optical system configuration must meet the payload volume and mass requirements. Each design must filter sunlight to a narrow spectral band of approximately $1.02 \mu\text{m}$. This filtered signal then needs to be reflected and focused onto the photodiode. Multiple reflector telescope designs were considered to meet these requirements. The baseline optical design trade studies included the telescope-type selection, mirror substrate selection, mirror surface coating selection, and filter selection.

Telescope Type Selection

The first trade study conducted was centered around the telescope type. While there are a myriad of reflector telescope configurations to choose from, the four options considered represent the optimal candidates. The single off-axis parabola (OAP) and on-axis telescope designs require just a single mirror. In contrast, the other two designs, the Cassegrain and Newtonian reflector telescopes, require multiple mirrors. The added complexity of the additional mirrors is a major factor considered for the trade study. In addition, the relative costs of the systems, including mounts and optics is investigated. The effective focal length (EFL) of each telescope type is considered too, since it relates to the payload volume requirement. Folding the optics system with multiple mirrors is advantageous for the overall optical system size. Lastly, the obstructions and optical aberrations are considered, as they pertain to the optical system alignment and spatial resolution.

After conducting the trades study, it was determined that the single OAP telescope type is the best option. It cost the least among all the options. Although there is a high risk of aberrations, all of the telescope types are at risk of producing aberrations. The OAP design has the lowest manufacturing complexity compared to the alternative designs mainly due to the fact that there is no central obstruction. The relatively short effective focal length is not ideal, but there are commercial-off-the-shelf (COTS) options for the OAP mirror from major manufacturers that fit within the dimensions of the NanoSAM enclosure.

Mirror Substrate Selection

The next design consideration concerns the mirror substrate selection. The COTS mirrors typically consist of a mirror substrate coated in a reflective material. The cost, density, and coefficient of thermal expansion (CTE) are examined for Al 6061-T6, floated borosilicate, borosilicate, and fused silica. According to the trade study, the floated borosilicate mirror substrate is clearly the best option due to its low cost, low density, and low CTE. With that said, the consistency of the CTE between the mirror substrate and mirror coating was assigned a weight of 0.05. Further along in the design process, the relative importance of this property of the system was discovered. Athermalization of the optics system is dependent on the uniformity of the material comprising the system. Despite the price and high density of the Al 6061-T6, it is the ideal design option because it is also available as a surface coating.

Mirror Surface Coating Selection

The mirror surface coating is explored next. The relative cost, reflectivity around the target wavelength, surface quality, and durability are studied for Protected Aluminum, Enhanced Aluminum, Protected Silver, and Protected Gold. By a narrow margin, the Protected Aluminum is the ideal design choice. First, it is the least expensive option among the designs considered. These mirrors are upwards of \$200 each, so the cost is an important factor. Second, the durability and surface quality of the Protected Aluminum is fairly high. Even though the reflectivity of the Protected Aluminum is the lowest among the surface coatings, the reflectivity is still greater than 85 percent, which is more than sufficient for the optical system. Lastly, the all-aluminum COTS mirrors facilitate the athermalization of the optical system.

Filter Selection

To isolate the target wavelength, the incident sunlight passes through a bandpass filter. Light outside the pass band is rejected, limiting the signal reaching the mirrors and, ultimately, the photodiode. The filter types selected for the trade study were: linear variable filters, traditional coating filters, hard coating filters, and custom coating filters. Each of the filter types were evaluated based on their cost, transmission, and optical density. In addition, COTS filters with the desired center wavelength are difficult to source. In many cases, the nearest available center wavelength (CWL) is slightly offset from the target wavelength. As such, deviation from the target CWL is also considered. The results of the trade study indicate that the hard coating filter is the best option. Although the CWL is 10 nm offset from the target wavelength, its relatively low cost, high transmission in the passband, and relatively low transmission outside the passband make it the best candidate. Besides that, absorption due to the predominant atmospheric species aside from aerosol is still relatively low around 1.03 μm .

4.2. Requirements Flow-down

Concurrent with the trade studies for a solution and its corresponding components, the design requirements of the project was developed from the functional requirements mentioned in section 3.5, "Functional Requirements." When scoping the project with the customer, both the mission and design requirements for the project was developed. Since this year's NanoSAM project will focus on launch, the mission requirements are incomplete and were only used to drive the specifications and design requirements that can be found in this section. As a result, a requirements flow-down document containing three levels was created while including the motivation of each requirement.

In the requirements flow down, the level 0 requirements represent the functional requirements of the system and are the parent to level 1 requirements. All other requirement levels will be known as design requirements throughout the document. Level 3 requirements work toward level 2 parent requirements and so on such that the design requirements flow down from the functional requirements.

When developing the design requirements, the NanoSAM team reviewed the design specifications of its legacy system, SAM-II, to determine the specs that could be inherited to the NanoSAM project. The first design requirement, 1.1, describes the necessary vertical resolution of the NanoSAM atmospheric profile. This requirement was inherited from the SAM-II project to ensure that the resolution in NanoSAM will at least match the performance of its legacy system. The other design requirements that flow down from requirement 1.1 are necessary to ensure the 1 km vertical profile is maintained. To achieve this vertical resolution, the FOV of the optical system must be sufficiently small.

This value was determined by geometrically solving for the angle required to achieve a 1 km vertical height when in orbit. The equation and diagram shown below describe the calculations to used to determine the field-of-view.

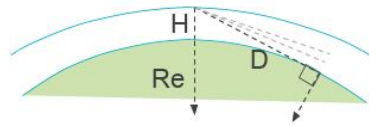


Figure 5. Vertical Resolution Diagram

$$D = \sqrt{(R_E + H)^2 - (R_E)^2} \quad (1)$$

In Fig. 5 above, R_e is the radius of Earth and is equal to 6378 km. The NanoSAM team decided to choose a mock orbit height of 500 km for calculations since this is a typical LEO orbit height that is within the range of values recommended by the customer. Performing this calculation gave a required field-of-view of 1.3 arcminutes.

The calculation with mock on-orbit conditions allow the NanoSAM team to be confident with the ability of this system to be extrapolated into a flight-capable system. Additionally, the required pointing accuracy of the system was also calculated using on-orbit conditions. Purchasing a commercial solar tracker that performs the pointing control of the system with the necessary pointing accuracy allows the team to ensure that the optical system field-of-view can be directed to the desired location. The final design requirement needed to maintain the required vertical resolution is the aperture of the optical system. The minimum aperture size was calculated based on the mirror position and the derived FOV.

Requirement 1.2 was not inherited as the SAM-II mission used a different wavelength than NanoSAM's 1.02 micron wavelength. This wavelength was determined after talking to Dr. Cora Randall from Laboratory for Atmospheric and Space Physics at CU Boulder. It is a wavelength particularly sensitive to aerosols and is, therefore, suitable to measure solar irradiance data at.

Next, to capture the desired image of the sun, the optical system must be sufficiently aligned. The driving factor behind the rigid alignment budget is the required modular transfer function (MTF). Meeting the required MTF guarantees that the system collects data with a spatial resolution that is at least as refined as SAM-II. The plot in Fig. 6 shows the MTF curves for various levels of obstruction given a circular aperture. The x -axis represents the normalized angular frequency of the image (ν_n), and the y -axis represents the MTF of the system. SAM-II had an obstruction of about 75%; therefore its MTF follows the red curve second from the left. The ideal MTF for SAM-II was found by determining the MTF value at the normalized angular frequency that corresponds to the 1 km vertical resolution. This gives an ideal SAM-II system MTF of 0.74, indicated by the black diamond in Fig. 6. As a result, NanoSAM should meet an MTF of 0.74 or greater to exceed the performance of SAM-II. Greater details regarding the MTF and its impact on the spatial resolution of the optical instrument are presented in the subsequent section.

The measurement stability requirement ensures that the MTF and collected data remain constant given different scenarios of testing. One such scenario is the different operating temperatures that the system would be tested in. The system must remain stable in an anticipated operating temperature range of 4°C to 26°C. The measurement error defines the allowable error in the collected data for the data to still be considered correct and viable.

Design requirement 1.4, which pertains to the system SNR, was a requirement that was developed after constructing a radiometric model to account for all sources of noise. In addition, the dynamic range requirement is necessary to make sure that the system does not saturate when encountered with excess irradiance. A previous aerosol profiling device, Polar Ozone and Aerosol Measurement II (POAM-II), experienced over-saturation and was unable to obtain any scientifically relevant data. To avoid this misstep, the NanoSAM system has developed a margin for acceptable excess irradiance.

The second functional requirement, which constrains the size of the payload's footprint or cross-section and all its associated design requirements, were developed specifically for the NanoSAM project. The relatively small size

in comparison to other legacy systems is the driving factor behind pursuing the NanoSAM project, since size will facilitate the possible production and deployment of a full constellation NanoSAM system.

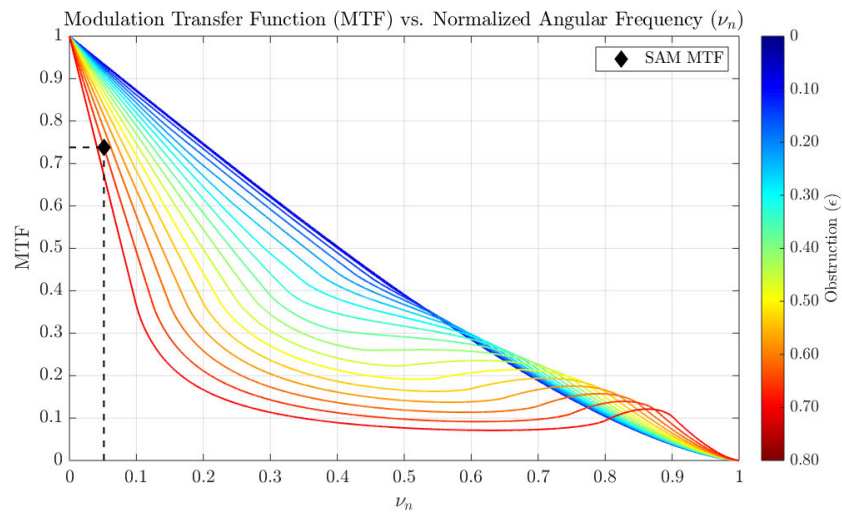


Figure 6. MTF Requirement Development

For the NanoSAM system to deploy a constellation of measurement devices the bus must be the adequate size to be compatible with standard CubeSat specifications. The team has designed a structure to house the radiometric and electronics systems which has the dimensions of a standard 1U CubeSat. From the CubeSat organization’s design specification document [43], the maximum allowable mass of a 1U CubeSat is 1.33 kg. Designing NanoSAM to meet the 1U specifications, only minor modifications would be required for the system to be flight-capable.

In addition to meeting the 1U specifications, the NanoSAM system must be housed within an enclosure that allows the team to perform verification and validation tests. This means that the enclosure must be removable from the optical and electronics systems such that the team can make adjustments as necessary. The enclosure must also be dust-proof to protect the sensitive components of the radiometric device such as the detector tube and the mirror. Additionally, the enclosure must not accept light into the optical system except through the designated area. This ensures that stray light does not affect the data collected by the photodetector and undermine the desired image. Finally, the NanoSAM structure needs to be portable and removable so the team can easily transport it to numerous locations for various tests.

There are three major capabilities that the electronics system of NanoSAM needs to be able to perform to satisfy the functional needs of the project. The first is data collection, as outlined in requirement 3.1. To collect data that is at least as valuable as SAM-II, the irradiance data needs to be sampled at a rate of 50 Hz and collected using 10 bits. The technology available to SAM-II engineers in comparison to today’s equipment means that both the sampling rate and bit size requirements can be easily met by the NanoSAM team.

The next major function the electronics and software system must perform is to packetize the data. This is necessary for the data to output to an external source. Once the data is packetized, it is then transferred via a serial connection to a laptop so that the team can verify the accuracy of the collected data. The accompanying software package will command the rest of the system to begin the data collection processes and the duration. The power capabilities of a small CubeSat also constrain the available power that the NanoSAM system can draw, as seen in requirement 3.5.

To generate these requirements, the NanoSAM team researched all aspects of past projects and held discussions with customers Jim Baer and Joe Lopez to determine the needs of the project’s main stakeholders. Baer is an optical engineer with many years of experience. He worked on the original SAM-II mission and, as such, is a valuable resource for the development of NanoSAM. Lopez is currently a systems engineer for Ball and was extremely supportive in creating the radiometric model. Additionally, the NanoSAM team worked in close conjunction with Joe Lopez to develop these requirements and further refine them. These design requirements are the main drivers of the engineering work presented in the following subsection "Resulting Design".

RQMT ID				RQMT Title	RQMT Text	Motivation
Level 0	Level 1	Level 2	Level 3			
1.0				Radiometry	The optical system of the payload shall be capable of collecting radiometry data.	The long-term mission goal of NanoSAM is to collect irradiance data in the stratosphere. The optical system will need to be capable of collecting radiometry data to achieve the long-term mission goals.
	1.1			Vertical Resolution	The optical system shall facilitate a vertical resolution profile of 1 km or less.	The vertical resolution of NanoSAM must at least be equivalent to SAM-II, its predecessor.
		1.1.1		FOV	The payload shall have a field-of-view of 1.3 arcminutes or less.	When placed in a 500x500 km circular orbit in the future, the FOV must be 1.3 arcminutes to achieve 1 km vertical resolution.
			1.1.1.1	Pointing Accuracy	The pointing accuracy of the payload shall be 30 arcseconds or less.	The pointing accuracy will affect the light entering the FOV of the optical system.
	1.2			Wavelength	The optical system shall reject 99.97% of incoming light outside of a center wavelength between 1.018 and 1.042 micrometers.	This is a wavelength at which aerosol particles can be detected. Other wavelengths at which aerosol particles can be detected have interference from other constituent absorption or Rayleigh scattering.
	1.3			Optical Alignment	The light rejection method used in the optical system shall be aligned to the pin-hole field stop.	The incoming light needs to align with the pin-hole field stop to successfully reach the photodiode.
		1.3.1		MTF	The optical system shall be aligned such that its MTF is at least 0.74.	The MTF requirement is needed so that the image obtained from the photodiode has a high resolution.
			1.3.1.1	Measurement Stability	The irradiance measurements of the system shall remain stable to within 1% across at least 5 tests.	The optical system will need to be capable of measuring radiometry data that is repeatable and precise throughout multiple tests.
			1.3.1.2	Allowable Measurement Error	The irradiance measurements of the system shall remain accurate to within 5% of theoretical signal.	The optical system needs to be capable of measuring radiometry data that is accurate.
			1.3.1.3	Optical Heating	The optical system focal length shall remain stable over the anticipated operating temperature range of 4C to 26C.	The operating range of temperature should not affect the alignment, precision, and accuracy of the optical system or the data obtained will not be accurate.
		1.3.2		Transportation Alignment	The alignment within the optical system shall not be affected by acceleration of 2g or below.	The optical system requires transportation that should not affect the alignment.
	1.4			SNR	The payload shall have an SNR of 3500 or greater for irradiance values of 50% maximum anticipated irradiance and above.	The SNR will ensure that the data collected will maintain its accuracy and effectiveness without being affected by noise. This will also allow NanoSAM to exceed SAM-II's performance.
	1.5			Dynamic Range	The payload shall not saturate for an irradiance input of 120% of the maximum anticipated solar radiance in the operational band.	The dynamic range is important in ensuring that the data in the window between the maximum and minimum irradiance signal is captured to the desired details.
2				Bus Compatibility	The payload shall be able to be extrapolated to a flight ready 1.5U CubeSat.	This is a customer-specified requirement for the system to be compatible with a CubeSat bus architecture.
	2.1			Payload Volume	The optics and electronics system shall fit within a volume of 10x10x10 cm.	The payload volume needs to fit within the chosen CubeSat form factor to be compatible with the customer's request.

Figure 7. Requirements Flow Down Part 1

	2.2			Payload Mass	The payload and bus architecture combined shall have a mass no greater than 1.33 kg.	The mass of the payload needs to be compatible with the commercial CubeSat bus architecture.
	2.3			Enclosure	The system shall be housed in an enclosure with external dimensions of 10x10x10 cm.	The volume of the payload and its enclosure needs to be compatible with the commercial CubeSat bus architecture.
		2.3.1		Sealed Enclosure	The enclosure shall be dustproof from the external testing environment.	Dust particles will affect the performance of the optical system due to its sensitive components and small photodetector surface area.
		2.3.2		Removable Enclosure	The enclosure shall be removable from the optical and electronics system and vice versa.	The enclosure is used to protect the optical and electronic components from external environment but the two systems need to be removable for testing and alignment. It will also simplify integration processes.
		2.3.3		Scattering Light	The enclosure shall not accept light entering the optical system besides through the designated area.	The optical system should not receive light from cracks or the integrity of the radiometry data will be affected.
3.0				Electronics System	The electronics system of the payload shall be capable of collecting, packetizing, and outputting radiometry data.	The electronics system is essential to ensure that the radiometry data can be measured accurately and retrieved.
	3.1			Data Collection	The payload shall be capable of collecting and terminating radiometry data collection.	Data collection is essential to obtain radiometry data.
		3.1.1		Sampling Rate	The irradiance data shall be sampled at a rate of at least 50 Hz.	The sampling rate is inherited from SAM-II to make sure that NanoSAM exceed its predecessor's performance.
		3.1.2		Data Collection Bit Size	The irradiance data shall be collected using 10 or more bits.	Data needs to be collected at a minimum of 10 bits to obtain desired precision.
		3.1.3		Termination	The optical system shall stop data collection once the solar irradiance drops below 25% of the previous irradiance measurement.	The system will need to stop taking data at some point, when the irradiance drops below the specified value the data will no longer be valid and the system will need to know to stop collecting data.
	3.2			Data Packetization	The payload shall be capable of packetizing radiometry data.	Data packetizing is needed before data can be transferred to an external source for post-processing.
		3.2.1		Data Storage	The payload shall be able to collect and store at least 100 Mb of data for 30 measurements.	Solar irradiance data is the critical data taken by the instrument and needs to be collected and stored.
	3.3			Data Output	The instrument shall be able to output solar irradiance data.	The data needs to be read in order to verify the functionality of the instrument.
		3.3.1		Data Output Method	The instrument shall output solar irradiance data through a serial connection.	The data will be transferred to a computer for analysis and verification.
	3.4			Software	The software shall command the payload to capture, store, and output irradiance data.	The software needs to connect the electronics and optical components to ensure the functionality of the payload.
	3.5			Average Power Draw	The payload shall draw an average of less than 4.5 W over 30 measurements.	The power required for the CubeSat to operate should be within reason and as low as possible to make sure that the power budget will be valid.
Requirements Flow Down						

Figure 8. Requirements Flow Down Part 2

4.3. Resulting Design

4.3.1. Optics Baseline Design Overview

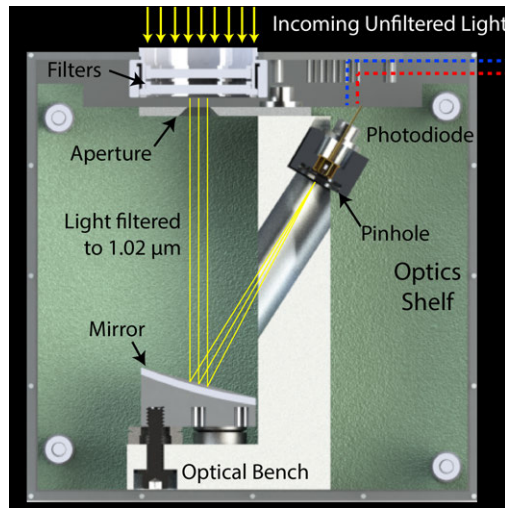


Figure 9. Optics Baseline Design Overview

This baseline design overview visualizes the flow of radiometric data from incident light to output voltage from the photodiode. The incoming light passes through a long-pass filter and band-pass filter, which isolate the wavelength of light that interacts with the atmospheric aerosols this mission seeks to measure. Specifically, around 85% of the light in the passband around $1.02\ \mu\text{m}$ is transmitted through the filters. This light then passes through a 20 mm x 5 mm rectangular aperture stop that defines the clear aperture of the system. The 25.4 mm diameter aluminum off-axis parabolic (OAP) mirror reflects the light at a 30° offset angle. The light then passes through a precision pinhole at the focal point 54.45 mm away. For nominal alignment conditions, the focal point of the OAP is located at the center of the pinhole field stop. The $15\ \mu\text{m}$ diameter pinhole limits the stray and scattered light that reaches the photodiode and sets the viewing angle of the optics system at 0.947 arc-minutes (.0158 degrees). After the focused light passes through the pinhole, it illuminates the active area of the photodiode resulting in an output voltage response.

Each of the optical bench components are rigidly mounted to the bench base plate. This solid aluminum 6061 plate constrains the position of the optical components once aligned. Integrated mounting systems and bores in the bench plate facilitate the alignment of the mirror to the diode block assembly. The diode block assembly constrains the position of the field stop plate and photodiode. The photodiode block is machined out of the same aluminum alloy as the mirror to maintain a consistent CTE throughout the optical bench. This minimizes thermal deformation and or shifting of the optics components. The integrated bench plate is mounted between two G10 fiberglass plates to thermally isolate the optics and constrain their position relative to the filter assembly.

4.3.2. Optics Detailed Design

Analytical Optics Configuration and Performance

The NanoSAM optics system captures, filters, and focuses incident aerosol-occluded sunlight onto the silicon photodiode. The optics system must meet functional and design requirements 1.0, 1.1, 1.2, and 1.3. Fig. 10 displays a scaled Zemax OpticStudio rendering of the NanoSAM optics system. It displays the path light follows through the NanoSAM optics system, and how it interacts with each optical component. Collimated unfiltered sunlight (depicted by yellow rays) passes through both a long-pass and band-pass filter, which filter the collimated light to the requisite $1.02\ \mu\text{m}$ wavelength. The collimated, filtered light (blue rays) then passes through a rectangular aperture stop that limits the desired amount of light that enters the optics system. The light then reflects off of a 30 degree off-axis

parabolic mirror that focuses the light through a pinhole field stop onto the silicon photodiode. The pinhole field stop limits the field-of-view of the optics system.

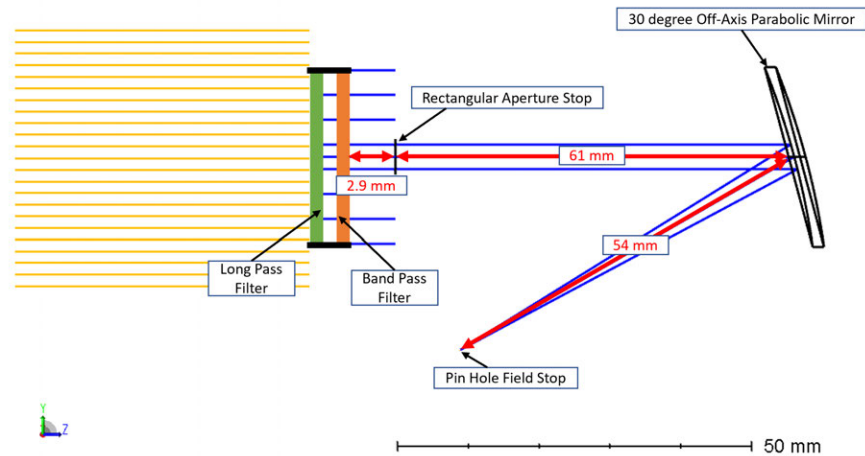


Figure 10. NanoSAM Optics System Zemax Model

Vertical Resolution There are a few considerations to be made when examining the vertical resolution of the NanoSAM optical instrument. To begin, the ideal diffraction-limited system is modeled. Due to the wave nature of light, a telescope’s maximum angular resolution is defined by the aperture size. The Rayleigh criterion gives the maximum angular separation between two point light sources which a telescope is able to resolve, given a circular aperture (Eq. 2). For a rectangular aperture, the right hand side reduces to $\frac{\lambda}{D}$. From the requirement derivation, it is evident that the angular separation corresponding to one kilometer is approximately 0.022 degrees (0.384 mrad). Therefore, at the target wavelength of 1.02 μm , the minimum required circular and rectangular aperture sizes are 3.31 mm (diameter) and 2.71 mm (width), respectively. According to the Rayleigh criterion, an aperture with larger dimensions is capable of achieving the vertical resolution requirement.

$$\theta = \frac{1.220\lambda}{D} \quad (2)$$

However, the Rayleigh criterion is not the only metric used to characterize the spatial resolution of optics systems. The modulation transfer function is another commonly used performance metric. Put simply, the MTF quantifies an optics systems ability to preserve image contrast[36]. The MTF varies with spatial and angular frequency. The frequency refers to the periodic contrast within an image, which is portrayed in the pinwheel diagrams below. Higher values of MTF (Fig. 11) correspond to sharper, clearer images. Conversely, lower values of MTF are indicative of low image contrast. The blurring and softened edges of the image for an optic with low MTF is shown in Fig. 12.

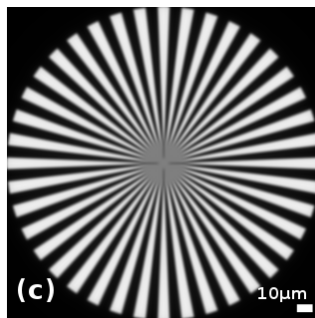


Figure 11. Pinwheel Diagram - High MTF

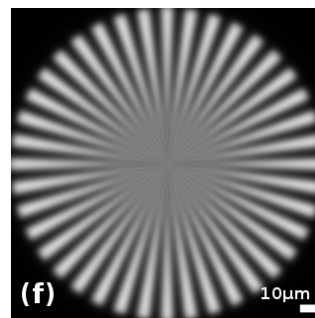


Figure 12. Pinwheel Diagram - Low MTF

Requirement 1.3.1 states that NanoSAM must meet or exceed an MTF of 0.74 at the cycle per kilometer frequency.

To assess the design solution for this requirement, one must first characterize the MTF of the NanoSAM optical instrument. For a rectangular aperture, the ideal diffraction-limited MTF curve is a straight line from one to zero for frequencies starting at zero cycles/km (zero cycles/mrad) and ending at the cutoff frequency, ν_c [38]. From earlier, the Rayleigh criterion defines the maximum angular resolution of the optical system. The inverse of the Rayleigh limit is the maximum frequency at which the optic can resolve any two points. Thus, the cutoff frequency represents the point at which no further contrast performance can be achieved. Generally, the spatial and angular frequencies are normalized by the cutoff frequency, and the x -axis spans from zero to one. The MTF curve for 20 mm wide aperture is shown in Fig. 13 alongside the ideal MTF curve for SAM II. Both points on the graph correspond to the MTF value associated with a single cycle per kilometer (the equivalent angular frequency is 2.57 cycles/mrad). The diffraction-limited MTF of the NanoSAM optical system is around 0.86 using this aperture size. Therefore, real losses can degrade the MTF of the system by around 14% before reaching the minimum for requirement 1.3.1.

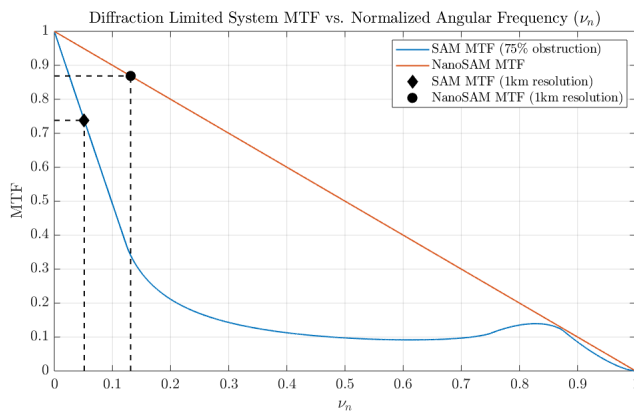


Figure 13. Diffraction-Limited MTF Comparison (SAM II and NanoSAM)

The optical performance section assesses the design solution with respect to the MTF-1.3.1 design requirement.

Stray Light The NanoSAM optical system was designed so that the effect of stray light scattering is minimized. The diameter of the Sun image on the pinhole is derived using Eq. 3.

$$d = EFL \cdot \theta = 54.45\text{mm} \cdot 0.0093\text{radians} = 0.506\text{mm}, \quad (3)$$

Note that d is diameter of the Sun image on the pinhole, EFL is the effective focal length of the off-axis parabola, and θ is the angular diameter of the Sun. The result of Eq. 3 shows that even if the image of the Sun drifts completely off the pinhole it will still remain on the surface of the pinhole disk and will not interact with the cylindrical walls of the detector block causing scattering, because the Sun image diameter is less than the pinhole disk diameter. Figure 14 displays a visual of the Sun image on the pinhole.

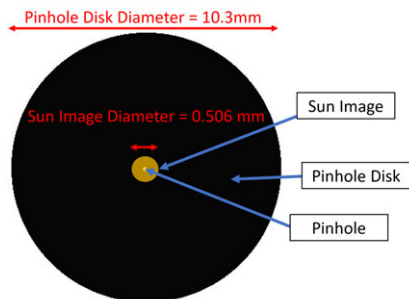


Figure 14. Sun Image on Pinhole with Dimensions

Spectral Filtering To isolate the effects of aerosol concentration on the transmitted sunlight, light which doesn't interact with aerosols must be excluded from NanoSAM's radiometric data. This drives Requirement 1.2, which prescribes a filtering of the light to a center wavelength of $1.02\mu\text{m}$ with exclusion of 99.97% of light outside the scientifically-relevant wavelength range. This exclusion specification corresponds to $1/\text{SNR}$ and thus ensures that the leaking light outside the passband doesn't contribute false data above the noise threshold of the system. The ThorLabs FLH1030-10 bandpass filter[41] has a passband centered at $1.03\mu\text{m}$ with a 10nm FWHM. This filter is rated to exclude 99.999% of light outside the passband. However, when the spectral transmission profile for this filter was mapped over the solar spectrum[28], it became apparent that the filter transmitted too much out-of-band light because the Sun emits much more strongly in the visible region than in infrared. In particular, to remain beneath the established SNR threshold the system would need to consider an effective pass region 57.1nm wide around the center wavelength. In other words, analysis of this data would assume that any light absorbed between 1.001 and $1.059\mu\text{m}$ correlates to aerosol absorption. This is not a good assumption - diatomic oxygen O_2 , for example, absorbs strongly at $1.060\mu\text{m}$, and this absorption could bias the aerosol absorption measurements. Narrowing the passband reduces this biasing; this is accomplished by adding a second filter, the ThorLabs FELH1000 longpass filter[40]. This filter cuts on at $1\mu\text{m}$, which is ideal for blocking the high-energy ultraviolet and visible light that makes up the majority of the solar emission spectrum[28]. Adding this filter reduces the SNR-limited pass region around the CWL to 23.9nm, halving the impact of the leaking light on the radiometric data. Because aerosols are the only significantly absorbing species in this region, between 1.018 and $1.042\mu\text{m}$, the combination of these filters meets the NanoSAM filtering and rejection requirements and is sufficient to isolate the effects of aerosols on the transmitted light. The effects of adding the filter are depicted in the plot below, which emphasizes how the longpass filter reduces the signal due to incident low-wavelength light by five orders of magnitude, significantly improving scientific validity of the aerosol occultation data. The signal peaks around the $1.03\mu\text{m}$ CWL, as desired.

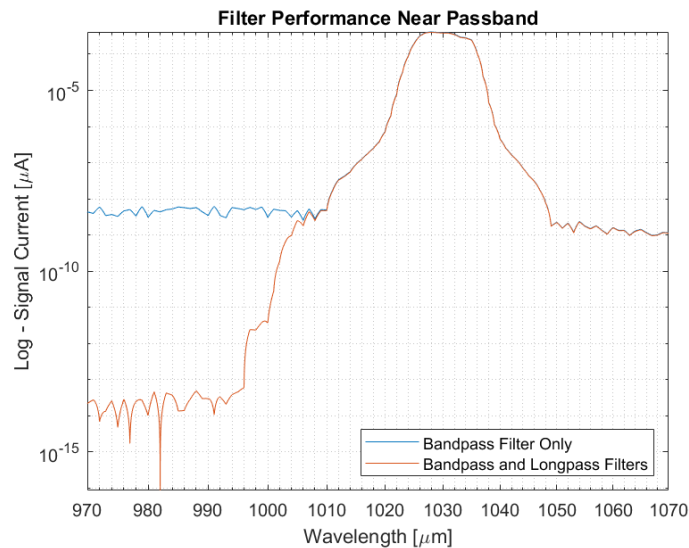


Figure 15. Spectral Performance of the Filter Assembly near the 1.03μ CLW

MTF Budget The modulation transfer function (MTF) is a measure of an optics system's ability to clearly resolve an image and is often used to categorize the performance of various optical systems. However, many factors such as defocus, tilting, in-plane and out-of-plane radial displacement, mirror irregularity, central obstructions, comatic aberrations, ripple noise, and more can significantly degrade the MTF of the optical system. Figure 16 illustrates positive focus and radial in-plane and out-of-plane displacement at the image plane. Zemax was used to model system MTF at the pinhole by combining degradations due to focus and radial in-plane and out-of-plane displacement. The Modern Optical Engineering textbook [38] was used to obtain the MTF degradations due to filter wavefront error.

Table 2 displays the MTF degradation budget of a feasible alignment configuration of the NanoSAM optics system.

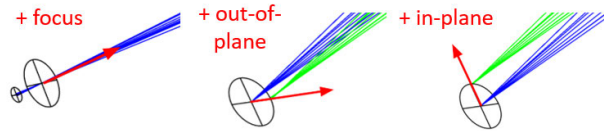


Figure 16. + focus, + out-of-plane, and in-plane Displacements

	NanoSAM (feasible alignment)	
Target MTF		
Best possible MTF of SAM-II at critical angular frequency with 50 mm aperture & 75% obstruction	0.74	
Predicted Mirror MTF with WFE		
Obtained using Zemax for angular frequency of 2.57 [cycles/mrad]	0.86	
MTF Degradation Factor		
Focus (Z') Displacement	0.94	45 μm error **
Out-of-plane (X') Displacement	0.97	30 μm error **
Filter TWFE	0.98	0.03 λ WFE
Filter TWFE	0.98	0.03 λ WFE
Analysis		
Combined Degradations = ∏ MTF Degradation Factors	0.88	
System MTF = Combined Degradations * Actual Mirror MTF	0.75	
Margin = $\frac{\text{System MTF}}{\text{Target MTF}} - 1$	0.01%	

** feasible displacement

Table 2. MTF Budget for Feasible Alignment Configuration of NanoSAM Optics System

The feasible alignment of the NanoSAM optics system in table 2 shows the MTF degradation budget of the NanoSAM optics system with a feasible alignment error of 45 μm of focus displacement and a maximum out-of-plane radial error of 30 μm in order to meet the target MTF of SAM II resulting in a margin of 0.01%. This shows that MTF-1.3.1 requirement is achievable by an undergraduate student optics team using off the shelf optical components.

Thermal Effects A major concern for the optical instrument involves the athermalization of the system. In general, athermal systems rely on uniform material properties throughout. This is most readily accomplished by constructing the system out of a single material[37]. With this in mind, the NanoSAM’s optical system is comprised of predominantly Aluminum 6061-T6. There are a few parts in the assembly which are not the aluminum alloy. The most notable are the stainless steel spherical washers between the back surface of the mirror and the optical bench plate. The difference in thermal expansion of the stainless steel washers and the aluminum bench misaligns the mirror and pinhole.

A simple analysis is performed to assess the severity of this misalignment of the optics components. The normal thermal strain, ϵ , on a material is given by Eq. 4, where α is the linear coefficient of thermal expansion and ΔT is the uniform temperature change. The difference between the changes in length for the steel washers and equivalent aluminum washers gives an estimate for the shift of the mirror (Eq. 5).

$$\epsilon = \alpha \Delta T \quad (4)$$

$$|\Delta L_{sys}| = L(\alpha_{Steel} - \alpha_{Aluminum})\Delta T \quad (5)$$

Notice that there are two unknowns in Eq. 5, the temperature change, ΔT , and the shift of the system, ΔL_{sys} . The system shift is set to one micron, which is well below the tolerances set during the MTF analysis. Then, the corresponding temperature change is computed. A range of CTEs for stainless steel are used for the analysis to examine the differences in the required ΔT . The resulting temperature changes can be seen in Fig. 17.

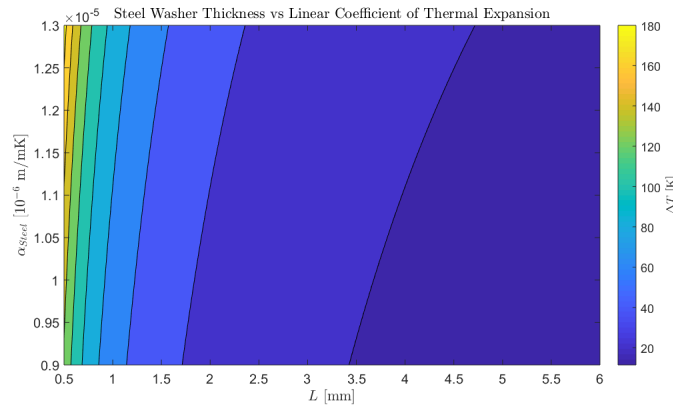


Figure 17. System Shift Due to Thermal Expansion of Steel Washers

The stainless steel spherical washers are each around 4mm thick. A 20 Kelvin temperature change is required to shift the mirror by one micron. It is not expected that the NanoSAM instrument experiences this magnitude of temperature change during testing and data capture. Therefore, the effects of the temperature change on the alignment of the system are assumed to be minimal.

Physical Optics System Assembly

The following section describes the design and development of the optical bench solid model. The functionality of the optical bench is to constrain the position of the physical components in the configuration dictated by the optical layout. In addition, the bench design employs adjustable features to allow for the high precision alignment required by the optical performance budget. The alignment process is discussed in detail in the "Optics System Alignment Verification and Validation" section below; the focus of this section will be on the optical bench and the satisfaction of its requirements. The detailed design process of the optical bench was driven by the functional requirements titled Radiometry-1.0 and Bus Compatibility-2.0. The basic dimensions of the current design are 45x45x90mm.

The current optical bench model consists of six main components and can be seen in Fig. 18 below. Each of these components help to satisfy their own list of design requirements. The components include the base bench plate, mirror, aperture plate, photodiode block, alignment shims, and the tooling plate. To better convey the functionality of each of these components as well as how the presented optical bench satisfies its driving requirements, a component by component detailed description is given below.

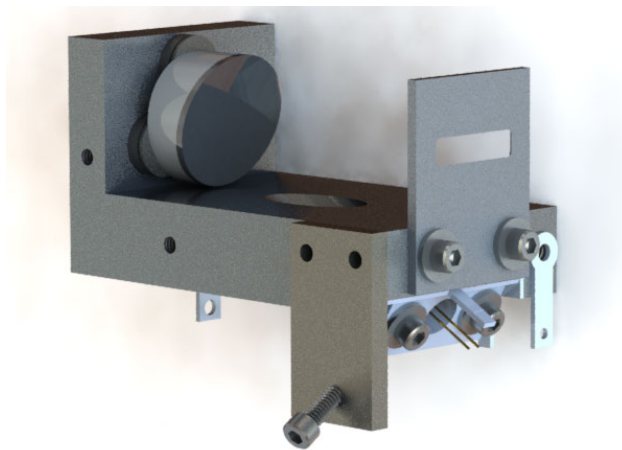


Figure 18. Optical Bench Design

Bench Plate The bench plate design shown in Fig. 19 is the skeleton of the of the optical bench. Each of the remaining 5 components will be integrated into the bench plate in order to constrain the optics' relative positions. The shape of the bench was designed to satisfy the Optical Optical Alignment-1.3, Payload Volume-2.1, and Payload Mass-2.2 requirements. The choice of constructing the bench plate out of aluminum ensured it was light and has the same coefficient of thermal expansion as nearly all other components making up the optical bench. The resulting uniform coefficient of thermal expansion ensured that the Optical Heating-1.3.1.3 design requirement was met. Early design shapes of the bench plate were created based on the geometric relationship between the OAP mirror, aperture plate, and pin hole field stop. Each iteration of these early designs were monitored to ensure the bench plate satisfied the Bus Compatibility-2.0 requirements. Once a draft layout for the optical bench and ergo bench plate was determined, an accurately scaled SolidWorks ray tracing (output from Zemax) was used to virtually align the system for nominal conditions. The integrated Zemax rays and current optical bench design in its nominal condition can be seen in Fig. 20 below. Note that during the manufacturing phase of the bench plate, it was determined that the best method of machining this component was in two separate pieces. These pieces were then mounted together via high precision pins and UNC #6 bolts. See the "Optics Manufacturing" section for an in depth description of the machining process.

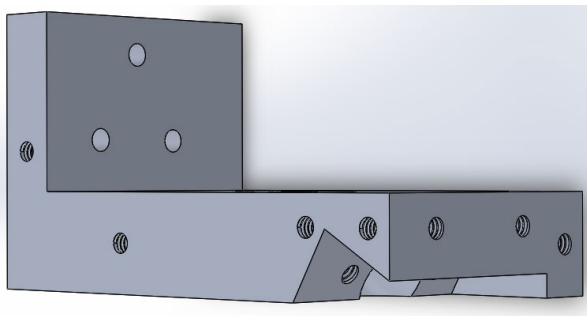


Figure 19. Bench Base Plate

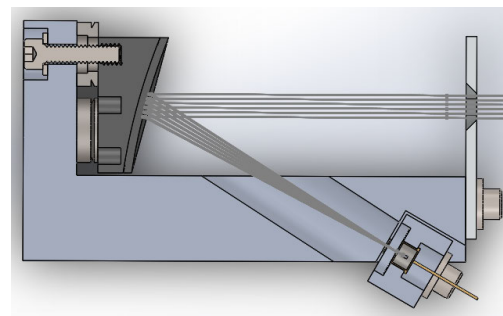


Figure 20. SolidWorks and Zemax Model Integration

The MTF-1.3.1 requirement also had a large influence on the final design of the bench plate. As described in the MTF analysis above failure to align the pinhole and focal point of the mirror within the 45 μm focus error and 30 μm radial error range results in the failure of the MTF-1.3.1 design requirement. As the CNC machines found in the aerospace machine shop are not be able to meet this precision requirement, the need for built in adjustments to correct the inevitable error arose. The effect of the added adjustments on the bench plate is seen at the cavity in which the detector block sits. The three perpendicular faces that make up the cavity are normal to the three optical axes described in Fig. 16. These faces provide a surface to shim against during the alignment phase.

Mirror The Edmund Optics aluminum 30° off-axis parabolic mirror was chosen based on the requirements discussed in the "Analytical Optics Configuration and Performance". The off the shelf mirror from Edmund's comes with three pre-drilled UNC # 6 threaded mounting points spaced 120° apart. These mounting points are used to secure the back of the mirror to the optical bench with three spherical washer sets separating the bench plate and back surface of the mirror.

Aperture Plate The aperture plate design was driven by the Vertical Resolution-1.1 and MTF-1.3.1 design requirements. While studying the performance of the optics, it was determined that an aperture of at least 20 mm along the vertical viewing axis was required to ensure the instrument was capable of collecting radiometric data (Radiometry-1.0). The physical plate was designed with a rectangular clear aperture of 20mm x 5mm with a 1mm radius of curvature in each of the four corners. To meet the MTF-1.3.1 requirement, the clear aperture of the aperture plate must be properly aligned relative to the mirror. To satisfy this requirement the remaining geometry of the plate was designed to include the two mounting points seen at the bottom of the plate. The nominal alignment of the designed aperture plate was verified within SolidWorks using the Zemax ray tracing. It was determined that the aperture plate can be mounted within the machine tolerances reported by the aerospace machine shop without introducing significant degradation in

the optical performance. The plate was manufactured out of 6061 aluminum to ensure it has the same coefficient of thermal expansion as the majority of the optical bench and satisfies the Optical Heating-1.3.1.3 requirement. Figure 21 below shows a rendering of the current aperture plate design.



Figure 21. Aperture Plate

Photodiode Block The functionality of the photodiode block is to constrain the relative position between the pinhole field stop, reflective half sphere, and photodiode, as well as ensure the feasibility of making the high precision alignment needed for the Optical MTF-1.3.1 requirement. A 3D rendering of the current photodiode block can be seen in figure 22. The 10 μm thick field stop plate is placed in the "top" cavity of the block and rests on the top surface of the photodiode canister. It is then tacked from above using epoxy applied at needle point. The lower two selves of the block act as a receptacle for excess epoxy flow. The top most self is used to constrain the position of the reflective convex half sphere alignment tool (see section "Optics System Alignment Verification and Validation - Alignment Tools"). The photodiode, seen in gold in Fig. 22, is inserted into the "bottom" cavity of the block. The clearance fits for the photodiode and reflective half sphere are set based on the ISO System of limits and fits where the diode cavity is machined for a press fit, and the sphere cavity is machined to a free running fit. The photodiode is secured in its position by filling the larger cavity, in which the leads protrude, with a electrically insulated epoxy.

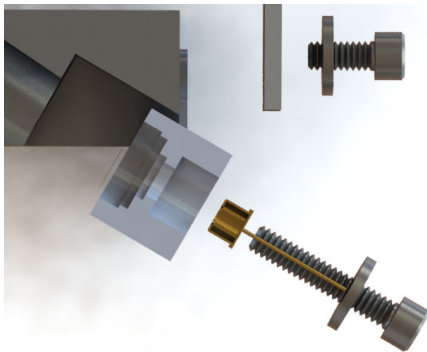


Figure 22. Photodiode Block - Exploded View

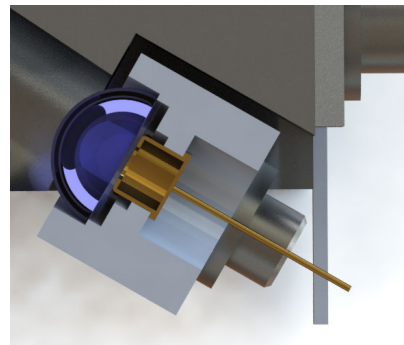


Figure 23. Photodiode Block - W/ Reflective Half Sphere

As stated above the photodiode block constrains the relative positions of the pinhole and photodiode. This design decision was driven by the overall Optical Alignment-1.3 requirement. The relatively small active area of the chosen photodiode requires precise knowledge of the location of the pinhole and ergo the size and location of the light footprint on the active area. The nominal aligned footprint of the light on the active area of the photodiode can be seen in figure 24 below. The highlighted blue point represents the nominal location of the pinhole when secured within the diode block. In order to keep the entire light footprint on the active area, the photodiode block must be capable of constraining the relative position of the pinhole and active area within $\pm 320 \mu\text{m}$ along the out-of-plane axis.

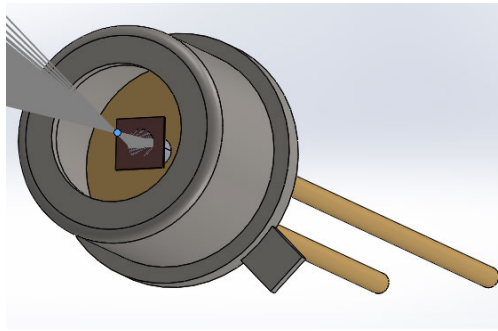


Figure 24. Light Ray Footprint on Active Area

An equally important function of the photodiode block is to work in conjunction with the bench plate to provide shimming surfaces along the optical axes described in Fig. 16. The three faces of the diode block positioned parallel to the bored out faces on the bench plate satisfy this requirement. The through holes in which the two bolts pass through the diode block are over sized in order to leave the block unconstrained along the three shimming axes during alignment. Once the required shim stacks have been implemented on each face, the two bolts can be tightened, and the belville washers on the outward face of the block will lock down the block keeping pressure on the shims. A single corner of the block is chamfered to produce a smooth interface for the tooling plate pressure screw (described below) used during alignment.

Optical Shims As mentioned above, the surfaces on the photodiode block and bench plate normal to the optical axes described in Fig. 16 are intended for use with shims to allow for precise adjustments. Various shim thicknesses were purchased to ensure that the photodiode block can be adjusted to within the allowable error range of $45\ \mu\text{m}$. Specifically, a $25.4\ \mu\text{m} - 254\ \mu\text{m}$ (0.001" - 0.015") shim stock set along with a single sheet of $12.7\ \mu\text{m}$ (0.0005") shim stock will be purchased from McMASTER-CARR. The shim stock were EDM wire cut at the CIRES Integrated Instrument Development Facility to be compatible with the shimming surfaces. Images of the focus, in-plane, and out-of-plane shim designs can be seen in figures 25 - 27 below.

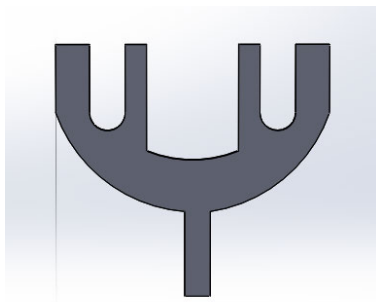


Figure 25. Focus Shims

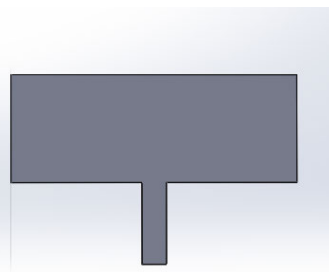


Figure 26. In-plane Shims

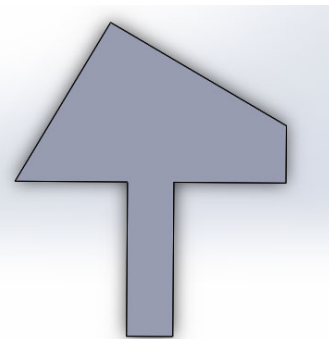


Figure 27. Out-of-plane Shims

Tooling Plate and Screw The functionality of the tooling plate and screw is to apply and release pressure on the shims stacks during the diode block alignment. Because the two bolts that lock down the diode block can only produce pressure on the focus shim stack, a method of creating pressure on the in and out of plane shim stacks was needed. To accomplish this, the tooling plate was designed such that the threaded screw hole is along the axis that connects the corner shared by the shimming faces and the chamfered corner interfacing with the screw on the photodiode block (see Fig. 28). This ensures that tightening the screw will create pressure on all three shim stacks with a majority of

the pressure on the in and out of plane shim stacks. The tooling plate was constructed out of 6061 aluminum alloy and will be removed after the alignment. The screw itself is a stainless steel UNC # 6 socket hex head cap.

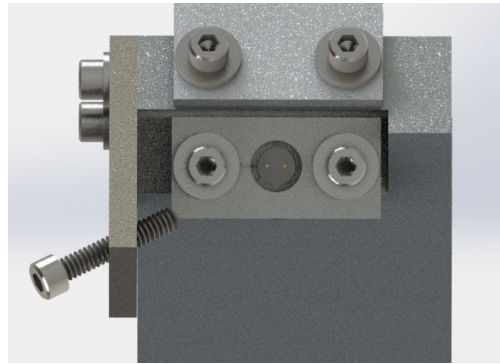


Figure 28. Tooling Plate and Screw

Sighting Tabs The final integration test of the NanoSAM instrument involves mounting the sealed system on a solar tracker and gathering solar irradiance data. With such a narrow FOV, it will be challenging to orient the optics toward the Sun. As a result, a pair of sighting tabs give the user a visual aid during the solar alignment of the instrument. The tabs are mounted on either side of the optical bench along the ideal optical axis of the OAP (see Fig. 18). The terms primary and secondary tab will refer to the tabs nearest to and furthest from the Sun in the aligned position, respectively.

Holes in the each of the tabs allow light to travel along the length of the optical bench. Light passing through the primary tab produces a bright spot in the plane of the secondary tab. A crosshair centered on the hole in the secondary tab casts a shadow that can be seen outside of the enclosure. Aligning these tabs requires centering the crosshair on the bright spot produced by the primary tab. The tabs pivot about points in the plane of the aperture stop. In this plane, these points are slightly offset to allow two axes of adjustment during alignment.

Mounting Hardware In order to maintain consistency across the bench, all of the mounting interfaces use UNC # 6 stainless steel socket hex head cap screws. This screw size and thread type was used by the manufacture at Edmund optics for the three mounting points in the back of the mirror. The aluminum threads in the optical bench have an optimal torque spec of 5.3 in-pounds. The stainless steel Helicoils inserts for the diode block interface have an optimal torque spec of 10.1 in-pounds. Given these torque specifications, the Optical Alignment-1.3 requirement was satisfied and the design was simplified by the use of UNC # 6 screws throughout the system.

In conjunction with the mounting screws, stainless steel UNC # 6 flat washers are used to better distribute the loading at most of the mounting interfaces. There are three interfaces, however, that do not use the standard flat washers. Two being the belville washers used on the diode tube and the sighting tabs (described above), and the third being the three stainless steel M6 spherical washer sets used between the back of the mirror and the bench plate. These spherical washers were chosen to help meet the MTF-1.3.1 requirement. Because the MTF performance of the mirror is reduced by distorting the reflective surface through uneven pressure at the mounting points, spherical washers were implemented to reduce the effect of surface defects present on the back surface of the mirror and on the bench plate. The thermal analysis in the "Analytical Optics Configuration and Performance" section showed that adding these steel washers would not significantly effect the Optical Heating-1.3.1.3 design requirement. Figure 29 below shows an exploded view of the optical bench and how the mounting hardware is used to connect each of the components.

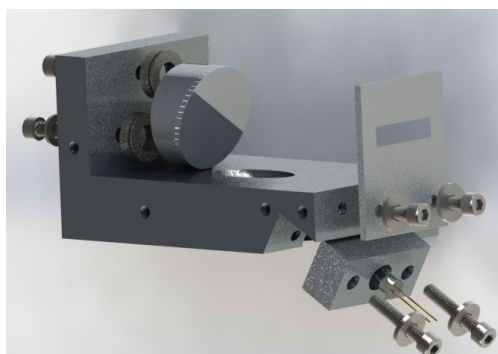


Figure 29. Mounting Hardware

4.3.3. Electronics Baseline Design Overview

From the trade studies, a silicon photodiode, sigma-delta ADC, microcontroller, and flash memory were selected as the components to turn a light signal to electronic signal, sample that electronic signal, move data between ADC and storage, and store data, respectively. All of these components are capable of working together. From the flash chip storage selection, microcontroller selection was narrowed to microcontrollers capable of communicating with flash chips. This was not difficult to meet, as most flash chips communicate over Serial Peripheral Interface (SPI), and most microcontrollers are capable of acting as a SPI master. To simplify things further, many ADCs also use SPI to communicate. The ADC must send data to the microcontroller at a sample rate of 50 Hz. With a 16 bit ADC, this is 800 bits/seconds. SPI is capable of carrying up to 10,000,000 bits/second, so it will be trivial to not only read from the ADC, but store readings between samples.

4.3.4. Electronics Detailed Design

The NanoSAM electronics system is responsible for measuring and recording irradiance data collected by NanoSAM. As discussed in the conceptual design section, this is accomplished with a silicon photodiode, an ADC, a microcontroller, and flash memory chips. These are organized as seen in the electronics block diagram (Fig. 30). This system must meet the design requirements 1.4, 1.5, 3.1.1, 3.1.2, 3.2.1, 3.3.1, and 3.5. The corresponding requirements titles are SNR, dynamic range, sampling rate, resolution, data storage size, external communication, and power draw, respectively. The baseline design for the electronics system will, as a result, also meet the critical project element E.3.

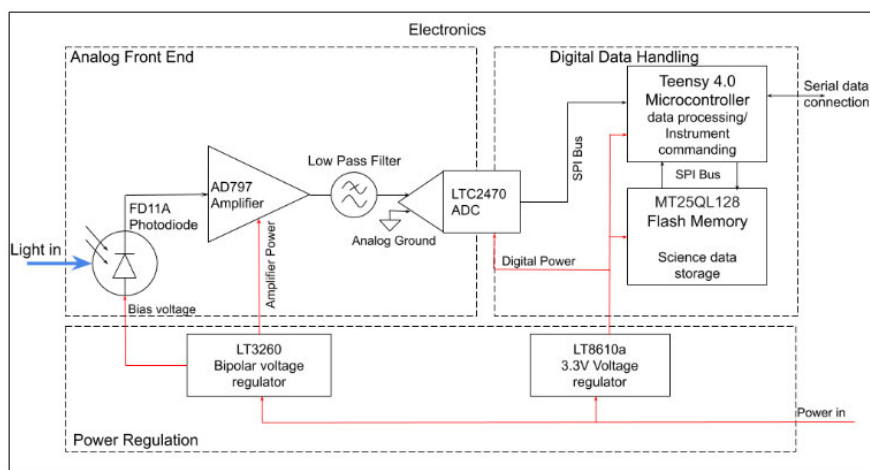


Figure 30. Electronics Block Diagram

Analog Electronics

The analog electronics design considerations include requirements for SNR, dynamic range, sampling rate and resolution. These requirements were considered when selecting components for the analog circuit. The primary concern among these requirements was the noise produced. The primary components included in this analog circuit are the photodiode, the transimpedance amplifier, and the analog to digital converter. These are arranged as seen in Fig. 31. The photodiode allows current through it proportional to the light incident on the active area. This current is measured by the transimpedance amplifier and converted to an analog voltage signal. This voltage is sampled by the analog to digital converter.

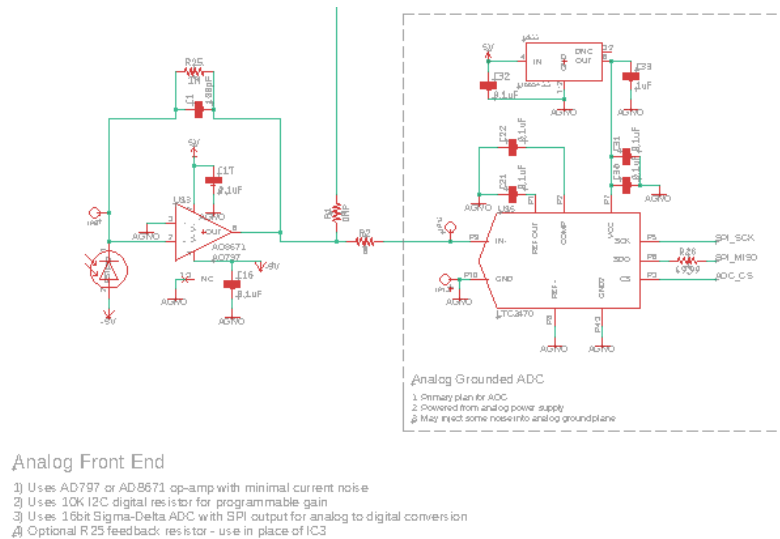


Figure 31. Analog electronics schematic

a. Photodiode The photodiode selected is the ThorLabs FD11A. This photodiode boasts an extremely low dark current, which helps as it is proportional to the dark noise. Additionally it has a low capacitance and low series resistance, although these are less critical factors, as we are not measuring a high speed signal, or a signal large enough to saturate the photodiode. Additionally this photodiode has a responsivity of .45 A/W at 1020nm. This is important as the photodiode must be able to detect light in the wavelength we are interested in.

The requirements affected by photodiode selection are the signal to noise and dynamic range requirements. If the dark noise is sufficiently large, it could drive down the signal to noise ratio. If the photodiode saturates too early, the dynamic range is impacted. The noise is proportional to the dark current, this is further explored in the SNR section of this report. The saturation is determined by the series resistance and bias voltage of the photodiode. Assuming a 50Ω series resistance and our expected signal, the required bias voltage is only $10\mu V$. This shows that with a 5V bias voltage, we will not saturate the photodiode.

b. Transimpedance Amplifier This project will use the AD8671 transimpedance amplifier produced by Analog Devices. While options with lower noise exist, this op-amp has an extremely low input current. This is important as the input current of the op-amp affects the accuracy of the readings of the photodiode current. The op-amp is powered by the $\pm 5V$ analog power supply and has a large enough power supply rejection ratio that noise from the power supply is not a concern.

The gain for this amplifier is controlled by a feedback resistor (R25 in Fig. 31). This resistor is currently sized to $1M\Omega$. This is based off of the expected current through the photodiode when receiving unattenuated sunlight through the current optical aperture and filters. It is sized such that this signal corresponds to 80% of the ADCs full range. This means that the dynamic range requirement is satisfied by this design. Similar to the op-amp itself, this feedback

resistor can easily be replaced during testing if a different gain value is desired.

To remove high frequency noise from the signal, capacitor C1 serves to create a low-pass filter with resistor R25. As the signal we expect to be measuring should never exceed 32 Hz, it is sized such that this filter has a corner frequency of 32.24 Hz. Again, it is trivial to replace this capacitor if a different corner frequency is desired. This helps reject any high frequency noise that might enter our system.

c. Analog-to-digital converter The analog to digital converter selected for this project is the LTC2470. This is a 16 bit, sigma delta, single ended or differential input ADC. The differential nature of this ADC allows for it to sink its current into either the analog or digital ground planes while still sampling relative to the analog ground plane. Footprint locations for both options have been included in the printed circuit board design for either option, allowing for the test of both configurations. The advantage of having the ADC on the analog ground plane is that there is significantly less noise on the reference voltage ground. This would be somewhat compensated for by the fact that both the signal and analog ground are sampled, theoretically removing any noise present in the digital ground. However, exactly how well this works remains to be seen. However, having the ADC on the analog ground would inject some amounts of noise from the serial lines connecting it to the digital electronics into the analog ground plane. This may or may not prove to be a significant issue.

The requirements associated with the ADC are the resolution and sampling rate requirements. The 16 bits the ADC has exceed the 10-bit requirement, and the LTC2470 is capable of sampling at 208Hz. We will either only keep every third sample or average every three samples to bring that down to the 50 Hz requirement, depending on the noise of the real system. Taking every third sample is marginally simpler, but averaging every three samples allows us to increase the SNR.

Digital Electronics

The digital portion of the electronics components consist of the microcontroller and flash memory. These are connected to each other and the ADC via SPI bus. The digital components are responsible for satisfying requirements for the data storage size and external communication. The digital electronics consist of a microcontroller and flash memory chips. The digital portion of the schematic can be seen in Fig. 32.

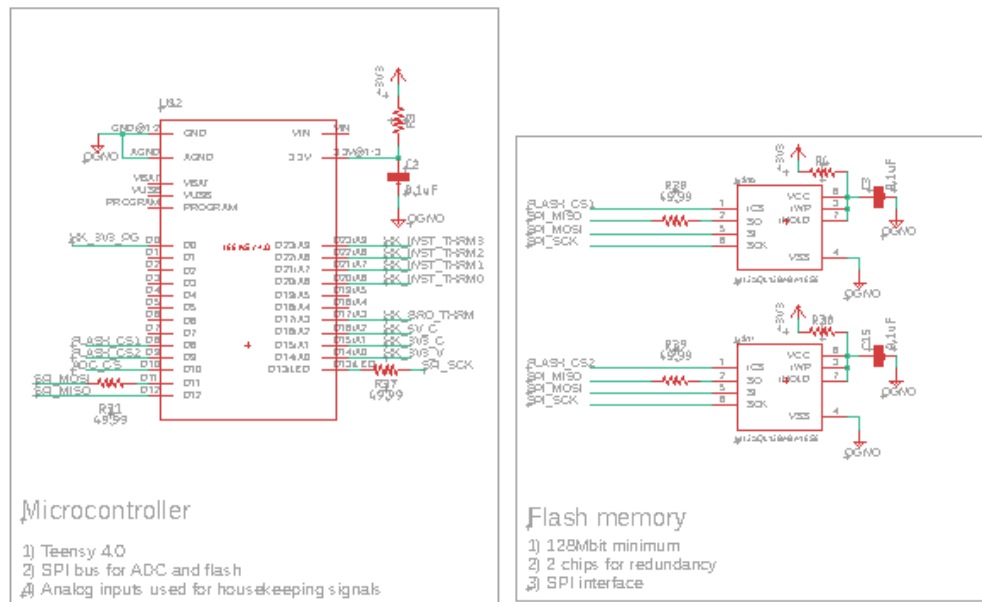


Figure 32. Digital electronics schematic

d. Microcontroller The microcontroller is responsible for retrieving data from the ADC, storing it in flash memory, and sending it to a connected PC. To satisfy requirement 3.3.1 it must be capable of outputting serial data to an external computer. In order to satisfy requirement 3.1.1, it must be able to read and write over SPI sufficiently fast to store the data from the ADC. The Teensy4.0 was selected as the microcontroller for this project, as it supports multiple SPI busses, is sufficiently fast, and can communicate over USB. This microcontroller is based around an ARM Cortex-M7 processor running at 600MHz. The Teensy has 1024Kb of RAM and 2048Kb of flash memory on board. Additionally it has two on board ADCs, each with seven channels. These ADCs will be used for housekeeping measurements. It also has an on board real-time clock. This will be useful for time-stamping data.

e. Flash Memory The electronics must be capable of storing two days worth of on orbit measurements to satisfy requirement 3.2.1. Using our 500km reference orbit, it was found that the NanoSAM satellite could be expected to observe 30 events per day. Each event is assumed to last at most 10 minutes. With a 50 Hz sampling rate, this amounts to 900,000 samples per day. With 16 bits for the ADC data and 32 bits for the timestamp, and holding enough data for two days, the total required data is 86.4 Mb. The flash chip selected is the Micron Technology MT25QL128ABA1ESE. It is a 128 Mb SPI flash chip. The electronics design includes two of them for redundancy.

Power Electronics

The power electronics are responsible for providing power to the analog and digital circuits, as well as ensuring that there is sufficiently low noise on the analog power lines. To ensure this, there are two separate power regulators on the circuit board, a 3.3V 2.5A switching regulator that provides power for the digital electronics where noise is much less of a concern, and a low noise dual supply inverting charge pump for the analog electronics. The requirement associated with the power electronics is requirement 3.5, that the instrument will not draw more than 4.5 W. The power electronics schematic can be seen in Fig. 33.

f. Analog Power Regulator The analog electronics are powered from an LTC3260. This is an adjustable dual supply with low noise linear regulators on its output. It can supply up to 50 mA on each output, which is sufficient for powering the analog circuit. It will be configured to supply positive and negative 5V, however this is adjustable with replaceable resistors. The datasheet for this part lists up to $100 \mu V_{rms}$ noise on each of the linearly regulated outputs, this is sufficiently low for the electronics, as shown in the signal to noise ratio section. Careful board layout is necessary when using this part. This is explored further in the circuit board considerations section.

g. Digital Power Regulator The digital electronics do not have strict requirements on noise, however they draw a lot more power than the analog electronics. Because of this, and LT8610 was selected as the power supply. This device supplies 3.3 V and up to 2.5 A, which is more than sufficient for the current draw of the digital electronics. Like the analog power supply, this device also requires care be taken during layout. This is also covered in the circuit board layout discussion.

h. Power Budget Requirement 3.5 states that the instrument electronics will not draw more than 4.5 W of power. Upon analysis, our electronics are expected to draw only 0.8 W of power. This analysis was done as a worst-case power draw. The maximum current draw from the data sheet for each part was multiplied by the input voltage to get the power drawn for each part. All the analog power draws were added together to find the power draw on the analog power supply. The quiescent current of the power supply times the input voltage was added to this power draw. A similar process was undertaken for the digital components. Each part had its power and current draw calculated and summed. This total current draw was used to find the efficiency of the digital regulator at that current draw. That efficiency was used to find the total power consumed by the digital electronics. These two powers were added to find the total electronics power draw. The power drawn by each component can be seen in Fig. 34. It can be noted that although the analog electronics require much less power, the power draw for the analog power supply is much higher. This is due to the significantly lower efficiency of the analog power supply.

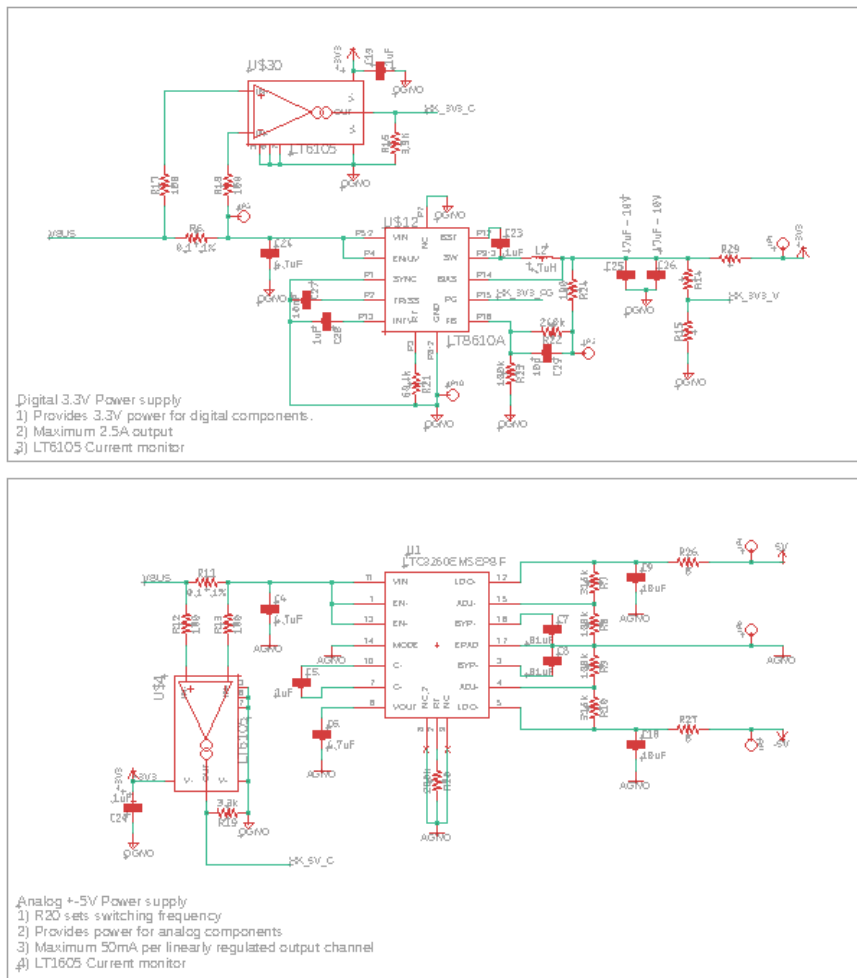


Figure 33. Power electronics schematic

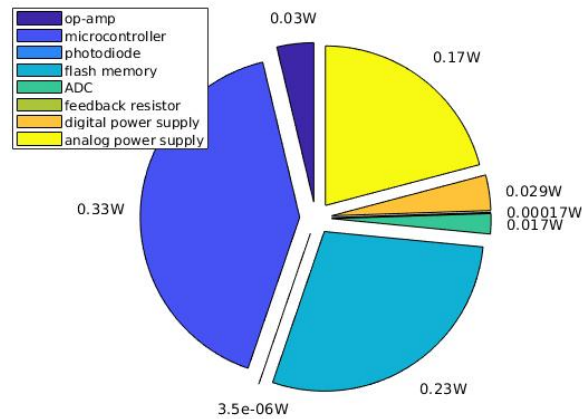


Figure 34. Power usage by component

These power electronics represent a small risk to the overall success of the mission as they create unexpected noise that will affect the SNR. Methods used to mitigate this risk is discussed in "Risk Assessment", section 8.

Circuit Board Considerations

All the electronic components (with the exception of the photodiode) are mounted to a single four layer PC104 printed circuit board. This board will be mounted underneath the optical bench. There is a cutout at the front of the board to allow for cable routing and connections on the instrument enclosure.

i. Ground Planes In order to minimize noise on the analog electronics, separate digital and analog ground planes were used. The ground planes are connected near the board's power connector. This is known as the "ground star point" and is typically the point where all grounds connect. Using this technique prevents most of the noise associated with digital electronics and communication from affecting our measurements. Figure 35 shows the ground planes. Additionally, there is a 3.3 V digital power plane on the digital half of the board. This was done mostly to simplify routing.

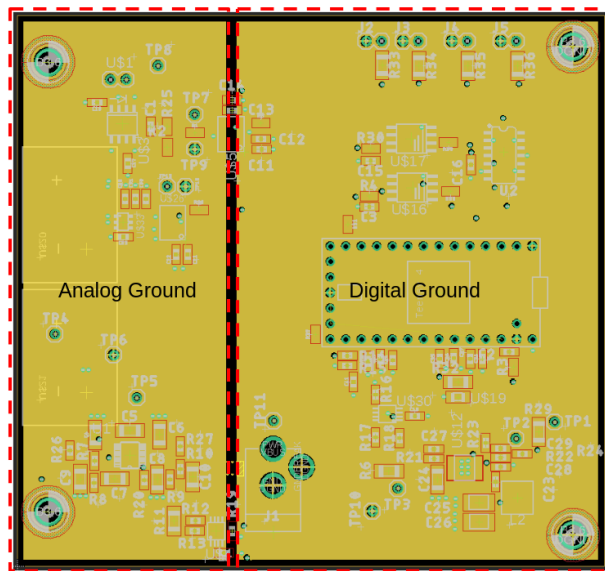


Figure 35. Analog and digital ground planes. Star connection point not shown.

j. SPI Bus Routing With four nodes on the SPI bus (two flash chips, the ADC, and the teensy), care must be taken to maintain signal integrity. All traces for this bus are on the same layer and are directly above an uninterrupted ground plane. Each signal is series terminated for $50\ \Omega$ of resistance. Series termination consists of placing a certain resistance at the source for a serial signal. This helps prevent the drivers from receiving reflected signals and damps overshoot. An example of a series terminated network can be seen in Fig. 36.

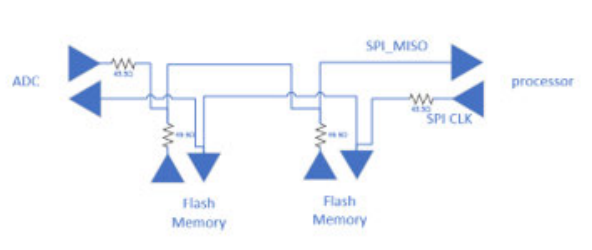


Figure 36. Series termination on a SPI bus

k. Power components layout The power components required the most thought in the layout. The datasheets for both components listed specific layout patterns that were followed. A comparison of the datasheet and implemented

Signal-to-Noise Model

Noise Sources	[e ⁻ /s]
Shot Noise	7358 x 10 ⁵
Dark Noise (Dark Current)	7900 x 10 ³
Quantization Noise	6.822 x 10 ⁶
Transimpedance Amplifier Noise	2.903 x 10 ⁴
Power Supply Noise	2.020 x 10 ¹

Figure 39. Summary: Contributions to Noise

The noise terms contributing to the SNR model accounting for a 16-bit ADC, an ADC margin of 20%, and an estimated photocurrent of $S = 0.207\mu\text{A}$ are given in a table in Fig.39. This calculation is accurate to the current design and results in an SNR of 3.258×10^5 . The calculated SNR gives a 9000% margin when compared to requirement 1.4 of 3500 SNR. It is important to note that a 12-bit ADC would meet the requirement with a margin of 477% with an SNR of 2.048×10^4 . However, the current design implements a 16-bit ADC with large margin for any complications and with no strain to other design constraints. The detailed calculation and derivation of the complete SNR model is documented in Appendix B.

4.3.5. Structural Baseline Design Overview

There were no formal trade studies completed for structural design options. The NanoSAM structure was designed after the Preliminary Design Review. It includes a plate module system to securely mount the optics unit, and an opaque solid enclosure to shield the optics unit from dust and light exposure outside the required bandwidth. The plate module system and enclosure model are shown below in Figures 40, and 41.

The primary purpose of the NanoSAM structural design is to integrate the optical and electronic sub-systems, verify that the instrument can be assembled in a 1U cross-section, and provide a housing for the system during testing. Section 5.5.1 Opto-mechanical Integration provides a detailed description of how the optics system integrates with the structural system. This includes the integration of the optical bench, plate module system, and enclosure.

The NanoSAM plate module system is held together by four threaded stainless steel rods, a collection of aluminum spacers and washers, and lock nuts on each end of the rods. The top plate module serves as a handle for transportation, the two G10 fiberglass plates serve as a mounting system for the optics unit, and the bottom plate is the printed circuit board with identical dimensions. The NanoSAM enclosure is built from an aluminum square tube, two removable plates on either side of the tube, and extrusions for the filter mount and electronics port. A more detailed description of the structural design is presented in Section 5.1 Structural Manufacturing, and Section 5.5 Integration of Parts.

4.3.6. Structural Detailed Design

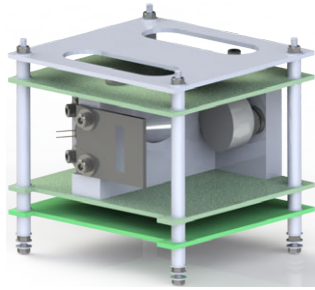


Figure 40. NanoSAM Plate Module System

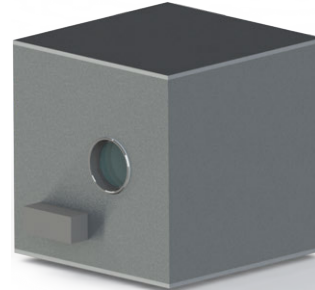


Figure 41. NanoSAM Enclosure

4.3.7. Software Baseline Design Overview

The NanoSAM software subsystem is responsible for the capture, storage, and transmission of irradiance data. The software consists of programming a Teensy 4.0 microcontroller with a C++ script using the PlatformIO IDE. As a result of our trade studies, the Teensy 4.0 microcontroller was selected as the best microcontroller due to its compact and powerful build. The Teensy 4.0 is best programmed with C++ given the ease of controlling the many digital I/O pins and interfaces that it offers. The PlatformIO IDE was selected to interface with and upload the code to the microcontroller due to its simple operation and the ability to operate on both MacOS and Windows computers.

4.3.8. Software Detailed Design

The NanoSAM software will receive a digital signal for the photodiode voltage from the built-in ADC on the Teensy 4.0. This digital signal will be in the form of a 12-bit binary number that represents the quantized photodiode voltage. The Teensy 4.0 will receive these signals at a sampling rate of 50 Hz. After receiving the digital signal, the Teensy 4.0 will then do a simple if-statement check to see if the digital signal is greater than the solar threshold value from the full integration test. Based on the output of the if-statement check, it will be known whether the Sun is in the FOV or not. If the digital signal is greater than the solar threshold value, the ADC will continue to be sampled and this if-statement check will continue checking the condition. If the photodiode voltage drops below the solar threshold value, the software script will break the data capture loop and data will cease to be collected. This if-statement check is necessary to fulfill requirement 3.1.3 for termination of data capture. In addition to performing this check, the Teensy 4.0 will take the digital signal and append a timestamp to it using a counter from the moment the software starts data capture. This will provide NanoSAM with accurate date/time of the digital photodiode voltage for post-processing. After the timestamp is added, the data will be packetized by adding start, stop, and parity bits in order to send the signal through serial transmission. By packetizing the data, design requirement 3.2 will be satisfied. From here, the Teensy 4.0 will both transmit and save this data. The data will be transmitted through a USB connection to a team member's laptop for real-time data checking during the integration testing. This USB connection to output the data to a laptop satisfies requirement 3.3.1 for the data output method. The Teensy 4.0 will also save the data through an SPI connection with the two Micron Technology MT25QL128ABA1ESE flash memory chips on the custom PCB. This storage of data on-board satisfies design requirement 3.2.1 regarding data storage. This overall software subsystem will be capable of data capture, storage, and output. Thus, this subsystem will fulfill the over-arching software design requirement 3.4 regarding the necessity of software for this project.

4.4. Critical Project Elements

After multiple trade studies, narrowing all the design alternatives to one solution can be challenging without knowing if the adopted decision will be able to meet the project purpose and requirements. Therefore, a list of

critical project elements were determined to ensure the design will meet any one of the specific objectives, ensuring the project's success. The list below presents the project elements that are critical to the overall success.

- E.1 Radiometer detects and measures solar irradiance in a narrow near-infrared band.
- E.2 The optical instrument aligns with the pinhole field stop so the specified wavelength of light can reach the detector for accurate measurements.
- E.3 The instrument SNR and sample rate are the same as SAM-II or better.
- E.4 The instrument field-of-view facilitates a vertical resolution of 1 km or less.
- E.5 When the detector stays within its operating temperature, the baseline measurements remain stable over the duration of data collection for the collected data to remain accurate.

Recall that the main purpose of NanoSAM is to be capable profiling stratospheric aerosols in the future while performing better than previous instruments. Since the particles can be detected in a narrow near-infrared band, the radiometer that will be constructed this year must be able to detect and measure solar irradiance. The next element regarding the alignment of the optical instrument is significant in the success of the project. With a pinhole field stop of only 15 micrometers, the light entering the filters of the payload must align within the specified tolerance of the photodetector to collect irradiance data. In addition, the SNR and sample rate of NanoSAM must at least meet or exceed the values of its predecessor, SAM-II, to achieve better data density. Similarly, the FOV element was inherited and should be better than SAM-II as well. Finally, the baseline measurements before or after solar irradiance measurements will need to be stable during its operating temperature so that the data collected is repeatable throughout tests and experiments. As a result, the accuracy of the data can be presented with confidence.

To summarize, if any of the critical project elements are not met, certain requirements and specific objectives will not be met, resulting in a failed project. Therefore, the detailed designs of the electronics, optics, mechanical, and software subsystems in the preceding subsections were chosen to ensure that the critical project elements will be met.

5. Manufacturing

Aanshi Panchal, Josh Horst, Matt Weber, Jared Cantilina, Jacob Romero

This section will detail the manufacturing of our project for all of our major subsystems. This project is manufacturing heavy, because the parts are unique and the majority of the allotted budget was assigned to optical and electronic components. Before the project was halted, the manufacturing phase was complete however the final integration was not complete.

5.1. Structural Manufacturing

The structural parts manufactured and purchased are succinctly described below in Table 3.

Manufactured	Enclosure Tube, Enclosure Plates, Plate Handle, Fiberglass Optical Plate Mounts
Purchased	Rods, Spacers, Nuts, Screws Washers

Table 3. Manufactured and Purchased Structural Parts

5.1.1. Structural Parts Manufactured

Below is a list of the structural parts that were manufactured in the Aerospace Engineering Machine Shop.

1. **Enclosure Tube:** The Enclosure Tube was manufactured from a stock 10 x 10 cm 6060 aluminum square tube. It was initially cut with the horizontal band saw, then faced off with the manual milling machine, and further manufactured with the CNC milling machine as in Figure 42. Large vice grips were used to reduce vibration during the milling process. The optical filter mounting hole, and sighting window were then hand-tapped with a specialty SM1 optical thread tap, and a 3/8" BSPP pipe tap. Lastly, the four clearance holes corresponding to the Enclosure Plate tap locations were counter sunk with a deburring tool.
2. **Enclosure Plates:** The Enclosure Plates were manufactured from a stock 1/4" 6061 aluminum plate. The internal face of the plate was profiled with the CNC milling machine, and the bottom Enclosure Plate's M3 clearance holes were drilled, shown in Figure 43. The tap holes corresponding to the four clearance holes on the Enclosure Tube were drilled by fitting the Enclosure Plates onto the Enclosure Tube, and carefully hand milling through the clearance holes. The holes were then hand-tapped with a #1-64 tap.
3. **Plate Handle:** The Plate Handle was manufactured from a stock 3 mm 6061 aluminum plate and cut with the Wazer Waterjet cutter. It is shown in Figure 43.
4. **Fiberglass Optical Plate Mounts:** The Optical Plate Mounts were manufactured from G10 fiberglass plates and cut with the Wazer Waterjet cutter. They are shown in Figure 43.



Figure 42. Enclosure Tube with Plates

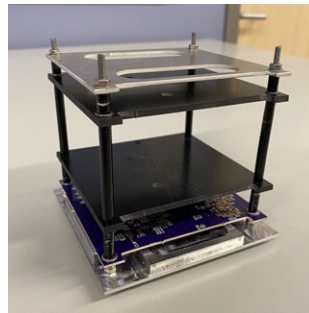


Figure 43. Plate Module Assembly



Figure 44. Plate Module Assembly within Enclosure

5.1.2. Structural Parts Purchased

The rods, spacers, nuts, and washers were purchased from a third-party supplier with specifications congruent with a 1U CubeSat model from Pumpkin Space Systems. The #1-64 screws were also purchased from a third-party supplier.

5.2. Optics Manufacturing

The optical parts manufactured and purchased are succinctly described below in Table 4.

Manufactured	Diode Block, Optical Bench, Aperture Stop, Optical Shims, Tooling Plate, Sighting Tabs
Purchased	Off-Axis Parabolic Mirror, Filters, Filter Mount

Table 4. Manufactured and Purchased Optics Parts

5.2.1. Optical Parts Made

Below is a list of the optical parts that were made in the Aerospace Engineering Machine Shop. The primary challenge in optical manufacturing for this project is ensuring that the parts were made to the required tight tolerances because the performance of the system relies heavily on the manufacturing precision. These concerns were overcome

by creating a detailed manufacturing plan and reviewing it with Matt Rhode, the lead manufacturer of the Aerospace Engineering Machine Shop. In doing so, many foreseeable problems were solved before manufacturing commenced.

1. **Diode Block:** The diode block was manufactured from a stock 4" x 4" 6061 aluminum block. First, the stock material was cut with the vertical band saw, and faced to ensure that both sides were flat and parallel. Then, using brand-new end mill bits, the CNC machine ran the compiled G-code and made the hole that holds the Alignment Sphere, the Field Stop, the Field Stop glue deposit, and the Photodiode. Using precision pins, these holes were measured to the order of 0.001" (or about $25.4\mu\text{m}$) to verify that the holes were within their respective tolerances ($\pm 25\mu\text{m}$ for the Field Stop hole and $\pm 50\mu\text{m}$ for the Alignment Sphere hole.). If the tolerances were not met due to the hole being too small, the G-code was modified to cut an additional 0.001" in diameter to drive the hole to the required tolerance. Next, the CNC machine was used to shape the body of the diode block, and the stock material around the block was cut with the vertical band saw. After that, all excess material was shaved off to dimension with a manual mill. Finally, the diode block goes back into the CNC machine to pocket out the hole that the photodiode leads protrude out of.

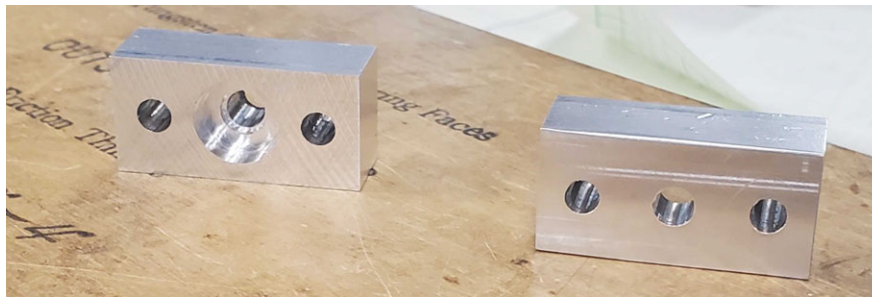


Figure 45. Manufactured Diode Block

2. **Optical Bench:** The Optical Bench was manufactured from a stock 4 x 4" 6061 aluminum block, and its manufacturing process may be split into three phases I, II, and III.

- I First, the two blocks corresponding to the base and body of the Optical Bench were cut with the horizontal and vertical band saw, faced on each side, and precisely cut to dimension on the top and bottom faces. Then, using a common origin point, the clearance and tap holes on both attachment faces were milled, and the 1/8" pin holes were reamed. Next, the clearance holes on the external side of the base block were counter-bored. After the body block's holes were tapped and the pins inserted, the two separate blocks were mounted together by #6-32 bolts to become one solid piece.
- II The Optical Bench now appears as Figure 46. Then, the block is precisely cut to dimension on each face, and the various #6-32 tap holes were drilled using the CNC milling machine. Lastly, the L-shaped portion is milled as an open pocket, as in Figure 47.
- III After the combined block is L-shaped and precisely cut to tolerance, the two pieces were dismounted. Next, the diode block cavity was cut at a thirty degree angle using a sine bar and the manual milling machine. Then, the angled through-hole was cut using a progressively larger drill bit up to the final 1/2" bit, and finished with a 1/2" end mill. Next, the diode block tap holes were drilled according to #6-32 helicoil tap specifications, and the two blocks were reconnected. Finally, the the holes were tapped and the #6-32 helicoils were inserted with a helicoil insert tool. The final Optical Bench is presented in Figure 48.



Figure 46. Optical Bench Phase 1

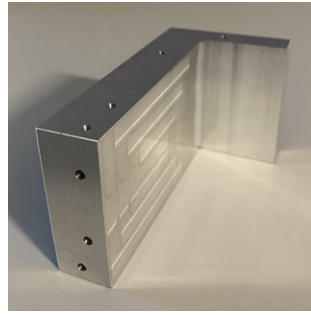


Figure 47. Optical Bench Phase 2

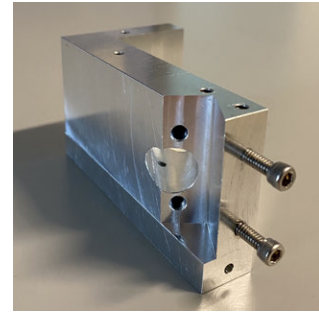


Figure 48. Optical Bench Phase 3

- Aperture Stop:** The Aperture Stop was made with a stock 3 mm 6061 aluminum plate. First, the stock material was faced off and cut to dimension with a vertical band saw and a manual mill. Then, the manual mill was loaded with G-code to position the mill in the correct location as the drill was lowered manually to drill the clearance holes that fix the Aperture Stop to the Optical Bench. Then, the drill is manually exchanged for an end mill and lowered manually to cut out the rectangle. Finally, a 0.25" chamber drill bit was used to create the chamber that goes around the rectangular pocket to limit scattered light from going into the optical system.

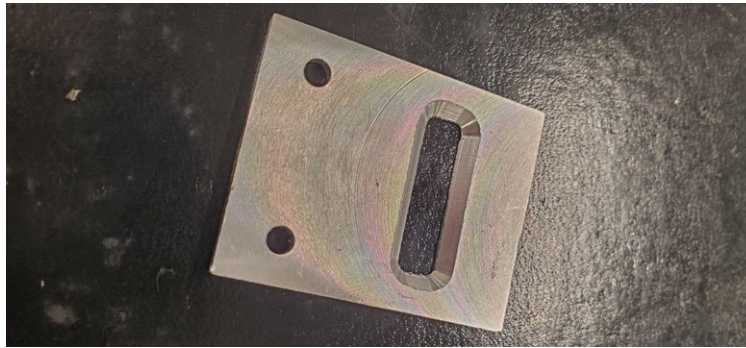


Figure 49. Manufactured Aperture Stop

- Optical Shims:** The optical shims were manufactured from aluminum of varying thicknesses ranging from 0.0005 to 0.015 inches ($12.7\ \mu\text{m}$ - $254\ \mu\text{m}$). The different shim sizes are necessary to achieve the required alignment precision when performing the shimming process. With the help of Nathan Showalt from Ball Aerospace, the team was able to design three unique shim shapes for each of the three shimming faces in SolidWorks. Utilizing the CIRES Integrated Instrument Development Facility, the team was able to manufacture the requisite number of shims needed to perform the alignment.



Figure 50. Manufactured Optical Shims

5. **Tooling Plate:** The Tooling Plate was manufactured from a stock 4 x 4" 6061 aluminum block. First, the block was cut into a thin plate with the horizontal band saw. Then, the plate cut to the approximate dimensions with the vertical band saw, and faced on each side to its exact dimensions. Next, the block was milled at a forty-five degree angle using the sine bar at the approximate location of the tap hole. The clearance holes of the Tooling Plate were then empirically marked with a sharpie, and drilled with the manual milling machine. Finally, the angled tap hole was threaded and the steel helicoil was inserted.



Figure 51. Manufactured Tooling Plate View 1



Figure 52. Manufactured Tooling Plate View 2

6. **Sighting Tabs:** The Sighting Tabs were manufactured from a stock 1/16" 6061 aluminum plate, and cut with the Wazer Waterjet cutter.



Figure 53. Manufactured Sighting Tabs

5.2.2. Optical Parts Purchased

The Aluminum and Gold off-axis parabolic mirrors were purchased from Edmund Optics. The 15 μ m precision pinhole and precision half-sphere (NBK-7) were also purchased from Edmund Optics. The two optical filters were purchased from ThorLabs.

5.3. Electronics Manufacturing

The NanoSAM electronics circuit board was originally manufactured by JLCPCB. Upon arrival, a design flaw was found where the analog and digital ground planes were not connected. Because the ground plane was an internal layer, this could not be fixed after manufacture. New boards with this issue fixed were ordered from OSHPark due to their faster delivery time. These boards were used in the final NanoSAM electronics system.

Off the shelf components from DigiKey were ordered, and a stencil for the PCB was purchased from JLCPCB to aid in the assembly process. The electronics system was assembled at the ITLL Advanced Electronics Center. Solder paste was applied to the PCB pads using the JLCPCB stencil. Components were placed by hand, and the solder was flowed in a reflow oven. The resistance between the power planes and the ground plane was measured to ensure no shorts were formed.

5.4. Software Manufacturing

There are no physical parts of the software subsystem that were manufactured by team NanoSAM. However, the Teensy 4.0 microcontroller was purchased from SparkFun Electronics as well as a Teensy header kit necessary for integration with the PCB. The first iteration of the integrated PCB included female headers soldered into the PCB while male header pins soldered into the Teensy allowed for the easy removal of the Teensy from the PCB for testing and storage purposes. The final integration of the PCB consisted of the male header pins on the Teensy soldered directly into the final PCB negating the need for female headers on the PCB.

The software manufactured for NanoSAM included many functionalities necessary for the success of this project. The first of which is the SPI transaction between the ADC and the Teensy. The SPI interface used the SPI Arduino library to allow the Teensy to be the master and the ADC to be the slave. The SPI library is necessary for the Teensy to gather data from the ADC and without which, the project would fail to achieve its purpose. The second main functionality of the software is the Serial Flash function that allows for data storage. The SerialFlash library is necessary for the communication between the Teensy and the NOR flash memory chips on the PCB. Functions within the SerialFlash library allow for the serial communication of digital photodiode data from the Teensy to the memory chips. Without this library and functionality, the project would critically fail because data storage is an integral part of NanoSAM's success. The third and final main functionality of the software for NanoSAM is the serial connection between the laptop computer and the Teensy. Although this requires an external piece of equipment, namely a micro-USB to USB 3.0 cable, the software needs to be able to serial print data to the serial monitor on the laptop. Being able to read the data from the Teensy in real-time allows for testing and verification of functioning software elements. For this reason, a serial connection and serial printing is necessary for the software subsystem and is considered a main functionality of the software and an important part of the success of this project.

5.5. Integration of Parts

5.5.1. Opto-Mechanical Integration

Opto-mechanical integration is the process of unifying the optical and structural sub-systems. After the diode block is aligned and fixed to the optical bench, as outlined in Section 6.1.2, the aperture stop is bolted and the tooling plate is removed. Figures 54, 55, 56, and 57 show the optical bench with the diode block and aperture stop mounted.



Figure 54. Optical Bench View 1 Figure 55. Optical Bench View 2 Figure 56. Optical Bench View 3 Figure 57. Optical Bench View 4

The optics system including the Optical Bench, Diode Block, Aperture Stop, and OAP mirror was intended to mount within the plate module assembly which was to be mounted within the CubeSat enclosure. Due to the project being halted, this did not occur, however, an example of how this may look is presented in the following Figures 59, 58, and 60.

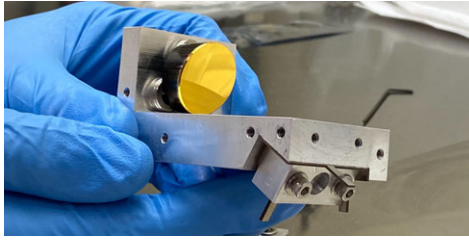


Figure 58. Optical Bench System

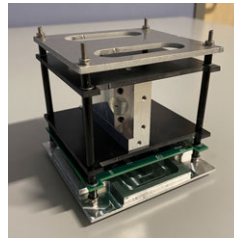


Figure 59. Plate Module Assembly



Figure 60. Aperture Stop and Filter Alignment View

The optics system is mountable to the plate module assembly by three #6-32 screws on its top and bottom faces. The plate module assembly is mounted to the Enclosure Plate by four nylon-insert lock nuts, and the Enclosure Plates are secured with four #1-64 screws. It is imperative that the Aperture Stop is aligned to the optical filter mount, as seen in Figure 60, to maximize the light through the system. The sighting window must also be aligned within tolerance so that the sighting tabs are visible. After alignment is verified, the optical filters were to be installed and opto-mechanical integration would be complete however our project before this could occur.

5.5.2. Electronics Integration

Figure 61 below shows the fully integrated electronics and software in NanoSAM's PCB. This figure depicts the necessary electronics components on the PCB, namely the digital power supply voltage, flash memory chips, transimpedance amplifier, analog power supply voltage, and the resistors and capacitors necessary for the circuitry to function properly. The software components included in this figure are the Teensy 4.0 with headers and the micro-USB cable to connect the Teensy to a laptop computer for testing. Figure 62 shows how the PCB is integrated in the plate module assembly.

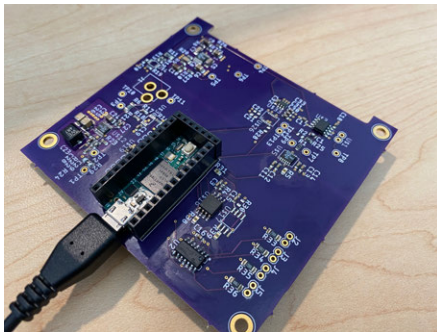


Figure 61. Fully Integrated Software & Electronics PCB

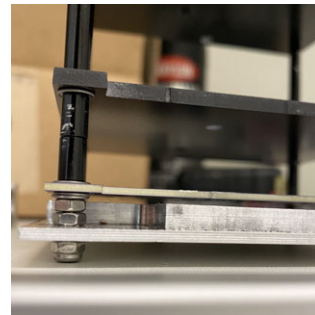


Figure 62. Electronics PCB Mechanical Integration

This electronics/software integration would have then been integrated with the optical and structural for our final integration test (Figure 40 and 41). Note that this includes that the electronics PCB board would be connected to the 9 Port Sub-D connection port that is placed on the rectangular enclosure tube, and the photodiode that is attached to the diode block in the optical bench is connected to the PCB so any gathered analog would be processed by the transimpedance amplifier and the ADC, which could then be processed by the software that is loaded into the Teensy microcontroller.

6. Verification & Validation

Jared Cantilina, Jaykob Velasquez, Conner McLeod, Sara Reitz, Quinn LaBarge, Jacob Romero, Jessica Harris

This section will detail the verification approaches and the corresponding equipment and logistics that are necessary to verify the design and functional requirements. It also details how the selected design will be validated. Below, in Figs. 99 and 100 the project test plan is shown. This matrix details how each project requirement is going to be verified, the necessary support equipment, and the data collected from these tests. The tests described in the test plan are smaller scale tests that will be performed during larger scale testing operations. These large scale tests are described in the following sections.

6.1. Optics Verification & Validation

6.1.1. Optics Component Integration Verification

Shortly after the manufacturing phase of the project, two qualitative component integration (i.e. "fit" and range of motion) verification tests were performed to determine if the machined and COTS parts were compatible. The tests allowed the team to fine tune the integration methods while gaining experience handling the optical components. The results of these tests were used to update the machine tolerances of components as well as the develop the proper integration procedures.

Diode Block Integration Verification

A description of the diode block assembly functionality can be found in "Optics Detailed Design". The integrated components of the diode block assembly are the photodiode, pinhole disk, chrome half sphere, and optical shims. The first fit test performed was on the photodiode. It was found that the press fit tolerance for the photodiode cavity worked as planned. A small amount of pressure allowed the team to press the photodiode into its cavity of the diode block. Its position was successfully constrained following the application of a non-conductive epoxy. Next, the team attempted to place and secure the pinhole disk. Epoxy was applied at needle point to the glue receptacle shelves around the photodiode. The disk was then placed on top of the photodiode canister. The epoxy proceeded to flow onto the top surface of the disk and compromised the pinhole. In a subsequent test, a revised method of tacking the pinhole was successful. The new method involved placing the pinhole disk using tweezers and tacking the disk on the top surface using small droplets of epoxy instead of placing the epoxy directly into the glue receptacle shelves.

An equally insightful test was the verification of the integration and removal method for the chrome half sphere. It was found that the 1 mm thick o-ring used to secure the half sphere in the photodiode was too large. This issue was remedied by cutting the o-ring into small pieces and strategically pressing the pieces around the half sphere. The chrome half sphere was observed to be successfully secured via the o-ring pieces and removable by pulling the nylon wire seated underneath the o-ring. Finally, it was verified that the integration and removal of the half sphere was possible with the presence of a focus shim stack.

Optical Bench Integration Verification

The verification test for the integration of the optical bench assembly was overall very successful. During this set of qualitative tests, the interfaces for the aperture stop, mirror, diode block, tooling plate, and sighting tabs were examined. Nearly all of these components "fit" as expected and were properly constrained by the optical bench. Two key exceptions were the mirror mounting points and tooling plate screw angle. The first machined iteration of the tooling plate was observed to have an incorrect compound angle for the tooling plate screw. This meant that the tooling plate screw did not contact the corner of the diode block, and was not able to apply compound pressure on the shim stacks. The plate was then re-machined, and the second iteration functioned properly. When examining the wave front error (WFE) of the OAP surface during the first alignment session at Ball, it was observed that the torque on the mirror mounts was directly related to increased WFE. When integrating the mirror into the final optical bench assembly, less torque was applied to these mounts and the WFE of the mirror was improved.

6.1.2. Optics System Alignment Verification and Validation

Alignment Tools

Fizeau Interferometer Figure 63 shows the ZYGO DynaFiz Interferometer used for the alignment procedure and the interferometer software (Mx). The interferometer has three main functional modes. The ALIGN mode allows the user to center the returning rays with respect to the interferometer. The VIEW mode allows the user to inspect a live display of the interferogram, or fringe pattern. Qualitative assessments are made using the live display. Lastly, the MEASURE mode allows the user to record measurements of the wavefront error, Zernike coefficients, MTF, etc. based on the interferogram. The various Zernike polynomials and corresponding fringe patterns measured by the interferometer are described in the "Zernike Coefficient Model" section below. The operational wave length of the interferometer beams is 633 nm.

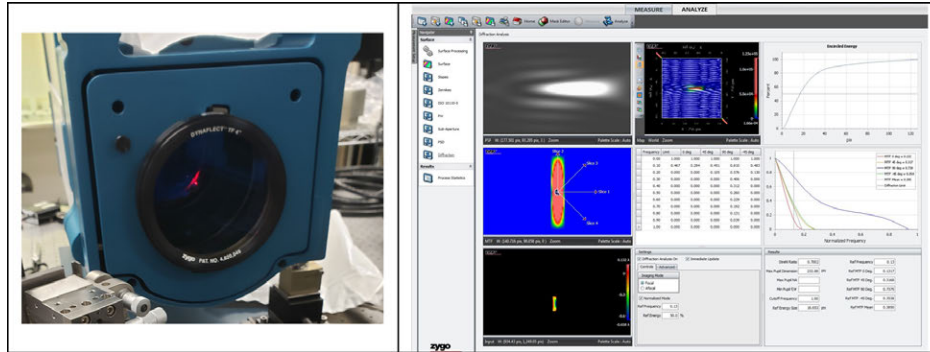


Figure 63. ZYGO DynaFiz Interferometer (left) and Example Software Output (right)

Optomechanical Hardware and Stages The optomechanical setup was constructed at Ball Aerospace during the first alignment session and was continuously updated up to the final alignment session. The optomechanics must allow the NanoSAM optical bench to be precisely tilted relative to the Zygo DynaFiz interferometer as well as allow for 3-axis translation of a return optic in order to align the optics system. A tilt stage allowed precise angle adjustments of the optical bench about 2 axes via adjustment of two micrometers. A 3 axis translation stage allowed precise translation of the return optic (i.e. the return sphere and chrome-coated half sphere) via adjustment of 3 micrometers. The optomechanics provided flexibility throughout the different phases of the alignment process allowing access to the tooling plate, sighting tabs, and the chrome-coated half sphere. Additional features were added to preserve the orientation of optical bench and allow for its repeated removal during the alignment process. Images of the various optomechanical hardware shown throughout the alignment process and further explanation of each stage is given in the Final Alignment Verification section below (see figures 69, 70, and 77).

Zernike Coefficient Model An optical model was developed using Zemax OpticStudio to plot Zernike coefficients as functions of in-plane tilt, out-of-plane tilt, and focus displacement which would correspond to the physical optomechanical setup implemented at Ball Aerospace. The equations from the model were translated into a MATLAB script that related micrometer translations of the tilt stage to the Zernike coefficient response. This allowed the optics team to input measured Zernike coefficients and retrieve physical displacement corrections to help drive the Zernike coefficient values to zero.

Figure 64 displays the commonly used Wyant Zernike term expansion. The Mx software developed for the interferometer uses the Wyant ordering of the Zernike polynomials. Note that Zemax OpticStudio uses standard Zernike fringe polynomials which differ from Wyant's ordering. The aberration and corresponding term order for each software is listed in table 5. The Zemax model used to describe the Z3-Z7 Zernike coefficient response to in-plane tilt, out-of-plane tilt, and focus offsets can be seen in figure 65 below. Note that the Zernike model described in figure 65 follows the Mx interferometer software ordering.

Aberration	Polar Equation	Interferometer Software Ordering	ZEMAX Software Ordering
Defocus	$2\rho^2 - 1$	Z3	Z4
Vertical Astigmatism	$\rho^2 * \cos 2\theta$	Z4	Z5
Oblique Astigmatism	$\rho^2 * \sin 2\theta$	Z5	Z6
In-plane Coma	$(3\rho^2 - 2)\rho * \cos \theta$	Z6	Z7
Out-of-plane Coma	$(3\rho^2 - 2)\rho * \sin \theta$	Z7	Z8

Table 5. Zernike Coefficient Description and Ordering

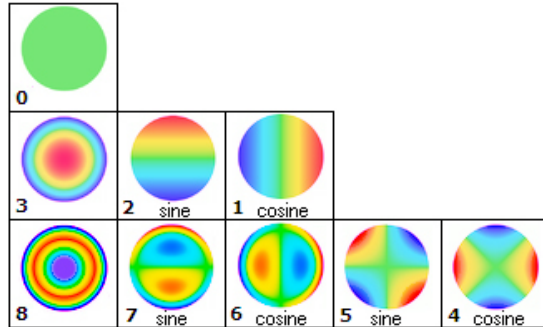


Figure 64. Wyant Zernike Term Expansion and Wavefront Pattern

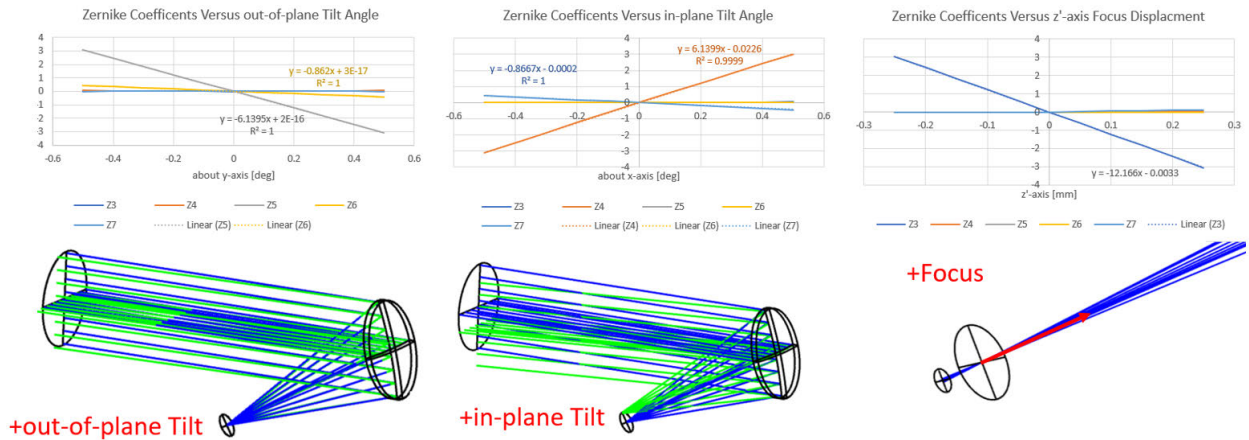


Figure 65. Zernike Coefficient (Z3-Z7) Response vs. In-plane Tilt, Out-of-plane Tilt, and Focus Displacement

From figure 65 it can be seen that the Zernike coefficient responses are relatively decoupled and are linear functions of the in-plane tilt, out of plane tilt, and focus displacement. The model also showed that the in-plane coma coefficient (Z6) and out-of-plane coma coefficient (Z7) are driven to zero when the vertical astigmatism coefficient (Z4) and oblique astigmatism coefficient (Z5) are driven to zero.

Return Sphere A return (AKA reference) sphere is a common accessory for interferometers and is essential when characterizing off axis concave surfaces. In general, return spheres are extremely high precision concave reflective

optics that, when aligned, are capable of returning focused rays back along the exact path in which they previously traveled. Because the precision requirements of these optics are so high ($< \lambda / 10$), purchasing a reference sphere was well beyond NanoSAM's budget. This meant that NanoSAM was required to borrow a reference sphere at Ball Aerospace's facilities during the mirror to interferometer alignment validation and verification steps.

Reflective Convex Half-Sphere A chrome coated NBK-7 10mm half ball lens was also required for the alignment process. In a similar fashion to a return sphere, when aligned properly, the reflective chrome convex half sphere returns incident rays back along the exact path in which they previously traveled. An important distinction to note is that the quality of the convex sphere will be nowhere near that of the reference sphere ($\approx \lambda/4$). The NBK-7 10mm half ball lens was purchased from Edmund Optics and coated through thermal evaporation at CU Boulders COSNIC fabrication facility. As this sphere is an alignment tool, it will be removed from the system following the diode block alignment verification step.



Figure 66. Interferometer Return Sphere



Figure 67. NBK-7 Convex Half Sphere Lens

Final Alignment Verification

The following sections describe the actions and results taken by the alignment team during the final alignment verification of the optics system. Prior to the final alignment session at Ball, the optics team fine tuned the alignment methodology in four preliminary alignment sessions. During these sessions, the team constructed the optomechanical setup described above, validated the mirror to interferometer alignment procedure, and practiced the pinhole alignment step using a 50 μm pinhole. This allowed the optics team to gain valuable experience operating the optomechanical setup and implementing the models developed to characterize the alignment of the system. Perhaps the most influential result of the preliminary alignment sessions was the development of the initial shim stack derivation procedure. Each alignment session conducted at Ball was supervised by the NanoSAM customer and professional optical engineer Jim Baer.

Mirror to Interferometer Alignment Verification This step of the alignment process involves the use of the interferometer, the OAP mirror, and a high precision return sphere. Figure 68 shows a conceptual diagram of this step of the alignment along with two key coordinate systems. The objective of this step is to align the OAP such that the culminated rays of the interferometer are along the optical (Z) axis of the mirror. The highest possible MTF performance of the OAP is achieved when the chief light ray is along this axis. Aligning the pinhole to the focal point of the mirror after the OAP has been aligned to the interferometer beams ensures the highest possible system MTF. After aligning the optical axis of the OAP to the interferometer, the sighting tabs are set to aid in pointing the system along the optical axis once the optical bench is integrated into the structure.

Acceptable alignment of the mirror relative to the interferometer is verified once the vertical astigmatism, oblique astigmatism, and coma coefficients (Z4-Z7) measured by the interferometer software are near zero, or between .15 and -.15 waves. Within this range, the COTS OAP was experimentally observed to produce the predicted WFE and MTF. This is accomplished by adjusting the tilt stage micrometers, which effectively control the in and out of plane tilt of the optical bench relative to the interferometer beams. Note in-plane tilt is rotation about the X-axis and out-of-plane tilt is rotation about the Y-axis. A return from optical system is required to obtain measurements of the Zernike coefficients. This is achieved using the high precision return sphere. The return sphere is aligned in-plane (Y'-axis), out-of-plane

(X' -axis), and and focused (Z' -axis) using the three axis opto-mechanical stage micrometers. It should be noted that the return sphere must be realigned after each tilt adjustment of the optical bench. The model describing the Zernike coefficient response to these adjustment was created and is described in "Alignment Tools" above.

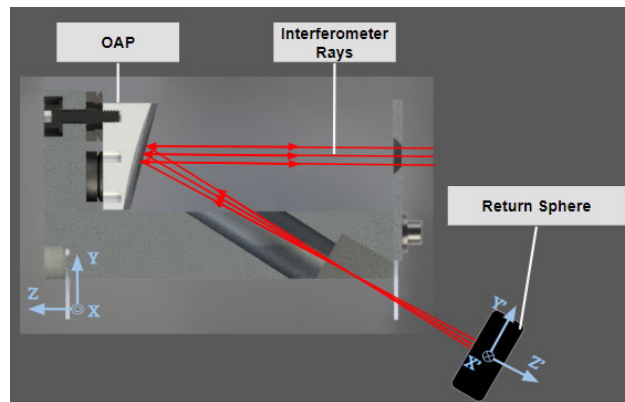


Figure 68. Conceptual Diagram for Mirror to Interferometer Alignment

To begin, the optical bench was secured to the tilt stage such that the position was constrained in 3-axes: vertically via the top plate of the tilt stage and in the two orthogonal directions by a straight edge cube and single point contact on a hex nut. An image of these components can be seen in figure 69. This configuration allowed the position of the bench relative to the interferometer rays to be maintained when removed from the stage. An image with the bench in position can be seen in figure 70.

The three axis stage with the reference sphere installed, was aligned such that the three axis adjustments were along the X' , Y' , and Z' axes using the inteferometer's return in align mode. Once a return was observed, the 3-axis stage position was locked. The return sphere, optical bench, and mounting systems in this configuration can be seen in figure 70. The return was then centred and focused using the three axis translation micrometers on the return sphere stage. The interferogram was used to fine tune the return. Specifically, once the fringe pattern was deemed appropriately centered and symmetric, numerical measurements of the Zernike coefficients were taken via the software. These measurements were then fed into the MATLAB Zernike model. This provided the estimated adjustments of the tilt micrometers required to null the Zernike coefficients.

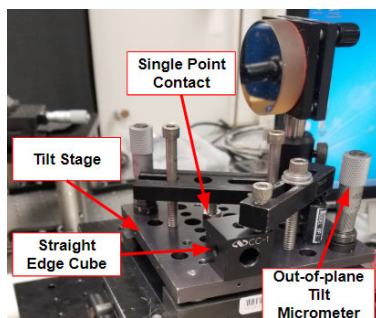


Figure 69. Optical Bench Position Constraint

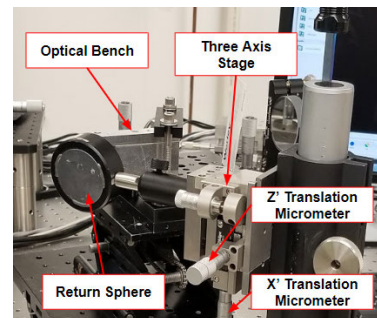


Figure 70. Mirror to Interferometer Alignment Configuration

The tilt micrometer displacements provided by the model were then implemented in the appropriate direction. This process was repeated continually until the astigmatism and coma Zernike coefficients (Z_4 - Z_7) under test were seen to be acceptably near zero, at which point the interferometer rays are deemed on axis. A final measurement of the aligned system was taken, and the wavefront error (WFE) and MTF performance of the OAP was recorded. A mask replicating NanoSAM's aperture was added in the software, and the the wavefront error and MTF performance of the OAP with the aperture mask was recorded.

Table 6 shows the Z4-Z7 Zernike coefficients for the aligned OAP. Plugging the vertical and oblique astigmatism coefficients into the analytical Zernike model gives that the mirror is misaligned by $\approx .13$ mrad in-plane and $\approx .11$ mrad out-of-plane.

ZFR	Value
4	0.045
5	0.038
6	-0.104
7	0.064

Table 6. Zernike Coefficients for Aligned OAP-Interferometer

Figure 71 shows the wavefront error across the surface of the aluminum OAP in its aligned configuration. The measured wavefront error is seen to range from 1.61λ to a -1.25λ . The wavefront root mean squared (RMS) error for the surface of the mirror was found to be $.46 \lambda$. This verifies that the mirror performance is in the range of the manufacturer reported $\lambda/2$ wavefront RMS error. A key discovery made from figure 71 is the trefoil pattern around the edge of the aperture. This pattern was seen to correspond with the screw hole mounting points on the back of the OAP. This suggests that mirror performance is related to torque on these mounting points. The pattern also shows that the performance near the center of the mirror is much better than the perimeter.

Figure 72 is a measure of the wavefront error within an approximate mask representing NanoSAM’s aperture. A quick inspection of the color bar shows that the range of wavefront has become much more regular. The WFE was seen to range from -0.66λ to 0.13λ . The WFE RMS of the clear aperture can be approximated by scaling the WFE RMS of the full OAP (0.46λ) by a ratio of the total WFE range measured in each configuration ie. $0.46 * 0.79/2.86 = 0.127\lambda$. Scaling this WFE RMS from a wavelength of $.633 \mu\text{m}$ to $1.02 \mu\text{m}$ gives a WFE RMS of approximately $.08 \lambda$ or $\lambda/12$ at $1.02 \mu\text{m}$.

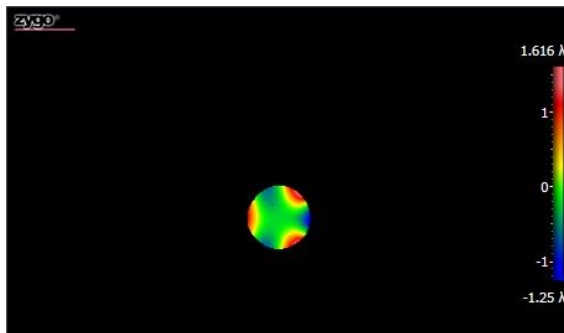


Figure 71. Aluminum OAP WFE

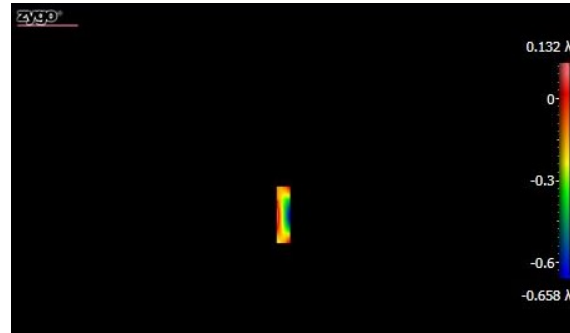


Figure 72. Aluminum OAP WFE with Aperture Mask

Following the WFE measurements, the MTF of the interferometer-OAP system was recorded over a range of spatial frequencies. The interferometer He-Ne laser outputs a 633nm beam. With NanoSAM’s 20mmx5mm aperture, the cutoff frequency is given by $\nu_c = 20\text{mm}/633\text{nm} = 31.6$ cycles/mrad. The spatial frequency of interest (1 cycle/km) corresponds to an angular frequency of 2.574 cycles/mrad. As a result, the normalized frequency used to evaluate the MTF is 0.08. The 90 degree MTF at 0.08 is approximately 0.85. Thus, the measured MTF of the OAP-interferometer system at the 1 cycle/km spatial frequency is close to the diffraction-limited value predicted by the NanoSAM teams’ MTF model^a. With that said, the OAP-interferometer MTF measurement neglects the image degradation due to pinhole misalignment and the degradation due the optical filters. The overall MTF budget of the optical system is outlined in the “Final Optics System MTF” section below.

^aThis model is separate from the Diffraction Limit curve labeled in the legend.

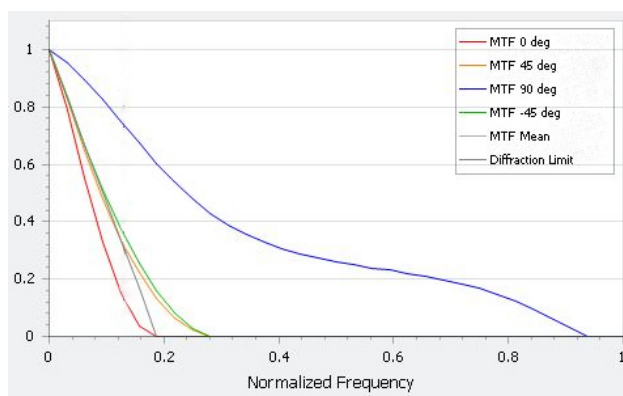


Figure 73. Aluminum OAP MTF with Aperture Mask

Following the mirror alignment, the sighting tabs were set. The tabs are tightened down until they are able to rotate about the pivot point with a little force. A piece of card stock is held behind the second tab to visually inspect the shadow cast by the cross-hair. Once the crosshair is centered on the bright spot, the tabs are tightened down further in their current positions. The tabs were successfully aligned during the final lab session at Ball Aerospace. The alignment was confirmed visually after the tabs were tightened into their final positions. Later that day, the pivot points were staked in the aerospace machine shop at CU Boulder. Figure 74 displays an image of the cross-hair resulting from aligned sighting tabs.

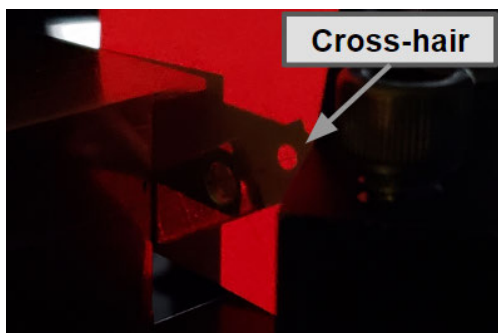


Figure 74. Aligned Sighting Tab Cross-hair Projection

Diode Block Alignment Verification The verification of the diode block alignment was performed in three distinct phases. An initial performance characterization of the chrome half sphere insured it was a viable return optic for use with the interferometer. The initial shim stack thickness were then derived to reduce the number of shim changes required by integrating the diode block and chrome half sphere onto the three axis translation stage. Finally, additional shimming of the diode block was performed to account for deviations from the initial shim stacks. The actions and results for each of these phases are described in detail below. A conceptual diagram describing the diode block alignment step can be seen in figure 75.

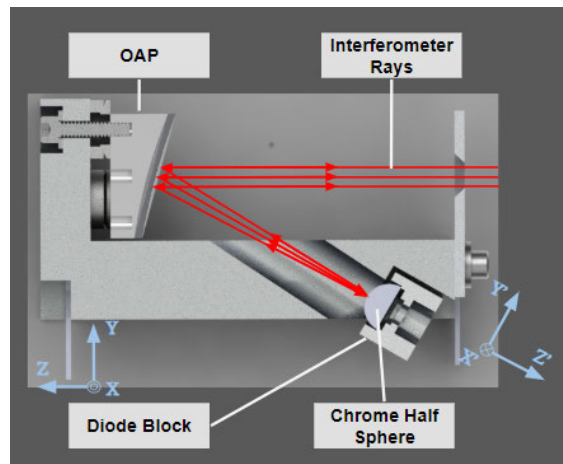


Figure 75. Conceptual Diagram for Diode Block Alignment Derivation

A fairly precise reflected wavefront is required to effectively utilize a return optic. Therefore, a preliminary characterization of the chrome coated half sphere's performance was essential. To begin, a transmission sphere was installed on the ZYGO interferometer. The transmission sphere transforms the collimated 633nm beam into a spherical wavefront for the characterization of curved surfaces. The diode block, with the chrome half sphere inserted, was mounted on a 2-axis tilt stage. From there, adjustments were made to the micrometers of the stage until a return from the chrome half sphere was visible in the interferometer live display. Further adjustments were made to center the return wavefront.

Data was successfully recorded which shows that the surface quality of the chrome half sphere is high. The full wave (peak-to-peak) of wavefront error is likely due to defocus, with the magnitude of Z3 being the largest. Spherical aberration and other aberrations are present but much less significant based on the magnitudes of the relevant Zernike coefficients. Strange artifacts in the chrome half sphere return were visible during the performance characterization, but they did not noticeably impact the performance metrics. The relative magnitude of the Zernike coefficients seen in figure 76 indicated that the chrome half sphere is an adequate return optic.

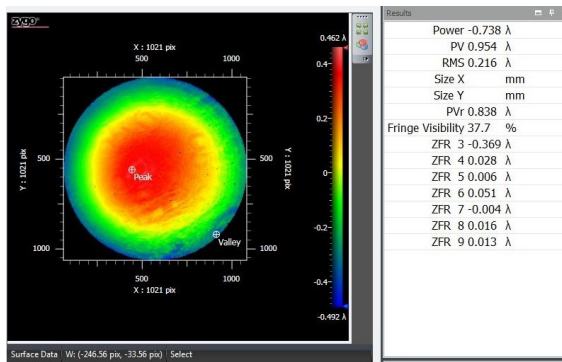


Figure 76. Chrome Half Sphere WFE and Zernike Coeff.

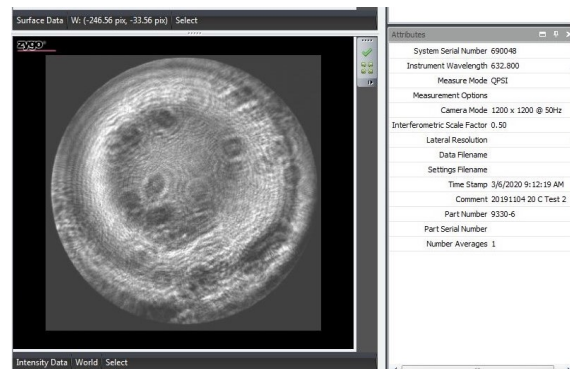


Figure 77. Chrome Half Sphere Surface

In order to reduce the number of shim changes once the diode block is mounted, the initial shim stack thicknesses were derived through the process described below. The diode block (with the integrated pinhole plate and half sphere) was secured to a cube via Teflon tape. The face of the diode block with the protruding chrome half sphere was positioned facing away from the rod connecting the cube to the 3-axis stage. The diode block was secured such that the shimming faces had an overhang relative to the co-planar faces of the cube. The rod was then secured into the 3-axis stage. The three axis stage was mounted such that the diode block was positioned within its cavity of the optical

bench and could be translated along the X', Y', and Z' axes seen in figure 75. An image of the physical configuration can be seen in figure 78. The three axis micrometers were used to translate the diode block until all three shimming faces of the diode block were in contact with the shimming faces of the optical bench. The micrometer readings in this configuration were recorded and used as "zeros" for describing the position of the diode block during the remainder of the initial shim stack derivation process.

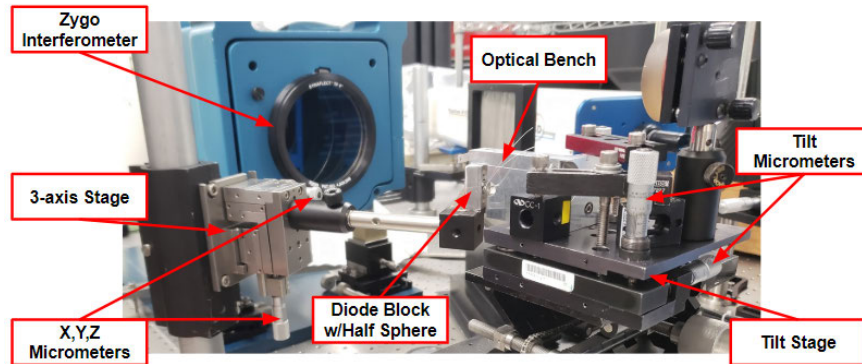


Figure 78. Diode Block in Starting Shim Derivation Physical Configuration

The diode block was then translated in each of the three axes until a return from the chrome half sphere was observed on the interferometer software. Once a return from the chrome sphere was observed, the return was centered on the align mode crosshair and focused using further adjustments of the 3-axis stage micrometers. The interferogram was used to ensure that the fringe pattern was focused, centered, and symmetric before a measurement was taken. The software was then used to measure the vertical astigmatism and oblique astigmatism Zernike coefficients. Because the astigmatism coefficients had been minimized in the mirror to interferometer alignment step, minimizing these coefficients by translating the diode block verifies its alignment in-plane and out-of-plane. The diode block was then translated in one axis by a small arbitrary distance, and the corresponding Zernike coefficient response was noted. The relationship between the Zernike coefficient response and micrometer adjustment was analyzed, and further adjustment was made until a near zero Zernike coefficient was observed. This process was repeated for the remaining two axes. Once all Zernike coefficients were deemed acceptable, a MTF measurement was taken, and the new micrometer readings were recorded. The aligned set of micrometer readings were compared to the "zeros", and the initial shim stack thicknesses were prepared in order to reconstruct the displacement of the diode block with out the presence of the 3-axis stage.

Table 7 shows the Zernike coefficient values used to verify the alignment of the diode block in the configuration described above. The micrometer "zero" readings, micrometer aligned readings, and the differences can be seen in table 8. The initial shim stacks were prepared to closely match the difference measurements given the shim thickness available.

ZFR	Value
4	-0.041
5	0.320

Table 7. Zernike Coefficients Reference for Aligned Half Sphere Position on 3-axis Stage

Axis	Zero Reading [mm]	Aligned Reading [mm]	Difference [mm]
Focus:	2.037	3.820	1.783
Horizontal:	6.360	6.045	.315
Vertical:	4.895	5.620	.725

Table 8. Micrometer Displacements for Initial Shim Stack Thickness Derivation

Following the initial shim stack derivation, the shim stacks and diode block were mounted to the optical bench. Once secured the team inspected the interferogram return from the chrome half sphere and measured Zernike coefficients 4 and 5 to characterize any discrepancies in the new diode block position. Just as in the section above, minimizing the astigmatism coefficients by shimming the diode block verified its alignment in-plane and out-of-plane. Shim changes were made until the half sphere was focused and aligned in and out of plane. Because the initial shim stack thicknesses derived were very accurate, only small out-of-plane (X') and focus (Z') shims stack variations were required. Finally, the chrome coated half sphere was removed from the diode block by pulling the fishing wire seated under the O-ring securing the half sphere within the diode block.

The resulting Zernike coefficients from this shimming process can be seen in the table 9. These values were measured from the return of the half sphere prior to removal.

ZFR	Value
4	-0.078
5	-0.008

Table 9. Zernike Coefficients for Aligned Diode Block

Pinhole Alignment Verification The objective of this alignment step is to verify that the radial and focus displacement of the pinhole is within the allowable MTF degradation margin and preform additional shimming of the diode block if necessary. Figure 79 shows a conceptual diagram of this step of the alignment. To accomplish this, the focus displacement error is calculated using a live view false interferogram produced by the pinhole plate surface. If light is observed to pass thorough the pinhole, the computed focus error can be used to determine the maximum radial error given that the out of focus light forms a round spot at the surface of the pinhole.

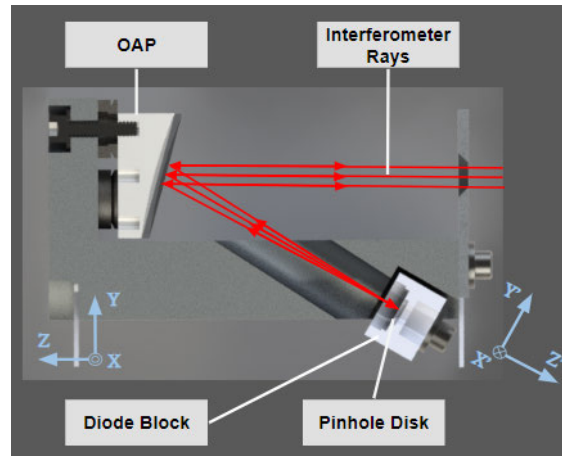


Figure 79. Pinhole Surface Return Conceptual Diagram

After removing the chrome half sphere from the diode block, a screenshot of the false interferogram return was taken and can be seen in figure 80. The alignment team was able to visually verify that without further shimming,

light was passing through the pinhole. At the time, an incorrect calculation of defocus using the number of defocus rings seen in the false interferogram led the team to believe that the system needed no further alignment. Due to the time constraints of the alignment session, this incorrect calculation was not verified. Given the team thought the system was properly aligned at this point in the session, the diode block bolts were fully tightened to maintain the diode blocks current position and allow for the removal of the tooling plate. During this process, the live view of the false interferogram was monitored to ensure locking down the diode block did not alter the number of defocus rings. After removing the tooling plate, it was verified that light was still passing through the pinhole. This completed the final alignment actions taken by the NanoSAM team in the spring of 2020.

It is now known that the system will not achieve the target imaging performance and needs further alignment steps. The correct analysis of the systems radial and focus error is described in detail in the following paragraphs. The further alignment actions that the team would have taken had the correct analysis been conducted is also described below.

Figure 80 is a screenshot of the final false interferogram output by the Zygo interferometer program after locking the diode block's position.

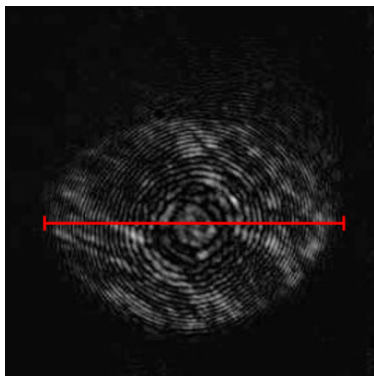


Figure 80. Pinhole False Interferogram

It can be shown that the number of defocus rings observed in an interferogram is proportional to the focus displacement error of the system. The full derivation of this relationship can be found in Chapter 1 of "Basic Wavefront Aberration Theory for Optical Metrology" by James Wyant and Katherine Creath [46]. Equation 6 describes the defocus displacement error of a system with a converging focus and circular aperture.

$$\epsilon_z = 8 * (f/\#)^2 * m\lambda = 8 * (2)^2 * 30 \text{ rings} * .633\mu\text{m} \approx 600\mu\text{m} \quad (6)$$

Where:

- ϵ_z : The focus displacement error
- $f/\#$: The F-number of the system
- m : The number of defocus rings across the aperture (i.e., counting the white rings from the center out)
- λ : The wavelength of the interferometer beam

Inspecting figure 80 reveals 30 defocus rings. Plugging this value into equation 6 along with NanoSAM's F-number of 2 and the interferometers wavelength of .633 μm yields a defocus error of approximately 600 μm . From this analytical focus error, the maximum possible radial offset that would result in light through the pinhole can be computed. A visualization of this geometric analysis is given in figure 81. The diagram shows that the maximum possible radial offset is equal to the radius of the $f/2$ cone of light along the plane of the pinhole surface plus the radius of the pinhole itself. For a 600 μm focus displacement error, the maximum radial displacement error that would allow light to pass through the pinhole is approximately 160 μm (see equation 7). As mentioned above, these displacements do not achieve the target imaging performance of the NanoSAM optics system. Given more time, the additional alignment actions described in the following paragraphs would have been implemented.

$$\text{Max. Radial Error} = 600\mu\text{m}/(2 * 2) + 15\mu\text{m}/2 \approx 160\mu\text{m} \quad (7)$$

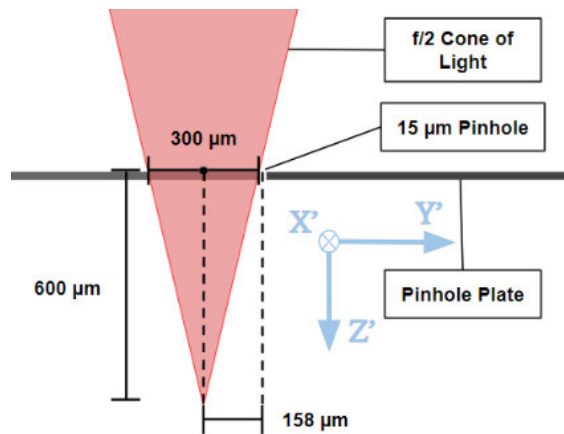


Figure 81. Maximum Radial Offset

The following sections describe the recommended steps that should be taken by future alignment teams to remedy the imaging performance the optics system. After removing the chrome half sphere, it is unknown whether the light is focusing before or after the pinhole. Accordingly, a test should be performed to identify if shims must be added or removed to reduce focus error. To begin, focus shims equal to half of the calculated focus displacement error should be removed. For example, if the focus displacement error is calculated to be 600 μm , then 300 μm of focus shims should be removed. The diode block should be re-secured using the tooling plate and the diode block bolts. If fewer defocus rings are observed in the false interferogram, then removing the focus shims has reduced the focus error. Conversely, if more defocus rings are observed, the focus error has increased. The 300 μm of additional focus shims should be added to the original shim stack to improve focus displacement error.

Equation 6 should then be used to confirm that adding or removing focus shims has successfully reduced the focus error. The scaling coefficient in equation 6 should be adjusted if the new focus error is not reduced by half (e.g. the 300 μm from above). If light is not seen passing through the pinhole, in-plane and out-of-plane shims must be added or removed until light is passing through the pinhole. To determine the size of the in-plane shims that need to be added or removed, the entire tilt stage should be adjusted about the in-plane axis via the tilt micrometer until light is observed passing through the pinhole. At this point, the current in-plane angle should be recorded. Tilt adjustments in the in-plane axis continue until light no longer passes through the pinhole. Again, the in-plane angle should be recorded. The entire tilt stage should then be returned to its original position (i.e. in which the rays of the interferometer are aligned to the optical axis of the mirror). The in-plane tilt angle offset corresponding to the midpoint of the two recorded tilt angle values should be equated to an in-plane translation of the diode block. The equivalent in-plane shim stack thickness should be added or removed to reduce the in-plane displacement error. An identical process should be performed to reduce the out-of-plane displacement error. With light ideally passing through the center of the pinhole, focus shims stacks should be adjusted to bring the focus error below the target MTF performance cut-off (45 μm). If light is still seen passing through the pinhole, then the system has met the alignment requirements. Otherwise, the in-plane and out-plane shimming process described above should be repeated until light is seen passing through the pinhole. The system should now be aligned.

Final Optics System MTF To compare the imaging performance of the NanoSAM optics system to SAM II, a MTF degradation budget accounting for misalignment and filter wavefront error was constructed. The degradation budgets seen below evaluate the system MTF (i.e. the actual imaging performance at the pinhole). Zemax was used to model the MTF degradation for the focus and maximum radial displacements (i.e. worst case scenario). Table 10 displays the

MTF degradation budget comparing the actual alignment achieved with the NanoSAM optics system versus a feasible alignment with the NanoSAM optics system (i.e. what the optics team expected to achieve if testing continued).

	NanoSAM (actual alignment)		NanoSAM (feasible alignment)	
Target MTF				
Best possible MTF of SAM-II at critical angular frequency with 50 mm aperture & 75% obstruction	0.74		0.74	
Actual Mirror MTF				
Measured using interferometer and scaled for angular frequency of 2.57 [cycles/mrad]	0.85		0.85	
MTF Degradation Factor				
Focus (Z') Displacement	N/A	600 μm error *	0.94	45 μm error **
Out-of-plane (X') Displacement	0.37	158 μm error *	0.97	30 μm error **
Filter TWFE	0.98	0.03 λ WFE	0.98	0.03 λ WFE
Filter TWFE	0.98	0.03 λ WFE	0.98	0.03 λ WFE
Analysis				
Combined Degradations = ∏ MTF Degradation Factors	N/A		0.88	
System MTF = Combined Degradations * Actual Mirror MTF	N/A		0.74	
Margin = $\frac{\text{System MTF}}{\text{Target MTF}} - 1$	N/A		0%	
		* calculated displacement		** feasible displacement

Table 10. MTF Degradation Budget Actual Versus Feasible Alignment

The actual alignment column in table 10 shows very poor imaging performance given the current misalignment of the NanoSAM optics system. The massive degradation in MTF is mostly due to the 600 μm focus displacement error. This large focus displacement is outside the bounds of the MTF model, thus the model gives an erroneous MTF value. In practice, the MTF value approaches zero for large focus displacements. Fortunately, because light was observed passing through the pinhole, the NanoSAM instrument is still capable of collecting radiometric data in its current alignment configuration. Because the Sun’s light rays are effectively collimated, the pinhole would be fully illuminated, resulting in light reaching the photodiode. Therefore, in the current alignment configuration, future tests (e.g. the measurements stability and final integration tests) of the NanoSAM instrument are still valid.

The feasible alignment column in table 10 shows the MTF degradation budget of the NanoSAM optics system with a feasible alignment error of 45 μm of focus displacement and a corresponding maximum radial displacement error of 30 μm (Eq. 7). These are the maximum allowable displacement errors which meet the target MTF of SAM II, resulting in a margin of 0%. Further improvements to the alignment would result in a higher system MTF. The feasible alignment column in table 10 shows that a 1 kilometer vertical resolution is attainable by an undergraduate student optics team using off the shelf optical components.

6.2. Electronics Verification & Validation

6.2.1. Component Tests

The first part of the electronics system that was tested was the individual components circuits. The results of these tests can be seen in Table 11.

a. Issues and Resolution As can be seen from Table 11, there were some issues with a couple of the components. Fortunately the electronics system was designed with many back up options to allow the system to function despite these issues.

The digital power supply was outputting 2.5V instead of the expected 3.3V. This issue was caused by a defect in the chip causing the feedback pin to be regulated to 0.75 V instead of the expected 1.25V. This was resolved by

Test	Requirement	Expected Result	Actual Result	Result after resolution
Digital Power Voltage	3.0: Electronics System	3.3V	2.5V	3.3V
Analog Power Voltage	3.0: Electronics System	+/-5V	+/-5V	
Amplifier Gain	1.5: Dynamic Range	1V/ μ A	1V/ μ A	
Flash input voltage	3.0: Electronics System	3.3V	3.3V	
ADC input voltage	3.0: Electronics System	3.3V	0V	3.3V
Amplifier input voltage	3.0: Electronics System	+/-5V	+/-5V	

Table 11. Component Test Results

removing the jumper resistor connecting the output of this power supply to the digital power plane. The digital power plane was then powered by the on-board linear regulator of the Teensy microcontroller.

The ADC chip footprint had an issue where the power pin was connected to the ground plane instead of the power plane. The result was that the ADC could not be powered. To resolve this, a wire patch was applied connecting the ADC input to an unused analog input on the microcontroller's on board 12bit ADC. The on-board ADC met our requirements for noise, resolution, and sampling frequency.

While these were intended to be temporary fixes while a new board was ordered, shutdown of manufacture and testing prevented a new board from being ordered. These fixes allowed testing to continue with an electronics system that met the requirements so other issues could be discovered and fixes included in the design of the new board.

6.2.2. System Tests

Once the individual components of the electronics system were verified as working, the system as a whole was tested to ensure that components were cooperating properly. These tests and results can be seen in Table 12.

Test	Requirement	Result
Microcontroller interfaces with peripherals	3.3.1: Data Output Method	Success
Electronics Noise	1.4: SNR	< 0.8mV
Photodiode dark current	1.4: SNR	< 0.8nA
Measurement Stability	3.1: Data Collection	N/A
Measurement Noise	1.4: SNR	N/A
Dynamic Range	1.5: Dynamic Range	N/A

Table 12. System Test Results

a. Microcontroller interfaces with peripherals In order to test the digital portion of the system, code was written that would read data from the Teensy microcontroller on board ADC and write the data to the on board flash chips. The code would also read data from the flash chips and send it over a serial connection to a PC. This would ensure the microcontroller could properly communicate with all the necessary peripheral components. The ADC input was connected to ground for the first test and 1V from the amplifier output for the second. In both tests, the data read from the flash chips matched expectations.

b. Electronics Noise and Dark current To determine the noise in the electronics portion of the system and the dark current of the photodiode, the electronics with integrated photodiode were brought to a dark room in the CU aerospace building. Code was run on the microcontroller to output the data from the ADC over a serial connection to a laptop at 50 Hz. When the room was dark, the output from the electronics system was a stable 1 Dn. Converting from ADC data numbers to volts can be done as follows, where V_{ref} is the ADC reference voltage, Dn is the ADC

data number, and R is the ADC resolution in bits.

$$V = V_{ref} \frac{Dn}{2^R} \quad (8)$$

From this, it can be seen that the voltage at the ADC input is less than $0.8mV$, and the noise was less than $0.8mV_{p-p}$. It is important to note that this noise measurement is the noise due to the electronics system alone, and does not account for sources of noise in the light signal itself, such as shot noise. This result matches the expectations from our noise model.

The dark current can be calculated by converting the amplifier voltage output to the equivalent current through the photodiode. This can be done as follows, with V being the voltage at the amplifier output, A being the amplifier gain, and I_r being the photodiode reverse leakage current, or dark current.

$$I_r = \frac{V}{A} \quad (9)$$

From the previous tests, it was shown that the amplifier gain is $1V/\mu A$. Using this, the dark current through the photodiode is less than $0.8nA$. This result matches expectations from the photodiode data sheet.

c. Measurement Stability and Noise While the dark room tests showed the electronics system is stable and low noise, this result had to be verified while the system was taking measurements of non-dark light sources. To do so, a stable light source would be made by powering a tungsten filament bulb with a lab bench power supply. The power supply ensures that a constant amount of power is supplied to the bulb. The bulb itself has a relatively constant efficiency once it reaches a constant temperature. The bulb would be left on for 15 minutes prior to starting the test to ensure the light being provided had constant irradiance. Various degrees of neutral density filter would be placed between this light source and the integrated electronics and optics system. These would produce various responses from the electronics system and the stability and noise at different light levels could be examined. Measuring the noise from this is important as it includes the shot noise of the light signal in addition to the electronics noise.

Due to the early end to testing and manufacturing, this test could not be performed. However, simulated results were produced to show what the data from this test was expected to look like using the set up given in figure 83. The simulated data can be seen in figure 82.

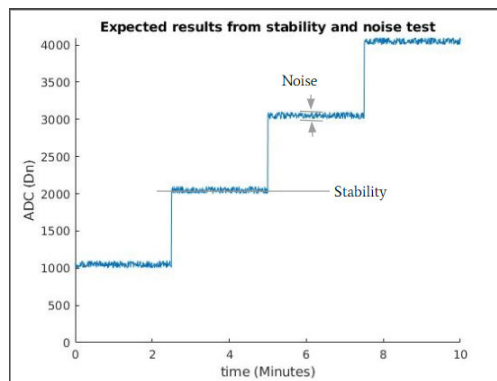


Figure 82. Expected results from stability and noise test

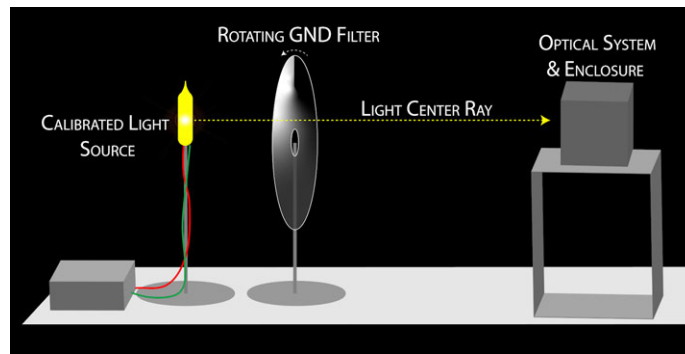


Figure 83. Stability test set up

d. Dynamic Range The final requirement to be tested was the dynamic range requirement. This would be tested during the final integration test where the instrument would track the sun over the course of a morning in order to correlate solar intensity with air mass. This requirement ensures that our system would not become saturated during the baseline measurements taken during a flight mission. In order to do this, the signal when viewing the unattenuated sunlight must remain below 90% of the ADC range.

The data taken during the final integration test can be used to correlate ADC signal to air mass. This can be used to extrapolate the ADC signal at zero air mass and show that the dynamic range requirement is met. Like the stability and noise test, this test was not performed due to the early halt to testing and manufacturing.

6.3. Mechanical Verification & Validation

The verification of the mechanical components will be fairly straightforward. The verification methods for the mechanical system will include demonstrations and direct measurements. Requirements 2.0 - 2.2 are concerned with bus compatibility verification, requirements 2.3 - 2.3.2 are concerned with enclosure verification, and requirement 2.4 is concerned with portability.

Requirement 2.1, 2.3.1, and 2.4 will be verified by simply mounting and dismounting the NanoSAM mechanical design within the enclosure. Requirement 2.3.1 will be simultaneously verified by directly measuring the dimensions of the test enclosure. After the enclosure is verified to be 1000 cubic centimeters, the NanoSAM instrument will be mounted inside to verify it is less than 1000 cubic centimeters. In doing so, requirement 2.4 will also be verified.

Requirement 2.2 will be verified by weighing the NanoSAM assembly prior to testing. This will verify that the mass of NanoSAM is less than 1.33 kilograms, the maximum allowable mass for 1-U CubeSat deployment.

Requirement 2.3.1 will be verified by inspection. First, all of the integrated components will be cleaned in a pseudo-clean room. Then, the prototype enclosure will be assembled in the pseudo-clean room. Inspection is focused on all of the openings of the rectangular enclosure tube to ensure that no stray light or dust can be seen through any potential openings during any integration tests going forward (Figure 84).

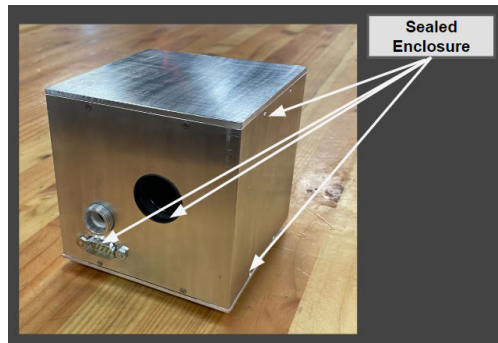


Figure 84. Places in the Enclosure Where Inspection will take place

Requirement 1.3 will be verified by directly inspecting the filter mount and aperture alignment. The axial distance from the filter mount to the aperture stop is 2.1 mm therefore it will be sufficient to confirm the alignment in this manner. The filter mount with the filters removed will be mounted on the enclosure, and the test engineer will view through the mount at a perspective normal to the aperture. If the aperture is fully visible through the filter mount then the component's alignment will be verified. If the components are not aligned, then corrective action will be taken as outlined in section 6.5.4.

6.4. Integration Verification and Validation

The most critical verification and validation test for the integrated NanoSAM system is the day-in-the-life solar measurement test. This simulation was done using data from CU Boulder's ATOC Skywatch Lab Solar Photometer, which is geographically identical to the proposed NanoSAM integrated test site on campus. Data here was taken in minute increments from 10:00a to 3:00p on 1 April 2020, comparable timing to the scheduled integration test. This spectral data was propagated through the NanoSAM optics system to produce a Langley plot:

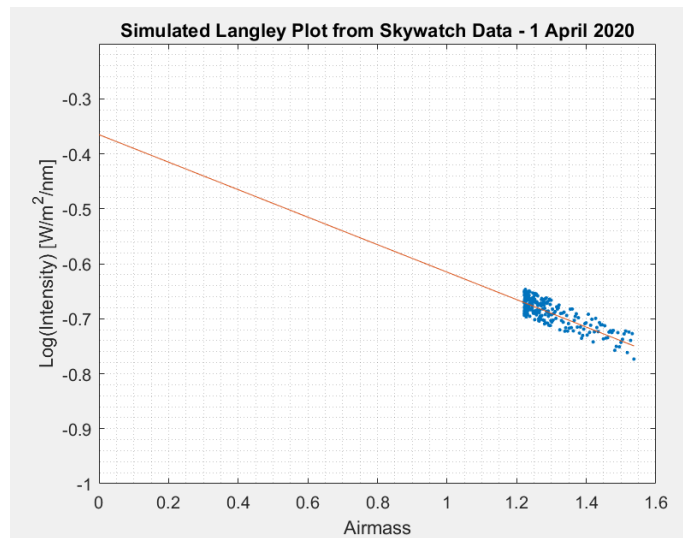


Figure 85. Langley Plot Simulation Result

This figure depicts the expected linear correlation between airmass and the log of the measured solar intensity. The red extrapolation line demonstrates how the intensity of the light increases as the amount of air between the instrument and the sun decreases moving left along the horizontal axis. At the zero-airmass intersect with the vertical axis, the extrapolated maximum solar intensity is calculated to be $684\text{W/m}^2/\text{nm}$. The established value for this zero-airmass intensity at 1020nm is $693.7\text{W/m}^2/\text{nm}$, so while the data is somewhat noisy and the extrapolation pushes far beyond

the region over which we have data, the calculated result agrees to 1.5%, which is quite good. It's important to note that the weather on this day was good (i.e. mostly clear skies), so any integration tests should be done on days with good weather for a valid comparison to this simulation. However, this simulated integration test indicates good agreement between the prototype NanoSAM measurements and established data, so NanoSAM would have passed integration testing.

7. Risk Assessment & Mitigation

Hui Min Tang, Jared Cantilina, Jacob Romero

The design solution discussed in the previous sections theoretically should meet all specific objectives, critical project elements, and requirements. However, in reality, there are plenty of possible risks that might undermine the NanoSAM project. To better manage risks, a risk analysis is performed to identify possible risks. First, a failure modes and effects analysis (FMEA) was executed. This step consisted of identifying failure modes, causes, and effects. For each failure mode, a number from one to five is assigned to three categories to assess its severity (SEV), occurrence (OCC), and difficulty of detection (DET). The three values are then multiplied together to produce a risk priority number (RPN). The RPN aids in the ranking of potential risks in the order they should be addressed. Failure modes with higher numbers take priority in the risk mitigation process.

Function	Failure Mode	Potential Effects	SEV	Potential Causes	OCC	Detection Mode	DET	RPN
Optical System Alignment	Optical system (mirror, filter, field stop, and detector) not aligned to specified tolerance.	Photodiode does not measure desired image. Signal strength too low. MTF does not meet requirement.	5	Vibrations on optical system. Pinhole and detector not aligned.	4	Determine alignment using a Fizeau interferometer.	3	60
SNR	SNR fails to meet desired value.	Signal is distorted by noise and will produce inaccurate readings. SNR does not meet requirements.	5	Optics or electronics thermal conditions are not satisfied. Unexpected dark current and other electronics noise. Weak signal strength. Errors in light source during testing.	3	Thermal analysis to ensure thermal conditions are met. A radiometric model will be developed at worst case conditions to ensure SNR is met at all times.	4	60
Measurement Stability	Irradiance measurements of the system does not remain stable and data points across 5 tests contains more than 1% of discrepancies.	Irradiance measurements are not repeatable; therefore the collected data is inaccurate and does not satisfy project requirements.	5	Photodiode contains bias. Photodiode oversaturated.	2	Perform multiple tests on payload with graduated neutral density filter and compare results.	5	50
Photodiode Saturation	An excess of solar irradiance above anticipated levels will cause the photodiode to become saturated.	The photodiode will not record accurate baseline measurements which will make all other measurements incorrect.	5	Improper optical alignment. Excess light is allowed in by the initial field stop.	3	Increase irradiance past expected baseline reading to ensure measurements are still taken and change with increasing irradiance.	2	30
Schedule	Project runs behind schedule.	Requirements and goals will not be met.	4	Lead time on components can change as well as longer than anticipated manufacturing and testing phases.	3	Review schedule weekly to determine progress and status of project	1	12
Manufacturing	Mechanical structure is manufactured out of specified tolerance	Cubesat will be misaligned and accuracy of data collection might be affected.	3	Available manufacturing equipment might not be able to reach specified precision.	2	Perform alignment procedure while the payload is within the mechanical structure.	2	12
Pointing System	Pointing system does not meet specified pointing accuracy requirements.	The optical system is not pointed toward the sun and records low and inaccurate readings.	5	Faulty COTS components. Solar tracker is damaged during transportation or testing.	2	The solar tracker will be pointed at the sun and irradiance measurements will be taken to ensure proper alignment.	1	10
Electronics Thermal Conditions	Heating from electronics caused increased noise in measurements.	Noisy measurements will cause measurements to create an inaccurate Langley plot.	4	Non-regulated temperature control within cubesat, especially in the electronics compartment.	2	Thermal analysis of electronics system.	1	8
Optics Thermal Conditions	Focused radiative source on the detector causes overheating.	Detector leaves operating temperature and gives incorrect measurements.	4	Excess light is allowed in by the initial field stop. Housing is not sufficiently thermally insulated.	2	Thermal analysis of optics system. Temperature readings are taken at detector.	1	8
Testing	Testing plan fails to verify all requirements.	Unable to verify some requirements. Unable to determine the success of project.	2	Testing equipment might not be available during testing period. Unable to procure equipment.	1	Inspect requirements biweekly to make sure each requirement has proper testing methods.	2	4

Figure 86. FMEA of NanoSAM

The top two failure modes with the same highest RPN are optical system alignment and SNR. The reason optical system alignment is the highest priority failure mode is due to the severity of the effects caused by unaligned optical system. Due to the small diameter of the pinhole there is a possibility that no light passes through the pinhole and onto the photodiode. This will result in no radiometric data being collected. Small misalignments outside the MTF budget bounds will mean the the MTF will also fail to meet its corresponding required value. As a result, critical project elements E.1 and E.2 will not be met since the radiometer will not be able to measure solar irradiance in a narrow near-infrared band and the wavelength of light will not be able to reach the photodetector.

The SNR is another high priority risk for the NanoSAM project due to its difficulty in detection and severity in its effects. The critical project element E.3 states that SNR needs to be greater than the value in SAM-II. Therefore, if the

SNR of NanoSAM project fails to meet its required value of 3500 and above due to weak signal strength, unaccounted noises, and thermal effects, the project will be considered a failure. In addition, SNR can be difficult to measure since the payload needs to be assembled for testing before using the data obtained to calculate the SNR. Hence, the SNR is the second highest failure mode in the the project’s priority.

The third highest failure mode is the measurement stability as it is one of the project’s critical project elements. The irradiance data collected by the radiometer needs to be repeatable so that the variability in the irradiance measurements can be analyzed and observed. In turn, the results attained can be reported with more confidence. Since these three factors play a large part in the critical project elements and specific objectives, they have a high priority to be addressed so that the risks can be minimized.

The goal for risk analysis is to prepare for risks and neutralize them as they appear throughout the duration of the project. Therefore, methods to mitigate these risks are used to decrease the severity, occurrence, or detection of possible failure modes. Mitigation methods were developed for all possible risks to mitigate the overall risk of the project. The actions that can be taken to lower the RPN of these failure modes are found in the table below. It shows all the failure modes in the same order as the FMEA and the anticipated SEV, OCC, and DET scores after applying the risk mitigation strategies to each failure mode.

Function	Current Controls	Recommended Action	S E V	O C C	D E T	R P N
Optical System Alignment	Manufacture to machine tolerance and follow tolerance document.	Use shim stacks to achieve better alignment. Measure with interferometer. Repeat process until desired alignment.	3	4	3	36
SNR	Build radiometric model with worst case scenario and design to assure SNR is maintained.	Add thermal insulation to ensure thermal conditions are satisfied. Increase initial field stop area to increase strength of signal. Add test points on all ground and power planes. Include jumper resistors. Use coin cell batteries as back up power source.	3	2	3	18
Measurement Stability	Purchase higher quality photodiode if required.	Perform multiple tests on photodiode before and after assembly. Adjust load resistance and reverse bias voltage of photodiode.	5	1	3	15
Photodiode Saturation	Select photodiode with large range to reduce chance of saturation.	If photodiode becomes saturated decrease area of initial field stop to decrease overall solar irradiance.	4	2	2	16
Schedule	Follow Gantt chart to determine status of project and tasks that needs to be completed.	Schedule internal deadlines to be 3 days ahead of course deadlines. Arrange 1 week of extra time for issue management.	3	2	1	6
Manufacturing	Manufacture current mechanical structure design to machine tolerance.	Manufacture another mechanical structure or make adjustments to existing structure to conform to specified tolerances.	2	1	2	4
Pointing System	Allocate additional budget to purchase additional solar tracker if needed.	Take care during transportation and testing. Budget properly to ensure additional funds are available if needed.	3	1	1	3
Electronics Thermal Conditions	Follow ICD to ensure each component draws no more than its allowed max power.	Keep all components power draw to 20% lower than max allowed power.	2	1	1	2
Optics Thermal Conditions	None	On basis of thermal modelling decrease area of initial field stop to decrease overall solar irradiance.	2	1	1	2
Testing	Follow test plan closely to monitor all requirements that needs testing. Plan testing logistics ahead of time and reserve testing equipment.	Create alternative testing methods for when testing equipments are unavailable	2	1	1	2

Figure 87. FMEA of NanoSAM with Mitigation Methods and New Ratings

To mitigate and minimize the top three risks, several actions will be taken on top of current controls. For example, the optical system alignment was previously relying solely on manufacturing components to precised machine tolerance found in a tolerance stack-up document. In reality, the manufacturing process was not perfect, so shim stacks were applied to the photodetector tube, and an interferometer was be used to measure the MTF and alignment metrics. This process was be repeated until the desired alignment and tolerance was achieved. See section 6.1.2 for a detailed description of this process. The new control method lowered the RPN of the failure mode since the photodetector will now be able to measure some irradiance data since the worst case scenario will still allow signal to reach the

photodiode. By developing and applying this mitigation strategy the optics team was able to get light to pass through the pinhole even though the requisite MTF was not met. Although the optics were not sufficiently aligned the presence of light through the pinhole indicates that the mitigation strategy was successful in its intended purpose.

For the SNR, an increase in the optical filter bandwidth will increase incoming signal, thus attaining a better signal-to-noise ratio. The project has a large amount of unassigned budget so filters with a larger bandwidth can be easily purchased if needed. To mitigate the risk of not achieving the required SNR a radiometric model with the worst-case scenario in mind was created. This ensures that unless there are massive unaccounted for sources of noise the required SNR of the system will be achieved. Besides that, switching regulators are the most likely culprits for unexpected noise entering the system. Because of this, our electronics system is designed with multiple backup options if these parts will not work. Jumper resistors allow for the power circuitry to be disconnected from the rest of the circuit. Test points on all grounds and power planes allow for the use of an external lab bench power supply. The digital electronics can be powered from the Teensy's USB connection, and footprints for coin cell battery holders are included to power the analog electronics. Coin cell batteries were chosen to power the analog section as a back up because the analog circuit has a very small current draw, and they are remarkably low noise. Subsequently, the RPN is lowered significantly using the above mitigation techniques. Although full integration testing could not be performed smaller tests to verify things such as dark current noise and noise within the electronics system were performed. Based on the results of these tests the team is confident that the SNR would meet the required value, indicating that the mitigation strategies worked as intended.

Currently the only control to ensure measurement stability of the system is to purchase a higher quality photodiode if the stability requirement can not be met. The photodiode has been tested independently of the rest of the system, so while a full integration test has not been performed the photodiode by itself The team also has excess budget that can be used to purchase higher quality photodiodes to ensure measurement stability in the anticipated operating environment. These failure modes, which present the highest cause for concern, are significantly mitigated by both the current controls in place, and the planned mitigation action.

Even though the project contains time and financial constraints, only the schedule poses a high risk for NanoSAM. The reason that budget is not a risk for this project is because the approximately 40% of the \$5000 budget is still unassigned. On the other hand, the schedule for NanoSAM is at a high risk of delays due to the requirement for precise alignment within the optical system. Through discussions with experts in the optics and manufacturing field, Mr. Jim Baer and Dr. Kathryn Wingate, the alignment process will require multiple interferometer testing that could delay the schedule. Additionally the alignment process falls along the project's critical path, meaning everything after the alignment is dependent on achieving the required alignment.

Of the five critical project elements, the risk of failing E.1 and E.2 are addressed in optical system alignment while E.3 and E.5 are addressed in the SNR and measurement stability failure modes. The reason why E.4 is not a risk is because the field-of-view that facilitates a vertical resolution of one kilometer or less can be achieved by adjusting the size of the aperture easily during the design phase. Since it is not a sensitive factor, the tolerance for the aperture size is large and does not pose as a risk of failure for NanosAM.

8. Project Planning

Hui Min Tang, Josh Horst, Jacob Romero

Throughout the project, the NanoSAM team needed to work efficiently and cohesively towards the satisfaction of all design requirements, critical project elements, and specific objectives. To aid in this process, the group applied some organizational and project planning tools commonly found in industry standards for project management. These tools include an organizational chart, a work breakdown structure (WBS), a work plan, and a cost plan.

8.1. Organizational Chart

The organizational chart illustrates the hierarchical structure of the NanoSAM team. At the top are the customer, Jim Baer, and the team's advisor, Dr. Zoltan Sternovsky. The customer defined the needs of the project and assisted

the team in the development of design solutions. Dr. Sternovsky aided the team with technical understanding of the project as well as helping to understand the format of the course.

Directly below the customer and advisor of the NanoSAM project is the project manager (PM), Hui Min Tang. The project manager organizes personnel, resources, and tasks throughout the duration of the project to maintain the organizational chart, work breakdown structure, and the workflow plan. The PM is also responsible for coordinating team meetings, solving logistical issues, preparing meeting agendas, and arranging the preparation of design reviews and reports. During every team meeting, the project manager reviews the tasks completed by the team from the previous meeting and what needs to be done before the next meeting to allocate resources to appropriate tasks. Consequently, the PM is able to keep track of the schedule closely and remind the team of both course and internal deadlines.

Below the project manager is the finance officer, Josh Horst, the systems engineer, Jacob Romero, and the safety and testing lead, Jaykob Velasquez. The finance officer is in charge of purchasing any necessary equipment, materials, or software the team will need. All purchases pass through the finance officer initially to keep track of all transactions and expenses so that the project will maintain within the given budget of \$5000. Next, the systems engineer is responsible for developing the requirements based on the customer's needs by acting as a moderator between various subsystems and maintaining a technical oversight of the whole project. The systems engineer is chiefly responsible for the development of top-level objectives and success measures. They are also responsible for requirements development and the concept of operations. Next, the safety and testing lead is responsible for acquiring test equipment and facilities along with obtaining any approvals needed during the testing phase. They are also responsible for the team's safety during manufacturing, integration, and testing. These three positions are accountable for leading the finance, safety, and successful completion of the project and as such are one level above the subsystem leads in the organizational chart.

The lowest level of the organizational chart includes all other group members and their specified subsystem leads. The subsystems that make up this project are software, manufacturing, structures, electronics, optics, and materials. Since NanoSAM project is heavily centered around optics, the subsystem consists of two co-leads. Even though each team member fulfill a leadership, the work done in each subsystem is shared by multiple people. This allows the rest of the team to contact the corresponding leads with questions about specific issues. By referencing this organizational chart, group members, the PAB, and any other outside personnel can easily determine the appropriate member to discuss their concerns, if any.

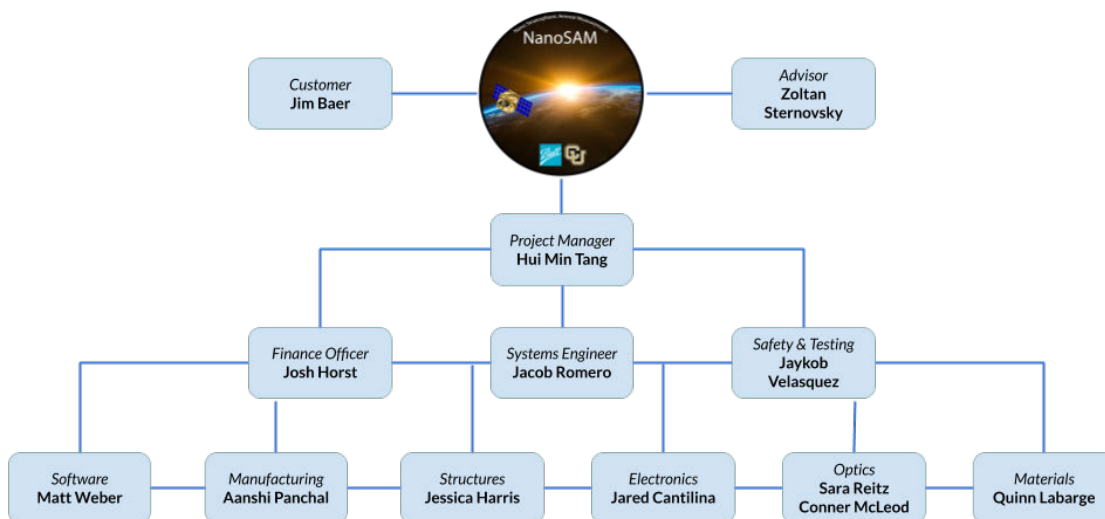


Figure 88. Organizational Chart of NanoSAM

8.2. Work Breakdown Structure

The following work breakdown structure (WBS) was developed to create specific work packages that need to be completed to achieve success in the project. Similar to the requirements flow down matrix, the WBS is hierarchical in nature. Creating the WBS this way allows the systems engineer and project manager to ensure all the requirements are satisfied through the completion of these deliverables. Each work package was created to satisfy the associated design and functional requirements. For example work packages 1.5.3.1 to 1.5.3.3 define the work needed to design and create the custom printed circuit board. The printed circuit board is vital to collect, packetize, and output the irradiance data in accordance with the third functional requirement. Furthermore, these tasks act as the building blocks of the schedule developed below. Upon completion of all the work packages, the project will be successfully completed.

- 1.0 NanoSAM
 - 1.1 Project Management
 - 1.1.1 Organizational Chart
 - 1.1.2 WBS
 - 1.1.3 Schedule
 - 1.1.4 Workflow Plan
 - 1.1.5 Project Budget
 - 1.1.5.1 Cost Plan
 - 1.1.5.2 Expenditure Plan
 - 1.1.5.3 Bill of Materials
 - 1.1.6 Design Reviews
 - 1.1.6.1 Preliminary Design Review
 - 1.1.6.2 Critical Design Review
 - 1.1.6.3 Manufacturing Status Review
 - 1.1.6.4 Test Readiness Review
 - 1.1.6.5 Spring Final Review
 - 1.1.7 Design Reports
 - 1.1.7.1 Project Definition Document
 - 1.1.7.2 Conceptual Design Document
 - 1.1.7.3 Fall Final Report
 - 1.1.7.4 Project Final Report
 - 1.2 Systems Engineering
 - 1.2.1 Project Objectives
 - 1.2.2 Critical Project Elements
 - 1.2.3 Functional Requirements
 - 1.2.3.1 Requirements Flow down
 - 1.2.3.2 Requirements Verification Matrix
 - 1.2.4 Concept of Operations
 - 1.2.5 Scope Tree
 - 1.2.6 Risk Management
 - 1.2.6.1 FMEA
 - 1.2.6.1.1 Risk Mitigation
 - 1.2.6.2 Risk Matrices
 - 1.2.7 Technical Specification Document
- 1.3 Optics
 - 1.3.1] Telescope
 - 1.3.1.1 Off-axis Parabolic Mirror
 - 1.3.1.1.1 OAP Solidworks Model
 - 1.3.1.1.2 OAP Solidworks Connection Model
 - 1.3.1.1.3 OAP Connection Tolerance Document
 - 1.3.1.1.4 Purchase OAP Mirror
 - 1.3.1.2 Filters
 - 1.3.1.2.1 Bandpass Filter Solidworks Model
 - 1.3.1.2.2 Longpass Filter Solidworks Model
 - 1.3.1.2.3 Filter Housing Solidworks Model
 - 1.3.1.2.4 Filter Housing Solidworks Connection Model
 - 1.3.1.2.5 Filter Housing Tolerance Document
 - 1.3.1.2.6 Purchase Bandpass Filter
 - 1.3.1.2.7 Purchase Longpass Filter
 - 1.3.1.3 Aperture Stop
 - 1.3.1.3.1 Aperture Stop Solidworks Model
 - 1.3.1.3.2 Aperture Stop Solidworks Connection Model
 - 1.3.1.3.3 Aperture Stop Tolerance Document
 - 1.3.1.3.4 Purchase Aperture Stop
 - 1.3.1.4 Field Stop
 - 1.3.1.4.1 Field Stop Solidworks Model
 - 1.3.1.4.2 Field Stop Solidworks Connection Model
 - 1.3.1.4.3 Field Stop Tolerance Document
 - 1.3.1.5 Mounting Tube
 - 1.3.1.5.1 Purchase Mounting Tube
 - 1.3.1.6 Pinhole
 - 1.3.1.6.1 Purchase Precision Pinhole

- 1.3.1.7 Reflective Concave Sphere
 - 1.3.1.7.1 Purchase Reflective Concave Sphere
- 1.4 Mechanical
 - 1.4.1 Optical Bench
 - 1.4.1.1 Two-tiered Flat Plates
 - 1.4.1.1.1 Flat Plate Solidworks Model
 - 1.4.1.1.2 Purchase Optical Bench Plate
 - 1.4.2 Optical Mount
 - 1.4.2.1 Mirror Mount
 - 1.4.2.2 Solidworks Model
 - 1.4.2.3 Purchase Spherical Washers
 - 1.4.3 Diode Tube
 - 1.4.3.1 Solidworks Model
 - 1.4.3.2 Precision Hemisphere
 - 1.4.3.3 Self-release Mechanism
 - 1.4.3.4 Purchase Shim Stocks
 - 1.4.4 Enclosure
 - 1.4.4.1 Purchase Rod Spacer Kit
 - 1.4.4.2 Purchase Stack Plates
 - 1.4.4.3 Purchase Enclosure Aluminum
 - 1.4.4.4 Purchase Rectangular Tube
 - 1.4.4.5 Purchase Black Paint
 - 1.4.4.6 Procure Nuts
- 1.5 Electronics
 - 1.5.1 Master Schematics
 - 1.5.2 Prototype
 - 1.5.3 Printed Circuit Board
 - 1.5.3.1 Circuit Diagram
 - 1.5.3.1 PCB Layout
 - 1.5.3.1 Order PCB
 - 1.5.4 Photodiode
 - 1.5.4.1 Circuit Diagram
 - 1.5.4.2 Photodiode Integration Document
 - 1.5.4.3 Purchase Photodiode
 - 1.5.5 Transimpedance Amplifier
 - 1.5.5.1 Circuit Diagram
 - 1.5.5.2 TA Integration Document
 - 1.5.6 Low Pass Filter
 - 1.5.6.1 Circuit Diagram
 - 1.5.6.2 Low Pass Filter Integration Document
- 1.5.7 Sigma-Delta ADC
 - 1.5.7.1 Circuit Diagram
 - 1.5.7.2 Sigma-Delta ADC Integration Document
 - 1.5.7.3 Purchase ADC
- 1.5.8 Microcontroller
 - 1.5.8.1 Circuit Diagram
 - 1.5.8.2 Microcontoller Integration Document
 - 1.5.8.3 Purchase Microcontroller
- 1.5.9 Flash Memory
 - 1.5.9.1 Circuit Diagram
 - 1.5.9.2 Flash Memory Integration Document
 - 1.5.9.3 Purchase Flash Memory
- 1.5.10 I/O Wiring
 - 1.5.10.1 Purchase Wiring
- 1.5.11 Master Integration Document
- 1.6 Software
 - 1.6.1 Master Flowchart
 - 1.6.2 Pseudocode
 - 1.6.3 Control
 - 1.6.3.1 Sun-scanning control
 - 1.6.3.2 Amplifier Gain Control
 - 1.6.4 Data Storage
 - 1.6.4.1 Flash Memory Integration Document
 - 1.6.5 Data Packetizing
 - 1.6.6 Data Transmission
 - 1.6.6.1 Data Output
 - 1.6.6.2 Command Input
- 1.7 Integration Testing
 - 1.7.1 Assembly
 - 1.7.1.1 SolidWorks Assembly Drawing
 - 1.7.1.2 Master Tolerance Document
 - 1.7.1.3 Interface Control Document
 - 1.7.1.4 Hardware Architecture Diagram
 - 1.7.1.5 Purchase Solar Tracker
 - 1.7.1.6 Procure Tripod
 - 1.7.2 Test Plan
 - 1.7.2.1 Testing Checklist
 - 1.7.2.2 Testing Flowchart
 - 1.7.3 Verification Activities
 - 1.7.3.1 Verification Analysis
 - 1.7.3.1.1 ZEMAX Model

- 1.7.3.1.2 Thermal Testing
- 1.7.3.1.3 SNR Calculation
- 1.7.3.1.4 Optical Heating Analysis
- 1.7.3.1.5 FOV Calculations
- 1.7.3.1.6 Pointing Accuracy
- 1.7.3.2 Qualification Testing
 - 1.7.3.2.1 Sampling Rate
 - 1.7.3.2.2 Dynamic Range Measurements
 - 1.7.3.2.3 Langley Plot Extrapolation
 - 1.7.3.2.4 Baseline Irradiance Measurement
 - 1.7.3.2.5 MTF Verification
 - 1.7.3.2.6 Measurement Stability
 - 1.7.3.2.7 Dynamic Range
 - 1.7.3.2.8 Measurement Allowable Error
 - 1.7.3.2.9 Optical Heating Testing
 - 1.7.3.2.10 Bandpass Filters Bandwidth
 - 1.7.3.2.11 Power Draw
- 1.7.3.2.12 Sampling Rate Bit Size
- 1.7.3.2.13 Data Storage Size
- 1.7.3.2.14 Data Transmission
- 1.7.3.2.15 Communication Timing
- 1.7.3.3 Inspection
 - 1.7.3.3.1 Payload Mass
 - 1.7.3.3.2 Payload Volume
 - 1.7.3.3.3 Payload Enclosure Volume
- 1.8 Power
 - 1.8.1 Power Distribution Diagram
 - 1.8.2 Power Budget
- 1.9 Safety Assurance
 - 1.9.1 Test Plan Safety Risks
 - 1.9.1.1 Safety Approvals

8.3. Work Plan

The work plan goes hand-in-hand with the work breakdown structure shown above. While the WBS shows the work packages that need to be completed in a hierarchical fashion, the work plan shows how the work will need to be completed in a chronological order. The Gantt charts below shows the work plan for both fall 2019 and spring 2020, beginning on September 16th and ending on May 4th. By carefully planning out the work that needs to be completed and setting reasonable deadlines, the NanoSAM team can stay on track and execute the project with success in the allotted time.

With that said, the dependencies in each task is important in scheduling. The complete list of tasks that needs to be completed can be found in Figs. 122, 123, 125, and 125 in Appendix C. Each row contains the row number and the name of the work with their corresponding start and end date. The rightmost column "Predecessor" shows the dependencies in some of the tasks. In Figs. 89, 90, 91, and 92, the dependencies can be visualized through the black lines with arrows connecting tasks with their predecessors.

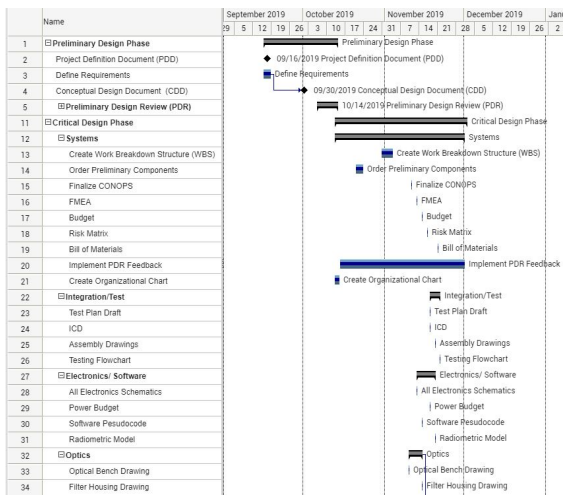


Figure 89. Part 1 out of 4 of NanoSAM Gantt chart

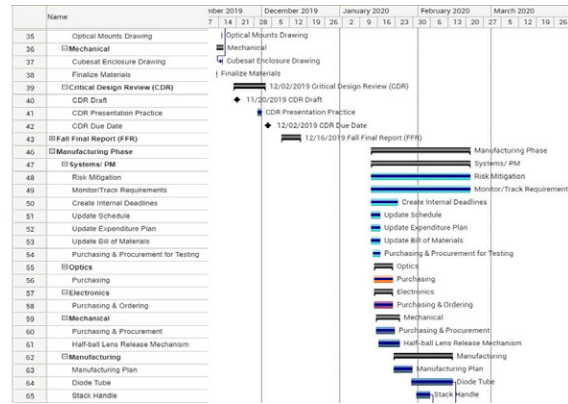


Figure 90. Part 2 out of 4 of NanoSAM Gantt chart

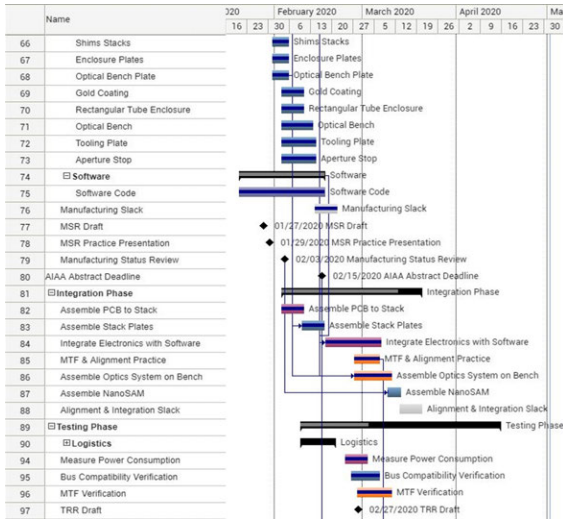


Figure 91. Part 3 out of 4 of NanoSAM Gantt chart

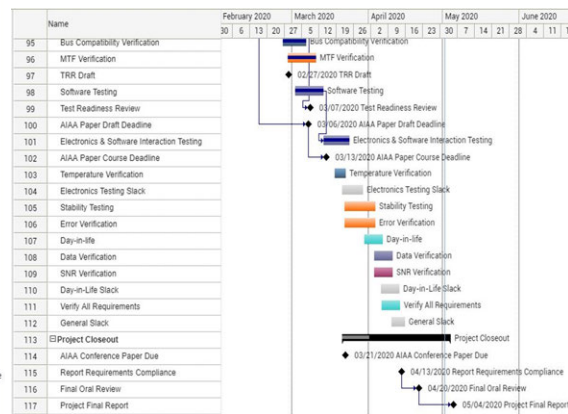


Figure 92. Part 4 out of 4 of NanoSAM Gantt chart

Fig. 89 begins with the preliminary design phase where the project goals were first defined. Then, in the critical design phase, the WBS was constructed. Preliminary designs and analysis was also created for the critical design review, which is the main milestone for that phase. Some preliminary mechanical drawings were also generated and included in the final fall report, which is the final milestone of the critical design phase.

As the spring semester began, the team started the manufacturing phase on January 12, 2020. This was when the team updated all project planning items such as the schedule, bill of materials, and expenditure plans while mitigating the risks stated in the previous section. In the mean time, all components were purchased or procured by January 22, 2020 so that manufacturing work can begin. The software accompanying the electronics was also developed simultaneously. The Manufacturing Status Review marks the final milestone of the manufacturing phase even though manufacturing continued throughout the next phase. During manufacturing, some components required reworking to meet the required tolerances. As a result, the manufacturing slack was used to allow the team to stay on schedule.

The integration phase began on January 22 and ended on March 13. During this time, the electronics and optical system was assembled together before being placed into the enclosure. The alignment of the optical system was

also implemented using an interferometer at an optical lab in Ball Aerospace Corporation. This was done over three alignment sessions over the course of two weeks.

The project was halted prior to spring break on March 18, so parts of the testing phase and the project closeout phase was not implemented. In the testing phase, compatibility tests of the integrated software and electronics subsystem was successfully performed. The final integration test of the complete payload with its enclosure would begin after all PAB members and logistical administrations have approved the project's testing procedures. The schedule contains a duration of about 17 days since the payload will most likely require multiple tests and adjustment to be successful. Finally, the project closeout phase begins on April 2 with the AIAA student conference and ends with the project final report after a report of whether all requirements are met is completed. In spite of circumstances, the AIAA conference paper, Final Oral Review, and the project final report in the project closeout phase was still completed.

From the task list and the detailed Gantt chart figures, the critical path of the project is calculated and mapped out. Figure 93 illustrates the flow of work and identifies the critical path of the project. The critical path is made up of a sequence of project network activities that adds up to the longest overall duration and is shown by the red arrows. In project management, it is important to note the critical path since they contain the most important tasks that, if missed, will delay the entire project. Therefore, it helps to determine the shortest time possible to complete the project. In Fig. 93, the sum of the duration of NanoSAM for spring 2020 totals at 100 days. Since there are 116 days in the spring semester, the team is allowed 16 days of slack. The reason for setting internal deadlines with time to spare is due to the high risk of falling behind schedule as mentioned in the FMEA of the Risk Assessment section. Some tasks that are along the critical path include the optical system alignment. If the optical system took longer than the allotted time to align, the integration and testing phases would not have been able to commence.

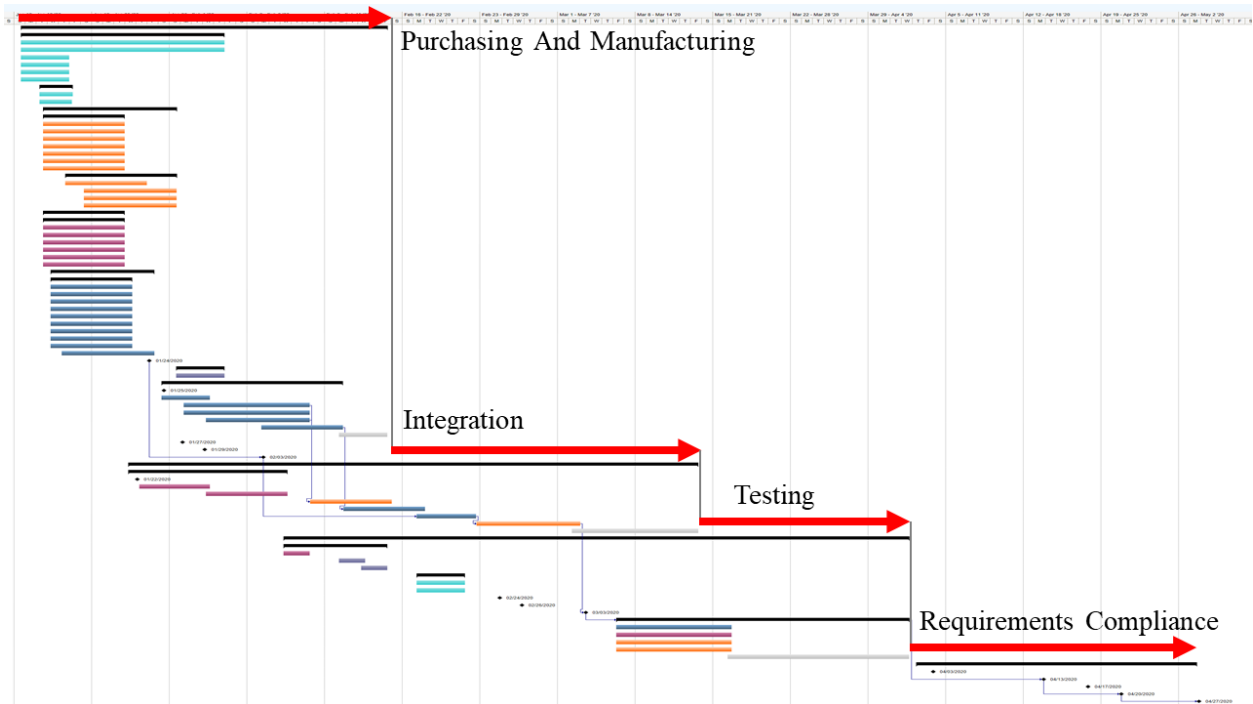


Figure 93. Gantt Chart with Critical Path.

With the extra margin assigned in the schedule, the NanoSAM project would be completed on time.

8.4. Cost Plan

The NanoSAM project had a total projected budget of \$3657 at the end of fall semester. It included 5 sections: systems engineering and project management, optical, electrical, and mechanical components, and testing and equipment use. This budget included spare parts, and an overestimation for shipping fees. The projected allocation of funds is presented in Figure 94. Note that this pie chart does not represent the actual cost.

When spring semester began, all components required for each subsystem, including testing, was purchased or procured. Components at risk of failure due to fragility, or manufacturing incompetence were procured in multiple quantities. These items include the OAP Mirror, pinhole stop, shim stock, and printed circuit board. The structural components were purchased in a quantity four times their required amount. This allowed the NanoSAM team to practice manufacturing techniques and produce early structural prototypes. The spreadsheet below presents the actual NanoSAM budget including each item's cost, quantity, specification, supplier and/or model number. These figures are separated by the five budget sub-systems: Systems/PM, optical, electrical, and structural components, and testing and equipment use.

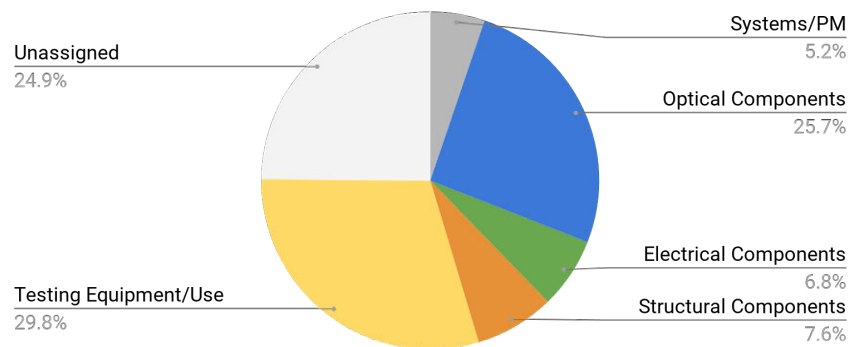


Figure 94. NanoSAM Projected Budget: \$3755

ASEN 4018: Senior Projects - NanoSAM									
Projected Final Balance:	4075.95								Order Complete
Updated Balance:	3687.29								Order In Progress
Shipping/Handling Balance:	294.56								
PROJECTED					UPDATED				
Systems/PM:									
Item:	Quantity:	Specs:	Supplier/Model:	Unit Cost:	Part Cost	Shipping/Handling Cost	Total Cost		
Pilot Deposit	1	One-time deposit	CU Boulder	200	200	0	200		
Gantt Chart Program	2	Monthly Membership	Google Gantter	5	5	0	5		
Printing	1000	Color-print	Fedex Print	0.05	35	0	35		
Optics:									
Item:	Quantity:	Specs:	Supplier/Model:	Unit Cost:	Part Cost	Shipping/Handling Cost	Total Cost		
O/A Parabolic Mirror	2	25.4 x 54.4 [mm] EFL, 30 [deg], Protected Al	Edmund Optics	214	520	8.99	528.99		
BP Filter	1	25.4 [mm], 1030 [nm], CWL, 10 [nm], FWHM	ThorLabs FLH1030-10	174	177.47	2.39	179.86		
LP Filter	1	25.4 [mm], 1000 [nm], Cut-on Frequency	ThorLabs FELH1000	177	174.22	2.39	176.61		
Filter-Mounting Tube	1	8.4 [mm] Interior threaded depth	ThorLabs SM1103	13	12.52	2.39	14.91		
Pinhole	2	Precision, Stainless Steel, 15 [µm]	Edmund Optics	52	53	3	56		
Aperture Stop	1	50 x 50 mm, 3 mm Al-6061	MetricMetals	20	0	0	0		
Half-ball Lens	1	N-BK7	Edmund Optics	48	147	11.99	158.99		
Shim Stock (12.7µm)	2	6" Wd. x 50" Lg. x 0.0005" Thick.	McMASTER-CARR 9502K56	34	68.06	3.03	71.09		
Shim Stock (25.4µm - 254µm)	2	6" Wd. x 50" Lg. x (0.001"-0.01") Thick.	McMASTER-CARR 9300K5	51	102.62	3.03	105.65		
Spherical Washers	3	4mm Thick, 12mm Outside Diameter	McMASTER-CARR 94007A030	36	57.96	3.03	60.99		
Electronics:									
Item:	Quantity:	Specs:	Supplier/Model:	Unit Cost:	Part Cost	Shipping/Handling Cost	Total Cost		
PCB	2	4-layer 100mm x 100mm	JLPCB	56	120	8.99	128.99		
Microcontroller	1	ARM Cortex-M7 at 600 MHz	Teensy 4.0	23	21.43	0	21.43		
Flash Memory	1	NOR Flash Chip	Digkey MT25QL128BA1E5E-#	20	5.4	0	5.4		
ADC	1	Sigma-Delta	Digkey LTC2470	20	10.04	0	10.04		
Passive Components	2	N/A	Digkey	75	101.89	8.99	110.88		
Photodiode	3	Silicon	FD11A	16	69.64	9.58	79.22		
Extra Components	1	-	Digkey		42.24	8.99	51.23		
Structures:									
Item:	Quantity:	Specs:	Supplier/Model:	Unit Cost:	Part Cost	Shipping/Handling Cost	Total Cost		
Rectangular Tube	1	100 x 100 x 2 mm, 24", Al-6060	MetricMetals	132	64.85	95.02	159.87		
Rectangular Plate	4	100 x 100 mm, 3 mm, Al-6061	MetricMetals	20	118.3	95.02	213.32		
Rectangular Plate	4	95 x 90.17 mm, 3 mm, Al-6061	MetricMetals	20	0	0	0		
Optical Bench Stock	1	4 x 4 [in], 2 [ft], Al-6061	McMASTER-CARR	20	74.27	3.03	77.3		
Microscrews	100	M1 x 5 mm, 0.25/pitch, 304 SST (Assorted Kit)	Uxcell - Amazon	0.05	13.99	0	13.99		

Figure 95. NanoSAM Final Cost Sheet 1

Threaded Rod	16	M3 x 120 mm, 0.5 mm/pitch, 304 SST	Uxcell - Amazon	0.5	7.67	0	7.67
Split Washers	100	M3 x 0.5 mm, SST	Uxcell - Amazon	0.12	2.81	15	17.81
G10 Fiberglass Plate	8	170 x 90 mm, 3 mm	Uxcell - Amazon	15	40.6	0	40.6
Spacer - 1	16	M3 x 70 mm, Al	Uxcell - Amazon	0.57	8.94	0	8.94
Spacer - 2	10	M3 x 45 mm, Al	Uxcell - Amazon	0.99	9.9	0	9.9
Spacer - 3	20	M3 x 8 mm, Al	Uxcell - Amazon	1.07	3.69	15	18.69
Nylon-insert Lock Nut	20	M3 x 0.5 mm, SST	Uxcell - Amazon	0.47	5.19	0	5.19
SMT Thread Tap	1	1.035" - 40 Thread	ThorLabs	93.36	93.36	2.39	95.75
Krylon Ultra-Flat Black Spray Paint	1	12 oz	Granger	8.23	8.73	0	8.73
Hand Tap	5	M1 x 0.25/pitch, 304 SST	Uxcell - Amazon	2	9.99	0	9.99
Optical Bench Bolts, Washers	1	UNC	McMASTER-CARR	99.84	69.52	24.65	104.17
Screwdriver	1	Number 0 Phillips, 6-3/4" Overall Length	McMASTER-CARR	3.34	3.34	0	3.34
Flat Head Screws	100	1-64 Thread Size, 1/4"	McMASTER-CARR	0.1148	11.48	0	11.48
Clear Sight	1	3/8 BSPP Male, Al	McMASTER-CARR	10.88	10.88	0	10.88
Testing:							
Item:	Quantity:	Specs:	Supplier/Model:	Unit Cost:	Part Cost	Shipping/Handling Cost	Total Cost
Solar tracker	1	11.1 lbs capacity, Solar Tracking Rate	iOptron Skyguider	428	919.99	96.7	1016.69
Tripod	1	11 L capacity, 3-way head	Magnus PV-3330G	20	0	0	0
Interferometer Use (Hourly)	10	Assume 10 hours of use	JILA	50	0	0	0
GND Filter	1	100 mm diameter GND	ThorLabs	436	194.78	10.96	205.74
Mounting Equipment	1	Stand and DC motor	Various suppliers	75	38	0	38
EDM Wire Shim Stack	1	EDM wire	CIRE		240	0	240

Figure 96. NanoSAM Final Cost Sheet 2

During the manufacturing phase, some components required reworking, so extra parts were purchased. The differences between the estimated cost from fall semester and the actual cost can be found in the bar chart below. Even though optics, electronics and mechanical costs increased, testing costs decreased significantly so the actual cost turned out to be lower than expected at \$3040.

As can be seen in Fig. 94 and 97, the margin takes up a large percentage of the NanoSAM budget. This margin is reserved for high risk components in case of uncertainties. The remaining predictive balance was allocated to unexpected expenses, such as an additional solar tracker or hourly interferometer rentals, and broken parts. In the end, the NanoSAM team utilized the free Ball Aerospace facility for the interferometer, resulting in the significant decrease in testing cost.

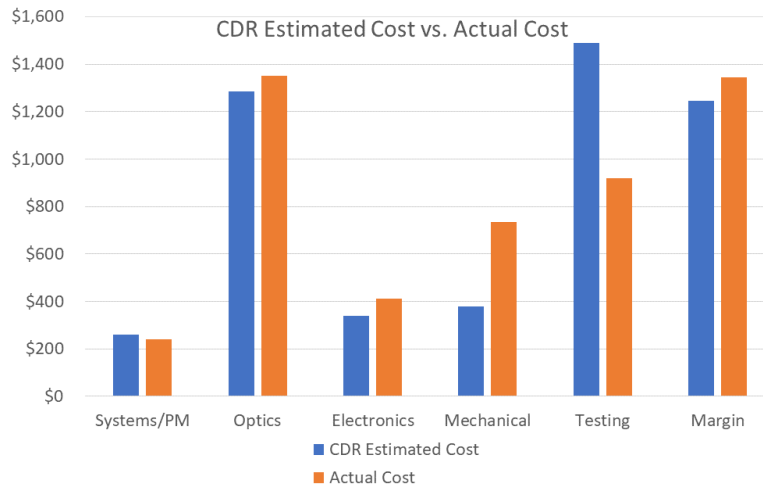


Figure 97. NanoSAM Actual vs. Predicted Budget

8.4.1. Uncertainty

Predicted budgets are inherently uncertain. The greatest uncertainty in our budget was the rental costs for alignment and testing equipment and facilities. The NanoSAM budget accounted for additional rental costs to address this; however, at the end of the the project, testing equipment did not cost as much while structural components cost more than initially thought. Another potential unanticipated project cost was a printed circuit board malfunction. The NanoSAM team was able to acquire custom printed circuit board from domestic manufacturers with short lead times and was able to respond quickly. The NanoSAM team also purchased an additional gold OAP mirror due to a longer lead time on the aluminium OAP mirror. These could not have been done without the allotted margin for uncertainties.

8.4.2. Industrial Cost Breakdown

The total industrial cost for the NanoSAM device when the project ended after 25 weeks was \$372,939. This accounted for all the materials and hourly services needed for manufacturing and a estimated industrial salary of \$31.25 per hour. An overhead rate of 200% was included into the salary and materials cost. If the project continued through to the end of April, following the expected schedule in fall, the total number of weeks spent on the project would be 30 weeks with 4393.8 hours of work. Adding the overhead rate to the corresponding salary and materials cost resulted in a total cost of \$422,889. A breakdown of the cost is shown in Fig. 98 below.

	25 Weeks			30 Weeks		
Item	Quantity	Per Cost	Total	Quantity	Per Cost	Total
Materials and Hourly Services	-	-	\$3,657	-	-	\$3,657
Salary	3861 hrs	\$31.25	\$120,656	4393.8 hrs	\$31.25	\$137,306
Overhead rate	200% above cost	-	\$248,626	200% above cost	-	\$281,926
	Total Cost		\$372,939	Total Cost		\$422,889

Figure 98. Industrial Cost Breakdown

8.5. Test Plan

The tests detailed in Table 13 describe the major tests that were performed or planned to be performed by the team to demonstrate the functionality of the NanoSAM. However, there are many smaller tests that need to be performed to verify all of the design requirements. The table given in Fig.99-100 describes, for each test, the requirements verified, the required support equipment, and the data collected. The data collected from each test would be compared to the required values from the associated requirements to ensure it has been properly verified.

RQMT Verifying	Test Description	Support Equipment	Data Collected	Date Performed
1.1	The vertical resolution of the optical system will be determined by using the calculated field of view and extrapolating it to an on orbit altitude.	Optical system, ruler	Optical system vertical resolution in km	N/A
1.1.1	The FOV will be determined analytically using measurements of the system's actual aperture diameter.	Optical system, ruler	Optical system FOV in degrees	N/A
1.1.1.1	The pointing accuracy of the solar tracker will be analytically determined using data from the solar tracker specifications.	Solar tracker	Pointing accuracy of solar tracker in degrees	N/A
1.2	Light at a wavelength between 1.018 and 1.042 micrometer will pass through filter onto the photodiode. The photodiode will collect irradiance measurements and ensure that light outside of the specified range of wavelength has been filtered by the band pass filter. Incoming light source will then illuminate the photodiode. This will ensure light of the desired wavelength is allowed to pass through the filters.	Variable wavelength light source, photodiode, black room or curtains to block stray light	Presence of measured irradiance data	N/A
1.3	Using an interferometer, the optical system will be aligned by getting the tip and tilt metrics and shimming the system until both are close to zero.	Optics system, interferometer, precision half sphere, half sphere removal tools, optical shims	Optical system tip and tilt metrics.	3/6/2020
1.3.1	During alignment of the system, the MTF of the system will be output by the interferometer.	Optics system, interferometer, precision half sphere, half sphere removal tools	Optical system MTF	3/6/2020
1.3.1.1	A regulated light source will be measured for irradiance with the optics system and compared to the theoretical value calculated by using a known light filament with a highly regulated power supply.	Regulated light source, optics system	Irradiance data from a regulated light source	N/A
1.3.1.2	A regulated light source will be measured for irradiance with the optics system and compared to the theoretical value for multiple levels of light attenuation across multiple tests.	Regulated light source, optics system, rotating GND filter	Irradiance data from a regulated light source.	N/A
1.3.1.3	A regulated light source will be measured for irradiance with the optics system and compared to the theoretical value over the anticipated operating temperature.	Regulated light source, optics system, thermally controlled environment	Irradiance data from a regulated light source.	N/A
1.3.2	The optical system will be transported and tested for alignment multiple times, ensuring standard transportation methods do not impact the alignment of the optical system.	Optics system, interferometer	Optical system tip and tilt metrics.	3/6/2020
1.4	An analytical model of the SNR will be produced with worst case scenarios in mind. Physical measurements of noise of the electronics will be made to incorporate into the model. The value derived from this model will be compared with the required value to ensure the SNR is met.	Electronics system, photodiode, oscilloscope	System SNR	3/11/2020
1.5	A regulated light source will be increased from 0% radiation to 120% maximum expected solar radiation and irradiance measurements will be taken to ensure the photodiode does not become saturated.	Regulated light source, optics system	Irradiance data from a regulated light source.	N/A
2.1	The optics and electronics system will be placed into the external housing and inspected to ensure a proper fit.	Payload, external housing	Payload Volume	3/7/2020
2.2	The overall system will be weighed using a scale.	Payload, scale	Payload Mass	3/7/2020

Figure 99. Test Plan Part 1

2.3	The optics and electronics system will be placed into the external housing and inspected to ensure a proper fit.	Payload, external housing	Enclosure Volume	3/7/2020
2.3.1	Sand and dust testing will be performed in a laboratory setting.	Payload, external housing	Presence of dust on optics system	N/A
2.3.2	The optical and electronics system stack will be removed from the enclosure and replaced multiple times to ensure a snug yet acceptable fit for the measurement system.	Payload, external housing	Demonstration Report	3/7/2020
2.3.3	The photodiode will be placed in the housing at points not exposed to the anticipated optical light path to ensure light is only being allowed in through the designated area.	External housing, photodiode, oscilloscope	Irradiance Data	N/A
3.1	During various tests data will be taken and captured, the presence of all recorded data will be checked for.	Payload, external computer source	Irradiance Data	2/30/2020
3.1.1	Data will be captured by the system for a set amount of time and analyzed to ensure sampling of at least 50 Hz.	Payload, oscilloscope	Irradiance Data	2/30/2020
3.1.2	Data will be captured by the system and specific packets of information will be examined to ensure 10 bit data transmission.	Payload, oscilloscope	Irradiance Data	2/30/2020
3.1.3	During various tests the incident irradiance on the optics system will be decreased such that the software will command the payload to stop capturing data.	Payload, oscilloscope	Demonstration Report	N/A
3.2	During various tests data will be taken and the group will output the data. Only if the data successfully outputs can the group say the electronics system has successfully packetized the data.	Payload, external computer source	Irradiance Data	N/A
3.2.1	During various tests data will be taken, including 100 Mb of experimental data during overall demonstration.	Payload, external computer source	Irradiance Data	N/A
3.3	During various tests data will be taken and the group will output the data to an external computer source to ensure all other aspects of the electronics system have performed the necessary functions.	Payload, external computer source	Irradiance Data	N/A
3.3.1	Once data has been collected by the electronics system it will be transferred to an external computer source via a serial port connection.	Payload, external computer source	Irradiance Data	N/A
3.4	The software will demonstrate its ability to command the payload to collect, store, and output irradiance data through basic functionality testing, code review, unit testing, and single-user performance testing.	Payload, external computer source	Software Test Report	N/A
3.5	A power budget for the system will be analytically formulated, and the electronics system will be tested to ensure the power draw conforms to the required value.	Electronics system, oscilloscope	System Power Metrics	N/A

Figure 100. Test Plan Part 2

The following table shows the overall test plan for the NanoSAM project. There are three main tests to verify the functional requirements of the system. The first is the optical system alignment. This test would ensure that the MTF of the system is at the required specific objectives level and that the optical system is aligned such that the measurement device would be able to collect the appropriate data to the required accuracy. Once the optical system is aligned, the team would be able to test the measurement device in a laboratory setting. This laboratory testing is also vital to ensure the measurement device is capturing accurate data. During this stability testing, the team would also perform smaller tests to verify the sampling rate, data bits, and other design requirements.

Performing this stability testing would prove that the measurement device is capable of collecting correct and scientifically accurate data. After conducting all the necessary laboratory tests, the team would then move onto the integration testing phase of the test plan. This test would be performed in an open space in front of the Ann H. J. and Smead Aerospace building. By testing the device in a dynamic environment, requirements such as optical heating and power draw can be verified. This test represents the closest environment to on-orbit conditions that the NanoSAM system can be tested in.

In the table below, the testing phases are presented in chronological order, with optical system alignment being performed first and integration testing last. This overall test plan creates a clear path to success for the team.

Table 13. Test Plan Overview

Test Phase	Location	Support Equipment	Requirements Verified
Optical System Alignment	Ball Optics Lab	Interferometer, Optical shims, Reflective concave sphere, torque wrench	MTF
Stability Testing	LAIR Lab	Gradient filter and associated equipment, highly regulated power source, tungsten bulb, oscilloscope	SNR, Stability, Error, Dynamic Range, Band pass filter, Sampling rate, Data bits, Data transmission
Integration Testing	CU Aerospace Building	Solar tracker, tripod, GPS, solar tracker to NanoSAM mount	Optical heating, Pointing accuracy, Power draw, Data storage, Payload mass and volume, Housing, Timing communication

8.6. Design Validation

To validate the function of the entire system, a full systems integration test will be performed. This will be the last test conducted and is designed to make sure that the assembled and integrated system functions as a whole. The test setup is described by Fig. 3 in Section 3.2. The data that is gathered during this test will then be used to create a Langley plot. In order to properly utilize the Langley plot method, data recorded during an integration test must include irradiance values with known zenith to find the airmass value of each data point as shown in Fig.102. By arranging the data in the form of Eq. 10 into a logarithmic scale plot, the optical depth can be estimated. Once the slope is known, the values can be extrapolated to zero airmass, which would be the expected irradiance at zero atmosphere (orbit). In Fig. 101, an example Langley plot is shown. As seen in Fig.101, the Langley Plot Method utilizes Eq. 10 to extrapolate out what the solar irradiance is at an airmass of 0, I_o . [27]

$$\frac{I}{I_o} = e^{-m\tau} \tag{10}$$

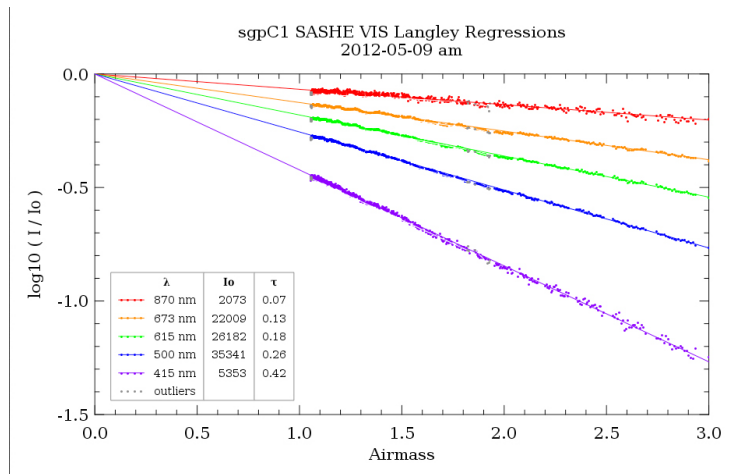


Figure 101. Example Langley Plot [3]

The test procedure with data processing overview is as follows. As mentioned previously, using Eq. 10 on the

test described in Fig. 3 will produce points similar to those seen in Fig. 101. Those points will then be used to determine τ . In order to determine m , the process described in Fig. 102 will be employed, with the zenith angle being measured directly during testing. The value of I will be gathered during testing and used in conjunction with the respective m and τ found during the processing stage. These values will be used to determine what I_o is for the wavelength that NanoSAM will sample at during the test, around $1.03 \mu m$. The results from this test, mainly the value of I_o , will be compared with known tabulated experimental data from official resources. The interpolated values for I_o will be used to determine if the NanoSAM project is able to produce results that other projects have also produced. If it is determined that the NanoSAM project does produce a value of I_o that satisfies the customer, then the design of NanoSAM will be validated.

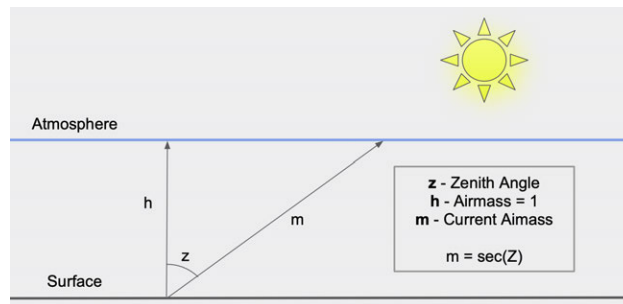


Figure 102. Airmass Determination Method

9. Lessons Learned

Quinn LaBarge, Conner McLeod, Jaykob Velasquez, Hui Min Tang, Aanshi Panchal, Matt Weber, Jacob Romero, Jessica Harris, Jared Cantilina

9.1. Optics

Diving into the design and development of an optics system was a fun and challenging experience. From the start of the semester the optics team was faced with the reality that this project would required an in depth understanding of fundamental optical theory. The optics team learned that attempting to jump into the design of the radiometer without first obtaining this baseline knowledge was a fruitless endeavor. Fortunately, with the help of Jim Baer, the optics team was able to build the required foundation in optics. An important part of this foundation was the comprehension of the extremely precise alignment requirements. As a result, the team was able to create a baseline design that facilitated alignment while also meeting the other requirements determined for this year's senior project.

The development of the NanoSAM optical instrument required the optics team to become familiar with advanced optical modeling software. At first the optics team underestimated the challenge of learning this software and eventually had to reach out to professionals in order to properly utilize the full capability of the optical software. Valuable knowledge was also gained when integrating the Zemax optical model with the mechanical SolidWorks model. The team learned that a back and fourth flow of information between the analytical optical models and solid models was essential to the success of the project.

As mentioned above, one of the most critical project elements involved the alignment of the optical system. Over the course of the project, the team pioneered an interferometric alignment procedure. While this procedure was viable in theory, it was very difficult to implement in practice. By the spring semester, the team had no hands on experience with the tools required for the alignment. When the time came to align the system, the optics team was forced to verify that each step of the alignment process was working as planned. This was a painfully slow process and spanned several lab sessions. Training with the interferometer setup, analysis software, and optomechanical stages prior to the alignment testing would have streamlined the process considerably.

9.2. Manufacturing

The manufacturing process was one of the most critical parts of the NanoSAM project. This was because all of the mission critical optical components was to be made with this manufacturing process. The importance of planning ahead was especially important, such as knowing tolerances for each part and having an idea for the typical manufacturing processes needed for each part. This especially played into the role of making a manufacturing plan with Matt Rhode and his assistant Nate to ensure that our parts could be manufactured in a relatively simple fashion. On a similar note of planning ahead, to ensure that manufacturing could be started as soon as possible, every person on the manufacturing team should have gotten their training as soon as possible in the first semester of projects to avoid the scheduling issues that came when second semester came around.

The phase "measure once, cut twice" became an important moto for this subteam as well. Many parts, including the high precision diode tube and the complex optical bench, had to be remade multiple times due to measuring mistakes. A way that this could have been easily mitigated was to have more time allotted to each part and not try to make things as quickly as possible.

However, everyone in the subteam thought it was a wonderful experience to learn how to use various tools such as CNC machine, mill, vertical and horizontal bandsaw. Useful measuring tools such as a sine bar, micrometer, and gauge pins were also interesting to use to ensure all of our tolerances were met.

9.3. Electronics

The lessons learned from electronics came mostly during the spring semester when everything was being put together. The first PCB that was ordered had an issue with the internal planes not connecting correctly. This occurred because the PCB CAD software removed the connection when exporting the board design to manufacture files. From this we learned to pay more attention to exactly what the software is doing when converting between design steps. Also a more thorough check of the design files before ordering would've caught this issue. The second set of boards had an issue with the footprint of the ADC, resulting in a switch to using the on board ADC of the microcontroller. This could've been caught by a more careful review of all the custom footprints on the board. However, this also showed how necessary all the risk mitigation and backup options built into the electronics system were. Despite these issues a working electronics system was completed and testing started while the issues were resolved and a new board ordered.

9.4. Software

Although the software for NanoSAM was fairly short compared to other projects, it took longer than expected to complete. Researching libraries and functions, then implementing them took a lot of debugging and trial and error to get working correctly. Starting earlier on the software would have been beneficial to allow time to learn the best and most efficient ways of programming the Teensy microcontroller. Pseudocode and functional block diagrams are the best way to start the programming process because they serve as benchmarks to keep the software going in the right direction and making sure it is functioning as it should. Frequent testing and debugging as the software develops is necessary to ensure efficient and functional code. Utilizing GitHub is important to allow version tracking of branches of the software, especially if multiple people are working on developing the code separately. An efficient way of developing the software during subteam meetings was to display the code on a large screen in front of the whole subteam and work on it together so multiple people could research libraries and functions when an error or bug occurs. Working on it collaboratively also allowed the entire subteam to be on the same page with the software rather than individuals working on it separately then later reporting changes to the code.

9.5. Systems Engineering

The optical nature of this project presented unique systems engineering difficulties, particularly in the requirements definition process. As the optics team and systems engineer learned more about the technical aspects behind the optics

of the project it greatly impacted the requirements of the entire project. One of the major lessons learned through the systems engineering portion of the project is that the team must quickly understand the technical knowledge behind the project, especially when the team has very little experience in the area of interest. By gaining an understanding of the optical aspects of the project the systems engineer, and by extension, the rest of the team can make informed decisions about requirements, risk mitigation, and design choices.

9.6. Project Management

Project management proved to be more complicated than expected throughout the project. When scoping the project, knowing the type of project and which project management method should be used would allow the team to be more efficient. However, the nature of the project and method used was not established until much later, halfway through the project. Besides that, due to the structure of the course, a Gantt chart was not developed until November. As a result, it was difficult to establish internal deadlines and milestones for the team to follow. Besides that, knowing what the team, as a whole, expects from the project would greatly increase the value of advisors and customer meetings. Future teams should focus on deciding project management methods early on and create Gantt charts or work plans as early as possible to keep track of milestones, making sure to update the Gantt chart once a week as more information becomes available. Other advice for future teams includes creating agendas for every meeting and keeping a good record of meeting notes. If all team members could read through meeting agendas and include topics that they would like to discuss about, meeting productivity and efficiency would increase greatly.

10. Individual Report Contributions

Jared Cantilina - Electronics Design, Electronics Verification, Risk Assessment, lessons learned, Electronics designs considered and selected,

Jessica Harris - Optics Designs Considered, Filter Selection (Appendix A), Electronics Detailed Design (4.3), Signal-to-Noise Model (4.3.4 and Appendix B), Electronics and Software Manufacturing (5.3 and 5.4), Electronics Integration and VV (5.5.2 and 6.2), Test Plan (8.5)

Josh Horst - Structural Baseline Design Overview (4.3.5), Structural Detailed Design (4.3.6), Structural Manufacturing (5.1), Optics Manufacturing (5.2), Optomechanical Integration (5.5.1), Cost Plan (8.4). I designed and described the plate module system and enclosure in Sections 4.3.5 and 4.3.6. I provided a detailed description of the structural and optics manufacturing process, and included many real images in Sections 5.1 and 5.2. I also described the integration of the optics and structural sub-systems in Section 5.5.1. Lastly, I presented the projected and actual cost plan for the NanoSAM team as well as an analysis of the uncertainty in our initial budget in Section 8.4.

Quinn LaBarge - Optics Subsystem Alternative Designs (4.1.2), Optics Baseline Detailed Design Overview (4.3.1), Optics Detailed Design (4.3.2 - Vertical Resolution, Thermal Effects, and Sighting Tabs), Optics Verification and Validation (6.1 - Alignment Tools Fizeau Interferometer, Final Alignment Verification), Lessons Learned

Conner McLeod - Optics Baseline Design Overview (4.3.1): Analytical Optics; Stray Light; MTF Budget, Optics Detailed Design (4.3.2) Optics System Alignment Verification and Validation (6.1.2): Opto-mechanical Hardware and Stages; Zernike Coefficient Model; Final Alignment Verification, Optics Lessons Learned (9.1)

Aanshi Panchal - Structural Manufacturing (5.1), Diode Tube, Aperture Stop ζ , Optics Manufacturing (5.2), Integration of Parts (5.5) Mechanical Verification & Validation (6.3), and Manufacturing Lessons Learned (9.2). I organized the whole Manufacturing section by planning out what needed to be said for each subsection as well and ensured that everything that needed to be said was said

Sara Reitz - Optics Designs Considered (4.1.2), Filter Selection (4.2.8), Baseline Design Optics (4.3.1), Optical Components (6.4.1), Spectral Filtering (6.4.2.a), Integration of the Optical Subsystem (6.5.4), Measurement Stability and Error Verification (7.1), Integration Verification and Validation (6.4), Lessons Learned (9)

Jacob Romero - Project Purpose, Project Objectives Functional Requirements, CONOPS Development, Requirements Development, Manufacturing Optical Shims, Risk Assessment Mitigation, Project Planning

Hui Min Tang - Project Purpose (2), Specific Objectives (3.1), CONOPS (3.2), Project Deliverables (3.3), Functional Requirements (3.5) Requirements Flow-down (4.2), Critical Project Elements (4.4), Risk Assessment & Mitigation (7), Organizational Chart (8.1), Work Breakdown Structure (8.2), Work Plan (8.3), Cost Plan (8.4), Lessons Learned-Project Management (9.6)

Jaykob Velasquez - Optics Baseline Design Overview (4.3.1), Optics Detailed Design (4.3.2): Physical Optics System Assembly, Optics Component Integration Verification (6.1.1), Optics System Alignment Verification and Validation (6.1.2): Alignment Tools; Final Alignment Verification, Lessons Learned (9.4)

Matt Weber - Electronics Designs Considered and Trade Studies (4.1.1), Software Design Overview (4.3.7), Software Detailed Design (4.3.8), Software Manufacturing (5.4), Electronics Integration of Parts (5.5.2), a little bit in Electronics Verification & Validation (6.2), Software Lessons Learned (9.4)

11. Appendix A: Alternate Designs Considered & Trade Studies

11.1. Alternate Designs Considered

11.1.1. Electronics System

The electronics system must meet the requirements Radiometry, Measurement Stability, Measurement Error, SNR, Dynamic Range, Data Collection, Data Storage, Data Output, and Average Power Draw. There are multiple ways of achieving these requirements, but all of them require a photodiode to turn solar radiation into an electrical signal, a way to read that electrical signal, memory to store the data, and a controller to send data.

Photodiode Selection

A photodiode is a light-sensitive semi-conductor. Incoming photons increase the energy of a valence electron in the P region of a P-N diode and drives it across a bandgap to the anode. A free electron from the N region flows into the absent electron's hole, drawing in another electron from the cathode. Light is thus converted to a proportional current. The relationship between incoming intensity is linear until saturation. Saturation occurs when there is not enough electric potential across the diode to sweep all electrons to the anode before they recombine with their holes.

Photodiodes are primarily differentiated by the structure and the materials used to make them. Fig. 103 below depicts a standard photodiode.

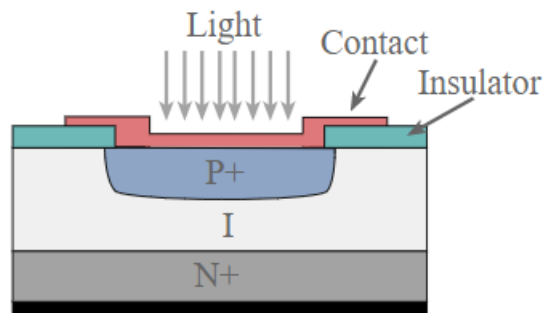


Figure 103. A cross section of a typical PIN photodiode, showing the P layer, the Intrinsic layer, and the N layer.

Photodiodes primarily differ in the semiconductor used. The most common are silicon, indium gallium arsenide, and germanium. Different materials allow for peak responsivity at different wavelengths. The responsivity is the number of amps of current produced per watt of incident light.

1. Silicon

Silicon (Si) photodiodes are primarily used for measuring wavelengths from 190-1100 nm. They also produce low dark current, ranging from 35 pA-600 nA (@ 5V). A large advantage is that the average price for a Si photodiode is less expensive than other materials, which addresses a critical element for the project [42]. Silicon photodiodes were used on SAGE-II.

Pros	Cons
Less noise than Ge photodiodes	Higher max bias voltage
Larger active area	
Produces low dark current	

Table 15. Summary: Pros and Cons of Silicon Photodiodes

2. InGaAs

Indium Gallium Arsenide (InGaAs) photodiodes are primarily used for measuring the near-infrared spectrum, from about 800nm to 1700nm. This coincides with our measured wavelength. However, they generally have a lower overall responsivity, particularly from 800 - 1100 nm. These photodiodes are very quickly responsive; the rise time of the current is on the generally between 300ps and 25ns. A downside of these photodiodes is their price. They are moderately expensive - more expensive silicon photodiodes but often cheaper than gallium photodiodes.

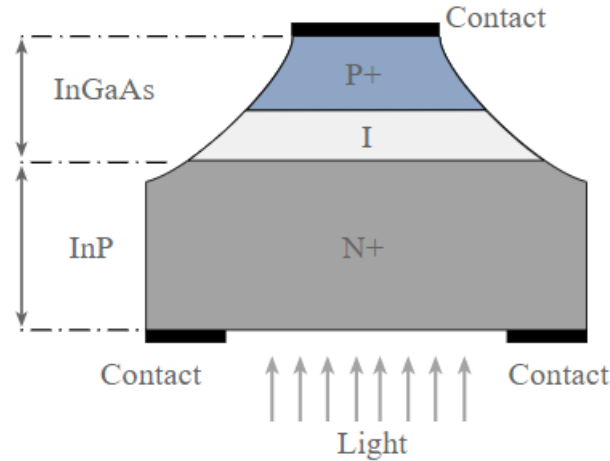


Figure 104. A typical cross section view of the heterojunction PIN photodiode

Pros	Cons
Can measure 1020 nm wavelength	Moderately Expensive
Low dark current	Smaller active areas
High speed (low rise time)	

Table 16. Summary: Pros and Cons of InGaAs Photodiodes

3. Germanium

Germanium (Ge) photodiodes are have the largest active area compared to the Si and InGaAs alternatives. However, they comes with several drawbacks. First, Ge photodiodes are quite expensive, generally hundreds of dollars each [42]. Second, their sensitivity at 1020 nm is quite low - Ge photodiodes are more responsive to longer wavelengths of incident light.

Pros	Cons
Large active area	Low responsivity at 1020 nm
	Very expensive
	Slow rise time
	Large dark current

Table 17. Summary: Pros and Cons of Germanium Photodiodes

ADC Selection

The analog signal produced by the photodiode must be converted to a digital value by an ADC for storage. ADCs vary in mechanism, which impacts their write speed and accuracy. Our requirements require high write accuracy, but

the required 50 Hz sample rate doesn't require substantial speed, so accuracy is weighed above speed in the following trade studies. These studies consider three ADC architectures: flash, successive approximation, and sigma delta.

1. Flash

Flash ADCs are the fastest and least accurate type of ADC available. They use a network of resistors and comparators to determine the voltage level of an input signal. This results in an extremely fast conversion, however inaccuracies in resistor network resistance means this ADC is less accurate than other types.

The primary advantage of a flash ADC is its speed. Flash ADCs have incredibly high sample rates compared to other ADCs. However for this mission the signal we will be measuring will not require a high sample rate. Flash ADC types are also common, easy to use, and cost less than other ADC types.

The primary disadvantage of a flash ADC is the low resolution and inaccuracies. Flash ADCs require 2^n comparators on the chip, where n is the resolution of the ADC. This limits the resolution of flash ADCs to around 8 bits. This mission will require a highly accurate conversion of relatively small signals, therefore this is a large disadvantage.

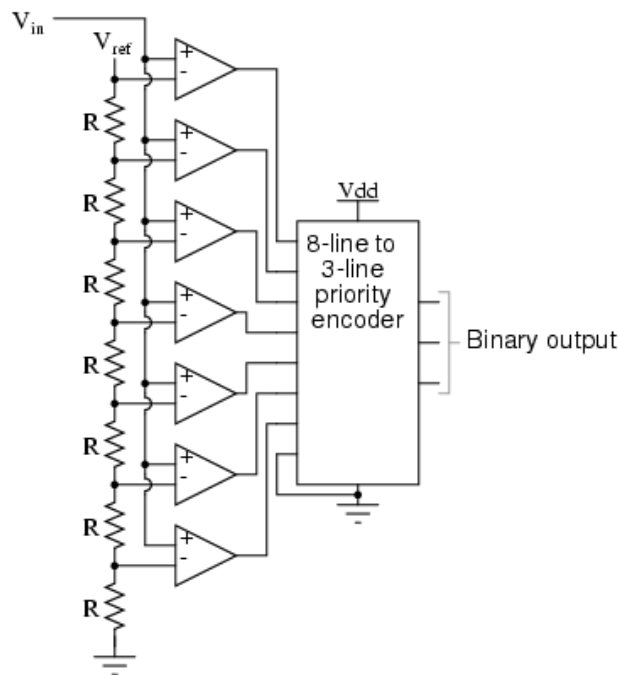


Figure 105. Flash ADC

Pros	Cons
High Sampling Rate	Low SNR
	Low resolution
	High Power Consumption

Table 18. Summary: Pros and Cons of Flash ADCs

2. Successive Approximation (SAR)

Successive Approximation (SAR) analog-to-digital converters have higher accuracy, low power consumption, low latency time, and are easy to use. The internal circuitry works as follows: (1) the analog signal is sampled and held by a latch, (2) the sample is compared to an analog voltage generated by a DAC. The ADC works from most to least significant bit. (3) outputs a digital approximation at the end of the conversion. A block diagram of the SAR ADC is presented below.

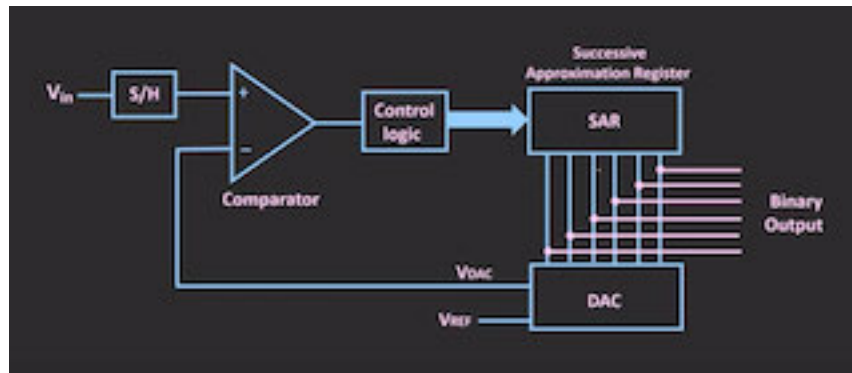


Figure 106. Successive Approximation ADC Block Diagram

Primary advantages of the SAR ADC are low power consumption, small volume, and increased resolution. The resolution of the SAR ADC ranges from eight to 16 bits, which fulfills our resolution requirement.

The primary disadvantage of the SAR ADC is its low sample rates for higher-resolution data. The ADC frequency is important for data processing and must meet the functional requirements of the system design. The SAR ADC also increases in size as resolution increases.

Pros	Cons
Low power consumption	Low sampling rate (for greater resolution)
Medium SNR	
Medium Resolution	

Table 19. Summary: Pros and Cons of SAR ADCs

3. Sigma-Delta

Sigma-delta ADCs offer very high resolution, high integration, and low power consumption. They include a 1-bit modulator, a digital filter or integrator, and a decimator. Sigma-delta ADCs utilize oversampling and noise shaping to provide a high resolution and low noise digital representation of the analog signal. A circuit diagram of the sigma-delta ADC is presented below. Sigma-delta ADCs are the most accurate of the options considered.

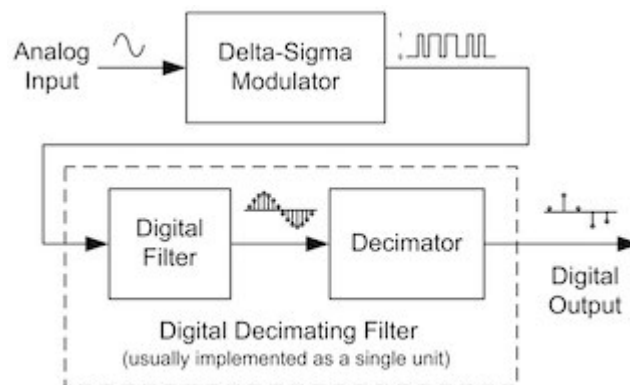


Figure 107. Sigma-Delta ADC Block Diagram

Primary advantages of the sigma-delta ADC are high resolution, low noise, and low cost. The utilization of digital filtering decreases the noise directly and simplifies our design. This will aid in acquiring a more accurate digital representation of the analog signal at a low cost and low power consumption.

The primary disadvantages of the sigma-delta ADC are low speed, and high latency time. The hardware of this ADC must operate at the oversampled rate which is larger than the maximum signal bandwidth. Additionally, Sigma delta ADCs can have significant latency times due to their complexity. This is not much of an issue for us because the data is simply stored and not used immediately.

Pros	Cons
High resolution	Low sampling rate
High SNR	High latency time
Low power consumption	

Table 20. Summary: Pros and Cons of Sigma-Delta ADCs

On-Board Controller Selection

1. Field-Programmable Gate Array (FPGA)

A field-programmable gate array, or FPGA, is a microchip consisting of configurable logic gates. This allows for custom integrated circuit design. FPGA synthesis tools allow for high level programming to be implemented in the FPGA fabric. FPGAs are extremely versatile, but are difficult to program, as they have a very steep learning curve. A microprocessor can be instantiated on the FPGA fabric to run high level C code.

The primary advantage of an FPGA for the on-board computer comes from its versatility. Any software or firmware required could be implemented on an FPGA, and it would be possible to create interfaces for all peripheral electronics.

The primary disadvantage is the complexity of programming an FPGA. While any possible interface could be created, it is extremely difficult to do so. The primary languages used to program an FPGA, Verilog and VHDL, are very different from more traditional programming languages, and are difficult to master.

Pros	Cons
Extremely versatile	Very complex
Allows for fast measurements	Difficult to program

Table 21. Summary: Pros and Cons of FPGA Controller

2. Micro-controller

A microcontroller is a microprocessor with integrated supporting electronics on a small circuit board. They are well suited to run simple repetitive tasks that are not very processor-demanding. They often have limited hardware interfaces, so compatibility with other components must be considered.

Pros	Cons
Low cost	Limited processing power
Small size	Limited interfaces
Simple programming	

Table 22. Summary: Pros and Cons of Micro-Controller

3. Single Board Computer

A single board computer (SBC) is a processor and supporting electronics on a single printed circuit board. These generally have much more processing power than a microcontroller, but are also limited in their hardware interfaces.

Pros	Cons
Low cost	Complex to code, not the best for prototyping
High speed	Large size

Table 23. Summary: Pros and Cons of Micro-Controller

External Memory Selection

An external memory source stores the data collected by the instrument. Considering the low sample rate and relatively few measurements per orbit, not much data storage is needed to store a substantial amount of irradiance data.

1. Solid State Drive (SSD) Card

Benefits of using an SSD would be having a very high storage capacity and be able to write fast while drawing relatively little power. However, they have the largest mass of options considered. Solid state drives consist of flash memory arrays controlled by an on card processor. These processors can be extremely susceptible to radiation damage, taking down the entire storage system when they fail.

Pros	Cons
High storage capacity	Larger volume/mass for CubeSat
Fast writing speeds	
Draws little power	

Table 24. Summary: Pros and Cons of SSDs

2. Micro-SD Card

Micro-USB cards are external memory cards that are similar to traditional SD cards with the benefit that they are smaller in mass and volume. SD cards are an extremely popular storage solution for CubeSats due to their price and ease of use. Many microcontroller boards have built in SD card slots. However, there are many drawbacks to SD cards in space. Like SSDs, they consist of arrays of flash memory controlled by a microcontroller. This microcontroller commonly fails due to radiation damage. Additionally, thermal expansion and contraction of the contacts between the SD card and SC card slot can cause failure of the SD card.

Pros	Cons
Small in volume and mass	Can be damaged by radiation
Cheap and easy to use	

Table 25. Summary: Pros and Cons of Micro-SDs

3. USB (Flash Drive)

Flash drives are very similar to SD cards, an array of flash memory accessed through a microcontroller over a USB interface. They also have similar pitfalls from radiation and interface. The advantage of USB drives is that they can plug into almost any system isn't useful for a a CubeSat application.

Pros	Cons
	Susceptible to radiation damage
	Large volume

Table 26. Summary: Pros and Cons of USBs

4. Flash chips

All the devices listed above use flash storage, and differ primarily in interface type. It would be possible to

bypass the interface and radiation sensitive controller by building a custom PCB (which is necessary anyway) with on board computer and flash memory chip. This would limit our on board computer to controllers that can interface with external flash memory.

Pros	Cons
More immune to radiation damages	More complex to use
Fastest read/write	Limits main processor selection

Table 27. Summary: Pros and Cons of NAND Flash

11.1.2. Optics Designs Considered

The NanoSAM instrument is required to take solar irradiance measurements in a narrow spectral band around 1.02 μm . Near the chosen center wavelength, atmospheric absorption is relatively low. Decreases in the transmission at this wavelength are directly correlated to aerosol extinction. Consequently, irradiance measurements gathered around this wavelength in the NIR spectrum are used to construct aerosol concentration profiles. To obtain these irradiance measurements, sunlight passing through the atmosphere must be filtered and focused onto a photo-detector.

There are a few key optical design considerations that are common to each of the design alternatives discussed below. First, the optical filters are considered. In order to isolate the target wavelength, the incident sunlight must be filtered. A bandpass filter rejects and or absorbs most of the light outside of the passband. In fact, in most cases, greater than 99% of the light outside of the passband is not transmitted. Placing a filter ahead of the photo-detector will ensure that irradiance measurements are gathered using light in the defined spectral region.

Next, the optics system will incorporate both an aperture stop and a field stop. The primary function of the aperture stop is to limit the amount of light entering the system. While the aperture stop controls the light collection, the field stop limits the amount of stray light and scattered light that reaches the photo-detector. Effectively, the pinhole diameter sets the field-of-view of the optics system. A 15 μm diameter pinhole has been selected which satisfies the FOV and vertical resolution requirements.

Then, the shape of the highly reflective primary mirror is examined. Generally, the primary mirror of a reflective telescope is either parabolic, spherical, or hyperbolic. Both spherical and parabolic mirrors are more easily obtainable than hyperbolic mirrors. Hyperbolic mirrors are often custom manufactured for a specific application, and custom optical components are prohibitively expensive. Furthermore, spherical mirrors are typically less expensive than parabolic mirrors. However, as one would expect, spherical aberrations are a greater concern for spherical mirrors. The use of parabolic mirrors is more common in reflector telescopes as they do not produce this geometric aberration. Both on-axis and off-axis parabolic mirrors are available to purchase through the prominent optics vendors. Off-axis parabolic mirrors divert the incident light away from the optical axis, providing more control over the focused light. Curved mirrors present in the optical system are expected to be parabolic.

Telescope Type

Various telescope designs are capable of focusing the captured sunlight onto the photo-detector within the payload size constraint. There are two main categories of telescopes to consider: refractor telescopes and reflector telescopes. Refractor telescopes utilize lenses to focus light, while reflector telescopes employ highly reflective mirrors to alter the path of incoming light rays. Reflector telescopes are often preferred to refractor telescopes for space-based applications for a number of reasons. First, lenses generate chromatic aberrations. These wavelength dependent aberrations severely degrade the performance of optical instruments and significantly increase design complexity. Second, in most cases, mirrors are smaller in size, less massive, and generally less expensive. Given the resources available for the project, both logistical and financial, telescope design options are limited to different types of reflector telescopes.

1. Cassegrain Telescope

The first telescope design considered is known as the Cassegrain reflector. Within the Cassegrain reflector family, there are a few different subtypes, but the main configuration is the same. A concave primary mirror is

used in conjunction with a convex secondary mirror^b. The image is reflected through a gap in the primary mirror onto the detector (Fig. 108). This gap limits the options for COTS mirrors. More importantly, drilling a hole through a solid precision mirror adds significant manufacturing complexity. Effectively, the Cassegrain reflector folds the path of the light to increase magnification while preserving space. Relatively large effective focal lengths can be achieved with limited space, which can mitigate the effects of certain geometrical aberrations (e.g. spherical, coma, etc.). Unlike some of the other telescope designs, the presence of a secondary mirror poses and issue. The central obstruction caused by the secondary mirror decreases the amount of light captured by the system. Additionally, central obstructions degrade the spatial resolution performance of optical systems. With that said, the Cassegrain reflector configuration is able to collect sufficient light depending on the aperture area. From a manufacturing perspective, adding a secondary mirror increases the design complexity. An optical window or spider vane mount is needed to secure the mirror in its aligned position.

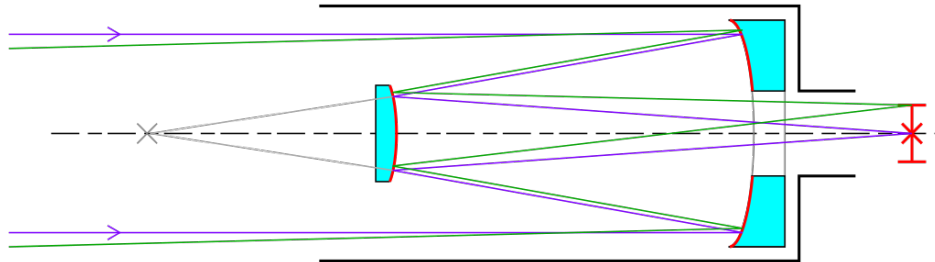


Figure 108. Cassegrain Reflector

Pros	Cons
Short overall length	Requires precise mirror alignment
Relatively long effective focal lengths	Relatively large secondary mirror
No chromatic aberration	Requires secondary mirror mount

Table 28. Summary: Pros and Cons of Cassegrain Telescope

2. Newtonian Telescope

The Newtonian reflector is the second telescope design explored. Similar to the Cassegrain reflector, the Newtonian telescope utilizes a secondary mirror to fold the path of the incident light rays. In contrast to the Cassegrain reflector, the Newtonian telescope secondary mirror is planar. The planar mirrors are relatively small. Still, the secondary mirror obstructs the optical tube. The secondary mirror for a Newtonian reflector also requires a mount, which greatly increases the manufacturing complexity of the optical system. Although, unlike the Cassegrain telescope, there is no gap in the primary mirror. Typically, the planar mirror is oriented at a 45 degree angle relative to the optical axis in order to focus the light 90 degrees off-axis (Fig. 109). Placing the focal point off of the optical axis is advantageous. To start, scattered or stray light is more easily rejected. That is, the light that reaches the photo-detector is more easily controlled. Furthermore, greater authority over the location of the focus point allows for more flexibility regarding the size and placement of the payload electronics.

^bGregorian telescopes utilize a concave secondary mirror. For the purposes of the trade study, Cassegrain telescopes are considered with the option to change the shape of the secondary mirror.

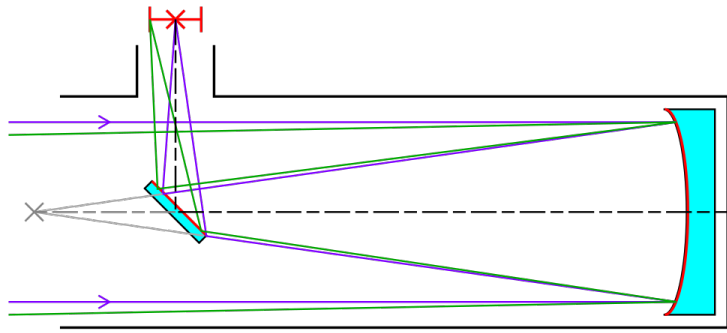


Figure 109. Newtonian Reflector

29.

Pros	Cons
Fewer curved mirrors	Requires precise mirror alignment
Low obstruction (relatively small secondary mirror)	Shorter effective focal lengths possible
No chromatic aberration	Requires secondary mirror mount

Table 29. Summary: Pros and Cons of Newtonian Telescope

3. Single OAP Telescope

The next telescope design utilizes a single OAP mirror. Compared to the multi-mirror reflectors, the single OAP telescope design is relatively simplistic. Collimated sunlight is reflected off of a single parabolic mirror to a focus point away from the optical axis (Fig. 110). In this configuration, the optics are not folded. Thus, shorter effective focal lengths are possible. There is no central obstruction with this single optic system, therefore the clear aperture area of the system is greater for a given aperture diameter. In other words, a smaller aperture is required to capture the equivalent amount of sunlight. Tilt and comatic aberrations are common when working with OAP mirrors. In addition, slight deviations from the ideal alignment can significantly impact the spatial resolution performance of the system.

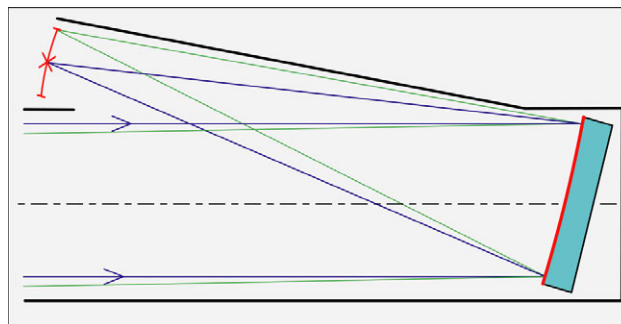


Figure 110. OAP Reflector

Pros	Cons
Requires a single mirror	Tilt aberrations are possible
No obstruction	Shortest effective focal lengths possible
No chromatic aberration	

Table 30. Summary: Pros and Cons of OAP Reflector

4. Prime Focus (On-Axis) Telescope

The final telescope design considered is the prime focus telescope. The PF telescope differs from the OAP reflector in two respects. First, the PF telescope reflects the incoming light back along the optical axis (Fig. 111). As a result, the photo-detector must be located in the optical tube, obstructing the field-of-view. Moreover, shielding the photo-detector from stray or scattered light in the the optical tube introduces another challenge. Secondly, the PF on-axis telescope necessitates the use of larger mirror to obtain an equivalent signal. Miniaturizing the optical system mandates shrinking the optics components.

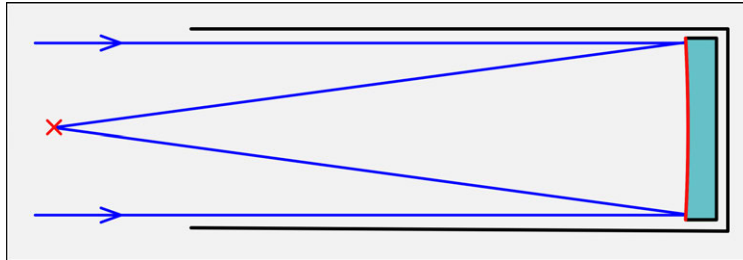


Figure 111. Prime Focus (On-Axis Telescope)

Pros	Cons
No secondary optics	Obstruction
No chromatic aberration	Larger Secondary Mirror ^c

Table 31. Summary: Pros and Cons of Prime Focus (On-Axis) Telescope

Mirror Substrate

The mirror substrate refers to the base material used to to construct the mirror. The mirror surface coating is considered separately. The reflectivity and absorptivity of the optical system are evaluated at the mirror surface. Therefore, the optical properties of the substrate do not need to be considered. The substrate selection is based solely on thermal and mechanical properties. Four metrics were considered when evaluating the substrates: the coefficient of linear thermal expansion, the consistency of the CTE, the substrate density, and the substrate material cost. It is worth noting that the substrate cost study was conducted by comparing uncoated mirrors with a 50mm diameter and 100mm focal length. The mirror size and focal length are not meant to represent the NanoSAM baseline design, but rather to provide a consistent metric for cost comparison.

1. Aluminum 6061-T6

Aluminum 6061-T6 is a commonly used substrate for OAP mirrors due to the consistency of the material properties throughout the optic. For an OAP with an aluminum surface coating, the CTE of the entire optic is consistent, eliminating thermal stresses due to temperature changes. The thermal and mechanical properties for this aluminum alloy were taken from a MatWeb data sheet[24]. The cost comparison is sourced from Edmund Optics' COTS mirror pricing.

Pros	Cons
Allows for consistent CTE	High CTE
	High density
	High cost

Table 32. Summary: Pros and Cons of Aluminum 6061-T6

2. Floated Borosilicate Floated borosilicate is a type of silicate glass that is distinguished by the "floated" manufacturing process used in production. Floated borosilicate is a popular substrate used for both spherical and

OAP mirrors. The thermal and mechanical properties for the floated borosilicate are taken from a Schott data sheet[34]. Again, the cost comparison data is sourced from Edmund Optics’ COTS mirror pricing. The resulting advantages and disadvantages of the floated borosilicate mirror substrate are tabulated below.

Pros	Cons
Very Low CTE	Consistent CTE not possible
Very Low Density	
Med-Low Cost	

Table 33. Summary: Pros and Cons of Floated Borosilicate

3. Borosilicate

Another silicate glass substrate to consider is borosilicate, also known as N-BK7. While borosilicate is more commonly used to manufacture lenses, it is also used for spherical mirrors. The thermal and mechanical properties for borosilicate are taken from a Schott data sheet[35]. Again, the cost comparison utilized Edmund Optics’ COTS mirror pricing.

Pros	Cons
Low Density	Consistent CTE not possible
Very Low Cost	Med-High CTE

Table 34. Summary: Pros and Cons of Borosilicate

4. Fused Silica

Fused silica is the final substrate material considered for the baseline design. Fused silica spherical mirrors are typically used for laser applications. The thermal and mechanical properties for fused silica are taken from a TOSOH data sheet[44]. Again, the cost comparison data is sourced from Edmund Optics’ mirror pricing. The advantages and disadvantages for fused silica are summarized below.

Pros	Cons
Very Low Density	Consistent CTE not possible
	Med-High Cost
	Med-High CTE

Table 35. Summary: Pros and Cons of Fused Silica

Mirror Surface Coating

As mentioned previously, the reflectivity and absorptivity of the mirror is evaluated at the mirror surface. Consequently, the mirror surface coating defines the optical properties. Mirror surface coatings are polished metal and/or dielectric coatings applied to the surface of a variety of mirror shapes including, but not limited to, parabolic, spherical, and flat mirrors. Metallic surface coatings are designed to be optimized for different regions of the electromagnetic spectrum. Aluminum, gold, and silver are commonly used, highly reflective metallic coatings. Dielectric surface coatings are often applied as an overcoat to a metallic surface to improve durability and enhance reflectivity. The mirror surface coatings considered for the NanoSAM optical system trade study are protected aluminum, enhanced aluminum, protected silver, and protected gold. The metrics considered to score the surface coatings include cost, reflectivity at the target wavelength (1.02 μ m), surface quality, and durability. Similar to the mirror substrate trade study, a 50mm diameter, 100mm focal length, spherical, floated borosilicate base mirror was chosen to provide a consistent foundation for cost comparison.

1. Protected Aluminum

The first surface coating to consider is protected aluminum. Even though the reflectivity is relatively low, protected aluminum is one of the most common polished metal mirror coatings utilized for applications in the visible and NIR spectra. An overcoat of silicon monoxide enhances the durability of the mirror, protecting the surface against abrasion. The advantages and disadvantages of the protected aluminum surface coating are displayed in the table below.

Pros	Cons
Less expensive	Low reflection % @ 1020 nm
Durable	
Precision surface quality	

Table 36. Summary: Pros and Cons of Protected Aluminum

2. *Enhanced Aluminum*

Enhanced Aluminum is a metallic aluminum surface coating with an additional multi-layer dielectric coating applied to the mirror. Similar to the silicon monoxide coating, the dielectric coat protects the aluminum from scratching and scraping as well as enhances the reflectivity of the mirror in the visible and ultraviolet spectrum. A summary of the pros and cons of the enhanced aluminum surface coating is given below.

Pros	Cons
Durable	Moderately expensive
Good reflection % @ 1020 nm	
Precision surface quality	

Table 37. Summary: Pros and Cons of Enhanced Aluminum

3. *Protected Silver*

Protected Silver demonstrates high reflectivity in the visible and infrared spectra, and thus silver surface coatings are used in applications across multiple spectral regions. Silver easily tarnishes in humid environments, so a protective coating is often applied.

Pros	Cons
Very good reflection % @ 1020 nm	Tarnishes easily
Precision surface quality	Very expensive

Table 38. Summary: Pros and Cons of Protected Silver

4. *Protected Gold*

Protected gold surfaces are optimized for applications in the NIR and IR spectra due to their high reflectivity in these spectral regions. The gold coatings are very delicate in nature and require a protective coating.

Pros	Cons
Very good reflection % @ 1020 nm	Very expensive
Precision surface quality	Poor durability

Table 39. Summary: Pros and Cons of Protected Gold

Filter

Another optical component of particular importance is the filter. The filter is used to isolate the narrow band of the EM spectrum where measurements will be taken. The transmission of light around the target wavelength, cost, and optical density are important factors to consider when selecting the filter for NanoSAM's optical system.

1. Linear Variable Filter

Linear variable filters transmit different wavelengths along the length of the filter. Utilizing a linear variable filter requires that the photodiode is precisely placed at the correct location along the filter length to intercept the desired wavelength [10]. Any wavelengths transmitted outside the passband must be rejected with some form of field stop near the photo-detector.

Pros	Cons
Can be centered at 1020 nm	Expensive
	Wide passband
	Requires alignment

Table 40. Summary: Pros and Cons of Linear Variable Bandpass Filtering

2. Traditional Coating

Traditionally-coated filters are less expensive than linearly variable filters and have relatively broad passbands. Filters made this way are generally less resistant to environmental stress due to the process by which dielectric material is applied to the filter substrate (often silica glass). Traditionally-coated filters typically transmit between 50 and 60 percent of incident light in the passband. Only certain center wavelengths are available off-the-shelf from the prominent optics vendors. Thus, this trade study assesses 990 nm and 1064 nm CWL filters, which are the closest equivalents to the desired 1020 nm CWL.

Pros	Cons
Inexpensive	Wide passband
	Low transmission
	Only available with certain CWL

Table 41. Summary: Pros and Cons of Traditional Coating

3. Hard Coating

Hard coating filters are also fairly inexpensive. Their very narrow passbands transmit more than 85 percent of incident light in the desired passband. Again, because these filters are acquired as COTS components, only certain wavelengths are available. The trade study assesses two filters, 980 nm and 1030 nm CWL, which are the closest to the desired 1020 nm CWL.

Pros	Cons
Inexpensive	Only available with certain CWL
High transmission	

Table 42. Summary: Pros and Cons of Hard Coating

4. Custom Coating

Although it is possible to commission a custom filter which combines the advantages of both the hard and traditional coated filters with a CWL at 1020 nm, a preliminary quote indicates that pursuing this option is likely not financially feasible [13]. As is the case for most custom optical components, the excessive price and lead time required remove them from consideration.

Pros	Cons
Control over CWL	Very expensive

Table 43. Summary: Pros and Cons of Custom Coating

11.2. Trade Studies

11.2.1. Photodiode Selection

The photodiode selection process considered the bandwidth, dark current, active area, cost, and responsivity at the desired wavelength. The responsivity at the desired wavelength and dark current was weighed the highest as it has the most impact on mission success, and cost was weighed the least as none of the options considered would consume a drastic portion of our budget.

Metric	Weight	Driving Requirements	Description and Rationale
Bandwidth	0.2	1.2	A larger photodiode bandwidth will correlate to more noise in data measurements from other wavelengths of light. The bandwidth was given a weight of 0.2 because having a narrower bandwidth around our desired wavelength limits the contribution of other wavelengths to our instrument noise.
Dark Current	0.3	1.3, 3.2	Dark current is one of the primary noise sources that the photodiode can have, so it was given a heavy weighting of 0.3. Having a calibrated photodiode that has minimal dark current is crucial to the success of NanoSAM since accurate data can only be made if noise is reduced as much as possible.
Active Area	0.1	1.2	The active area is the sensitive area of the photodiode that measures irradiance. While having a larger active area would be beneficial, it is not as crucial for mission success as the optics system will be able to focus the light to a small area, so the weighting for active area is given a value of 0.1.
Responsivity @ 1020 nm	0.3	1.2	The responsivity at the required wavelength is of grand importance because the photodiode must be able to generate a measurable current while measuring irradiance in order to produce relevant data. Thus, the responsivity at 1020 nm was given a large weighting of 0.3.
Cost	0.1	Project Budget	The cost of components is very important in every project with a limited budget. However, the average cost of these photodiodes is fairly negligible compared to other components of the mission. Therefore, the cost for this photodiode trade study was given a low weighting of 0.1.

Table 45. Photodiode Trade Study Metrics and Weighting

Metric	1	3	5
Bandwidth	1020 nm ± 1500 nm	1020 nm ± 1000 nm	1020 nm ± 500 nm
Dark Current	High	Average	Low
Active Area	Small	Average	Large
Responsivity @ 1020 nm	Low	Average	High
Cost	High	Average	Low

Table 46. Photodiode Metric Score Categorization. Note that the numbers in the responsivity section is the range where the photodiode is able to measure.

Metric	Weight	Si	InGaAs	Ge
Bandwidth	0.2	3	3	5
Dark Current	0.3	4	3	3
Active Area	0.1	4	2	5
Responsivity @ 1020 nm	0.3	5	4	3
Cost	0.1	5	3	1
Total	1	4.2	3.2	3.1

Table 47. Photodiode Trade Study Scoring

11.2.2. ADC Selection

The ADC selection process took into account resolution, noise, dynamic range, sampling rate, power consumption, and latency. Noise and Resolution were weighed the most as they directly affect the measurements.

Metric	Weight	Driving Requirements	Description and Rationale
Resolution	0.3	1.0, 3.1	The ADC is responsible for converting the continuous analog signal to an accurate digitized signal. It is imperative that the resolution of the ADC is great enough to deconvolve simulated aerosol concentrations from a radiation source, thus, the resolution of the ADC is very important and was subsequently given a weight of 0.3.
Noise	0.3	1.3, 3.1, 3.2	A low noise is required to accurately represent the analog signal in a digital form. The noise will be the largest source of error in digitally representing the analog signal. To get accurate and relevant data, the noise needs to be weighted heavier in this trade study and is thus given a weight of 0.3.
Dynamic Range	0.1	1.0, 6.1	A large dynamic range is optimal for our ADC design because the strength of the signal output will vary considerably. The ADC must be able to resolve weak and strong signals to measure the changes in intensity of our light source. However, the output of the analog front end electronics can be scaled to the range of the ADC, so the dynamic range is given a light weight of 0.1.
Sampling Rate	0.1	1.0, 3.2, 4.1	Sampling rate is important to precisely and accurately represent the continuous signal however our requirement of 50 Hz is very achievable for most modern electronics. Due to the fact that the ADC options considered can handle the required sampling rate, this metric was given a low weight of 0.1.
Power Consumption	0.1	6.0, 6.1	Power Consumption is important in our application because power will be limited by batteries however the spacecraft bus will supply this power which is outside of this project scope. The weight for the power consumption will be relatively low so the weighting in this metric is a low 0.1.
Latency	0.1	2.1.1, 2.1.2, 2.1.3	A low latency time is required to accurately clock the signal to a specific time stamp. The data acquisition must be synchronous with the analog signal to receive viable data. Latency is not critical and was therefore given a weight 0.1.

Table 49. Analog-to-Digital Converter Trade Study Metrics and Weighting

Metric	1	3	5
Resolution	< 8 bits	< 16 bits	< 24 bits
Noise	High	Middle	Low
Dynamic Range	Small	Average	Large
Sampling Rate (Typical)	> 1 kHz	> 1 MHz	> 100 MHz
Cost	High	Average	Low
Latency Time (Typical)	< 1 ms	< 1 μ s	< 1 ns

Table 50. Analog to Digital Converter Metric Score Categorization

Metric	Weight	Flash	Successive Approximation	Delta-Sigma
Resolution	0.3	1	3	5
Noise	0.3	2	3	5
Dynamic Range	0.1	3	3	3
Sampling Rate	0.1	5	3	1
Power Consumption	0.1	1	4	4
Latency	0.1	5	3	1
Total	1	2.3	3.1	3.9

Table 51. Analog to Digital Converter Trade Study Scoring

11.2.3. On-Board Controller Selection

The on board controller selection was based off of mass, hardware interfaces, ease of programming, processing power, power draw, and available software solutions. Hardware interfacing was weighed the most as it is critical that the controller can communicate with the rest of the components. Processing power was weighed the least as our application does not require much processing power.

Metric	Weight	Driving Requirements	Description and Rationale
Size & Weight	0.1	7	In order for this system to fit in a CubeSat, the mass must be limited to under the required mass and volume limits. Some options considered for the on-board controller have considerable mass, and must be considered in their selection. Due to the fact that the mass can be important for some options considered, this metric was given a 0.1 weight.
Hardware Interfacing	0.2	6.1	In order for this mission to be successful, the on-board controller must be able to interface with a number of different systems, such as the ADC, on-board storage, and spacecraft systems. Due to the vitality of the on-board computer, this metric was given the highest weight of 0.2.
Ease of programming	0.15	Resources	While some of the systems selected can be very easily programmed, some are extremely difficult. In order for this mission to be successful, the on-board controller will need to be programmed to acquire and store the data. This challenge is somewhat mitigated by the fact that multiple team members have experience with the different design options considered. The experience of the team members gives a relatively low weight of 0.15.
Processing Power	0.1	6.1	There is a large range in processing power available from these different design options. In order to successfully acquire and store data at the specified rate, the controller will need sufficient processing power. However, the required rates for collecting data are not difficult to achieve. Processing power is not a major concern so it was given a weight of 0.1.
Power Draw	0.1	6.1	Different controller options have different power requirements. In a space environment, power is generally at a premium. Selecting a system with a low power draw is important for mission success. Peak power draw is not a major concern so it was given a weight of 0.1.
Available Software solutions	0.15	Resources	Some design options require extensive custom software to achieve the necessary tasks, while others have open-source solutions already available. By leveraging existing software for the on board controller, the design time can be significantly reduced. A larger variety of software solutions will give more choices and make it easier for the group, therefore a score of 0.15 was given.

Table 53. On-Board Controller Trade Study Metrics and Weighting

Metric	1	3	5
Mass	less than .025kg	less than .01kg	less than .005kg
Volume	Large	-	Small
Hardware interfacing	No interfaces	Some interfaces	Many interfaces
Ease of programming	Difficult to program	-	Simple to program
Processing Power	Low	Middle	High
Power Draw	High	Middle	Low
Available Software Solutions	None	Some	Many

Table 54. On-Board Controller Metric Score Categorization

Metric	Weight	FPGA	Micro-Controller	Single Board Computer
Size & Weight	.3	4	5	1
Hardware Interfaces	.2	3	2	4
Ease of Programming	.15	1	3	4
Processing Power	.1	5	3	4
Power Draw	.1	1	5	3
Available Software Solutions	.15	2	3	4
Total	1	2.85	3.6	3

Table 55. On-Board Controller Trade Study Scoring

11.2.4. External Memory Selection

The external memory selection was weighed on complexity of use, storage capacity, speed, reliability, mass, and cost. Complexity of use was the highest ranked metric, as difficult to interface with storage options limit our controller selection. Reliability and mass were weighed second highest as they are both very large concerns for space missions.

Metric	Weight	Driving Requirements	Description and Rationale
Complexity of Use	0.3	Resources	The ability to a) use our external memory with our on-board computer and b) be able to use it with relative ease with the team's given expertise is quite crucial given the nine-month time limit for the project. A complex external memory system will make integration and implementation difficult and was therefore given a score of 0.3.
Storage Capacity	0.1	4.1	The storage capacity of the external memory is important given the relatively high rate of data collection and how often data will be captured. In the event of a missed ground station pass, the payload will have to store data on-board until the next downlink can be achieved. The storage capacity will most likely not be an issue and was given a score of 0.1 because of that.
Read/Write Speed	0.1	3.1.1	The read/write speed metric is simply how quickly the external storage can read the incoming data and store it. The read/write speed is an important metric as it will ensure no backups in the electronics system occur and that data will be collected efficiently. The group is not concerned about the read/write speed so it was given a score of 0.1.
Reliability	0.2	4.1	The ability for the external memory to be durable in space is crucial to the NanoSAM mission since the data should not be compromised due to any thermal and radiation damages. The external memory needs to be dependable and was therefore given a score of 0.2.
Size/Weight	0.2	7.1, 7.2	Since the completed instrument should be able to fit comfortably in a CubeSat, the mass and volume are important considerations to be a viable payload in the future. The size/weight is given its 0.1 weight because the given design choices are typically small so this metric is not as important as some others. Size and weight are important in implementing the project into a CubeSat so it was given a score of 0.2.
Cost	0.1	Project Budget	The cost of the external memory is important given the limited budget of this project. However, it is not weighted as strongly as other metrics due to the relatively low cost of the design choices for this selection. The cost is not a major concern for the group and was given a score of 0.1.

Table 57. External Memory Trade Study Metrics and Weighting

Metric	1	2	3	4	5
Complexity of Use	Impossible	Difficult	Medium	Easy	Trivial
Storage Capacity [GB]	<1	2	3	4	>5
Read/Write Speed [MB/s]	<100	100-200	200-300	300-400	>400
Reliability	Unreliable	Many Concerns	Some Concerns	Few Concerns	No concerns
Size/Weight	Too large	Large	Medium	Small	Negligible
Cost [\$]	>30	20-30	10-20	5-10	<5

Table 58. External Memory Metric Score Categorization

Metric	Weight	SSD	Micro-SD	USB	NAND Flash
Complexity of Use	0.3	2	5	5	4
Storage Capacity	0.1	5	5	5	4
Read/Write Speed	0.1	5	1	1	2
Reliability	0.2	4	3	4	5
Size/Weight	0.2	1	4	3	5
Cost	0.1	1	3	3	5
Total	1	2.7	3.8	3.8	4.3

Table 59. External Memory Trade Study Scoring

11.2.5. Reflector Telescope Type Selection

Table 61 describes the metrics used to evaluate each of the telescope design options. The relative weights of each metric are explained in the description and rationale entries of the table. To reiterate the justification for each weight, the cost of the optical components is a major factor. The mirrors and filters alone are hundreds of dollars each. The effective focal length directly affects the ability of the optic system to meet the size requirement. Manufacturing complexity expends the team’s limited resources. Meanwhile, the obstruction and optical aberrations which degrade the optical system’s spatial resolution are unavoidable to an extent.

Metric	Weight	Driving Requirements	Description and Rationale
Cost	0.3	Project Budget	The reflector telescope components are relatively expensive. Stock mirrors, lenses and filters may require a significant portion of the project budget. Thus, an understanding of the estimated cost for each telescope configuration is of paramount importance. As the group estimates that optical system cost will be the most expensive aspect of the project, and telescope type will play a major part in the overall cost the highest weight of 0.3 was given to the cost metric.
Manufacturing Complexity	0.2	1.1, Resources	The overall scale of the telescope is small compared to its predecessors, and miniaturization of optical instruments poses a challenge. Precision alignment and installation of multiple mirrors necessitates additional equipment, time, and material resources. Manufacturing the telescope will require a large amount of resources, therefore the complexity of manufacturing was given a weight of 0.2.
Optical Aberrations	0.1	1.1, 3.1	Optical aberrations introduce uncertainty into the telescope design. Different types of optical aberrations[8] alter the image at the sensor location. Aberrations will decrease the spatial resolution of the image, however a clear image is not vital to obtain accurate scientific data. For this reason the aberrations were given a weight of 0.2.
Effective Focal Length	0.25	1.1.2, 3.1	First, controlling the effective focal length of the telescope can mitigate certain optical aberrations. Second, the effective focal length affects the sensor size and placement. The effective focal length will need to fit within the 1U CubeSAT structure, so it is a vital parameter when selecting a telescope type. COTS options for precision mirrors with shorter effective focal lengths are limited. For these reasons this metric was given a weight of 0.25.
Obstruction	0.15	1.1.1	Obstruction of the optical tube affects the amount of light gathered (i.e. the effective aperture). Adequate illumination will be easy to obtain with all telescope designs. The obstruction also degrades the spatial resolution of the optical system, although it is not the most impactful degradation factor. Therefore, this metric was given a weight of 0.15.

Table 61. Telescope Type Metric Score Categorization

Table 62 outlines the scoring system for each of the above metrics. Due to the indefinite nature of each metric, qualitative assessments are used. The cost of optics components is heavily dependent on the vendor, material selection, and size. The challenges which define the manufacturing complexity are unique to each type of reflector telescope. Optical aberrations are difficult to quantify, however certain telescope attributes (e.g. EFL, surface quality, mirror shape, etc.) are judged to increase/decrease the risk of optical aberrations. A custom mirror would allow for a wide range of effective focal lengths for each telescope type. Furthermore, folded optics are rated higher due to their ability to fit a larger EFL within a smaller system. Lastly, the obstruction is dependent on the aperture size and size of the blockage. A detailed explanation of the scoring system is outlined in Appendix A.

Metric	1	2	3	4	5
Cost	High	High/Medium	Medium	Medium/Low	Low
Manufacturing Complexity	High	High/Medium	Medium	Medium/Low	Low
Optical Aberrations	High Risk	-	Moderate Risk	-	Low Risk
Effective Focal Length	Small	-	Medium	-	Large
Obstruction	High	-	Medium	-	Low

Table 62. Telescope Type Trade Study Metrics and Weighting

Applying the metric scoring system (see Appendix A for score justification), the following trade scores are assigned to the telescope types. According to the trade study, the OAP reflector is the appropriate design choice. Although the OAP is at risk for optical aberrations and has a shorter EFL, the optical tube is free from obstructions and only one mirror is required which decreases both the cost and manufacturing complexity.

Metric	Weight	Cassegrain	Newtonian	OAP	PF (On-Axis)
Cost	0.3	1	2	4	3
Manufacturing Complexity	0.2	1	2	4	3
Optical Aberrations	0.1	3	3	1	5
Effective Focal Length	0.25	5	3	1	1
Obstruction	0.15	3	3	5	1
Total	1	2.5	2.5	3.1	2.4

Table 63. Telescope Type Trade Study Scoring

11.2.6. Mirror Substrate Selection

Table 65 details the weighting scheme of the mirror substrate material trade study. Reviewing the metrics, the cost is a critical consideration as the difference in price between the substrate materials is a few hundred dollars. The density of the substrate is directly proportional to mass of the system. In addition to the volume constraint, CubeSats must meet a strict mass requirement. Even though the mirrors are highly reflective, they still absorb a portion of the incident radiation, which leads to a change in temperature. Thermal expansion of the optics system can be detrimental to the instrument performance.

Metric	Weight	Driving Requirements	Description and Rationale
Coefficient of Linear Thermal Expansion	0.25	1.1	Because reflecting telescopes use mirrors rather than lenses, the mirror substrate optical properties will not affect its performance. The thermal properties of the substrate, however, remain a key selection parameter. The CTE was compared directly using material data sheets. Limiting the CTE will provide greater thermal control on the system and was therefore given a score of 0.25.
Consistent CTE Benefit	.05	1.1	The benefit of a consistent substrate and surface coating CTE is a reduction in the thermal stress within the optic. A consistent CTE makes it slightly easier to perform calculations as everything will react the same way to thermal changes, therefore it was given a score of 0.05.
Density	0.3	7.2	Given the instrument must be compatible with a CubeSat platform, the mass of each component remains a key selection parameter. The values were compared directly using material data sheets. Higher density materials will increase the weight of the optical system. As weight is an important property when designing for space flight it is an important factor in overall selection, therefore a weight of 0.3 was given.
Cost	0.4	Project Budget	The budget of \$5000 will be a constraining factor throughout the design of the instrument. The telescope mirrors will likely require a sizable portion of the budget, thus finding the best value in mirror substrate is essential for success. The price's used in the comparison correspond to a 50mm diameter mirror with an effective focal length of 100mm. Optical components can become very expensive, by placing a higher emphasis on cost the overall cost of the optics system will be controlled. Therefore a score of 0.4 was given to the cost of the mirror substrate.

Table 65. Mirror Substrate Trade Study Metrics and Weighting

Table 66 below outlines the scoring system assigned to the previously defined metrics for the substrate material trade study. The CTEs of the various materials span from $2 \cdot 10^{-6}K^{-1}$ to greater than $10 \cdot 10^{-6}K^{-1}$. The consistency of the CTE is judged to be possible or impossible based on the combination of substrate and surface coating materials available for purchase. Only options with the same substrate material and surface coating will have a consistent CTE. Next, the densities of the substrate materials range from $2.2 \frac{g}{cm^3}$ to greater than $2.6 \frac{g}{cm^3}$. Equal divisions between these values define the intervals for the intermediate scores. Lastly, the cost scoring is divided into five \$60 intervals spanning \$60-\$300.

Metric	1	2	3	4	5
CTE [$\frac{1}{K} * 10^{-6}$]	$\alpha > 10$	$10 > \alpha > 8$	$8 > \alpha > 6$	$6 > \alpha > 4$	$4 > \alpha > 2$
Consistent CTE	Not Possible	-	-	-	Possible
Density [$\frac{g}{cm^3}$]	$\rho > 2.6$	$2.6 > \rho > 2.5$	$2.5 > \rho > 2.4$	$2.4 > \rho > 2.3$	$2.3 > \rho > 2.2$
Cost	$C > \$300$	$\$300 > C > \240	$\$240 > C > \180	$\$180 > C > \120	$\$120 > C > \60

Table 66. Mirror Substrate Metric Score Categorization

The scores for each substrate material are presented in Table 67. According to the trade study, the floated borosilicate substrate is the most appropriate design option by a large margin. The other two silica glasses are the next best options, whereas the aluminum alloy is by far the least viable option. The results of the trade study are counter to the expected results. Consequently, further research is necessary to validate the results of the trade study.

Metric	Weight	Aluminum 6061-T6	Floated Borosilicate	Borosilicate	Fused Silica
CTE	0.3	1	5	2	4
Consistent CTE	0.05	5	1	1	1
Density	0.3	1	5	2	5
Cost	0.4	1	5	5	3
Total	1	1.2	4.8	3.15	3.75

Table 67. Mirror Substrate Trade Study Scoring

11.2.7. Mirror Surface Coating Selection

The mirror surface coating metrics are detailed in Table 69. Again, the cost is the most important metric, giving it the greatest weight. Next, the reflectivity of the surface coating at the target wavelength is evaluated. Higher reflectivity is favored to minimize heat transfer to the optics system and to maximize the illumination of the photodetector. All of the mirrors are fragile and, therefore, the durability of the mirror is of less important than the other metrics. On a different note, much greater surface qualities are obtainable for more flight capable components. However, given the scheduling and budgetary constraints of the project, the maximum attainable surface qualities are all similar.

Metric	Weight	Driving Requirements	Description and Rationale
Cost	0.4	Project Budget	The budget of \$5000 will be a constraining factor throughout the design of the instrument. The telescope mirrors will likely require a sizable portion of the budget, thus finding the best value in mirror surface coating is essential for success. To distinguish the cost of different mirror surface coatings a spherical 50mm diameter mirror with a 100mm focal length was chosen. Then the type of surface coating was varied.
Reflection % @ 1020 nm	0.3	1.0, 3.0	Reflection % was evaluated using the Edmund Optics Metallic Mirror Coatings resource document. [11]
Surface Quality	0.15	1.0, 3.0	Surface quality was evaluated using the the scratch-dig specification described by MIL-PRF-13830B. [15]
Durability	0.15	1.0	Durability was evaluated using qualitative descriptions of the durability of each surface coating from the Edmund Optics Metallic Mirror Coatings resource document. [11]

Table 69. Mirror Surface Coating Trade Study Metrics and Weighting

Table 70 gives the scoring breakdown for the surface coating trade study. The cost is divided similar to the cost category developed for the substrate material trade study. Each surface coating is highly reflective. The reflection percentage, surface quality, and durability intervals are derived from the Edmund Optics resource pages.

Metric	1	2	3	4	5
Cost	C > \$400	\$400 > C > \$350	\$350 > C > \$300	\$300 > C > \$250	C < \$250
Reflection % @ 1020 nm	R < 80	80 > R > 85	85 < R < 90	90 < R < 95	95 < R < 100
Surface Quality	80-50 standard		60-40 precision		20-10 high precision
Durability	Poor		Average		Good

Table 70. Mirror Surface Coating Metric Score Categorization

The results for the surface coating trade study are given in Table 71. According to the trade study, the protected aluminum surface coating is the most appropriate design choice. Its lower reflectivity at the target wavelength is offset by its relatively low cost. Finally, off-the-shelf OAP mirrors are available in protected aluminum, and this will drastically simplify the ordering and manufacturing process.

Metric	Weight	Protected Aluminum	Enhanced Aluminum	Protected Silver	Protected Gold
Cost	0.4	5	4	3	3
Reflection % @ 1020 nm	0.3	3	4	5	5
Surface Quality	0.15	3	3	3	3
Durability	0.15	5	5	1	3
Total	1	4.1	4	3.3	3.6

Table 71. Mirror Surface Coating Trade Study Scoring

11.2.8. Filter Selection

The metrics used to assess the filters are described in Table 73. Unlike the previous optics system trade studies, the greatest weight is not attributed to the cost. Instead, the deviation from the target CWL is assigned the greatest importance. The transmission and optical density isolate the signal used to measure irradiance.

Metric	Weight	Requirements	Description and Rationale
Deviation from 1020 nm CWL	0.4	1.2.1	While the ideal instrument would transmit at 1020 nm, it is difficult to source affordable off-the-shelf filters centered at this wavelength. Incorporating a filter's deviation from the ideal CWL allows assessing how much deviation from the ideal CWL should be tolerated in favor of other criterion [11]. Large deviations from 1020 nm CWL will give extra light that does not need to be measured, or even incorrect wavelengths. This is a critical component of the optics system and was therefore given a weight of 0.4.
Cost	0.3	Project Budget	The budget of \$5000 will be a constraining factor throughout the design of the instrument. Acquiring a high-quality filter with well-characterized thermal performance could become very expensive. To mitigate this, a the prices for a variety of off-the-shelf filters were compared to custom filtering options for a 50 mm filter aperture. [7] Coating process and filter design most significantly impacted this parameter. As the cost of all optical components is a major concern to the group a weight of 0.3 was given to the cost of the filter.
Transmission	0.2	3.1	The transmission of the filter is necessary in assessing the responsiveness of the instrument to small changes in occultation. Transmission is reported as the percentage of incident light at the CWL which is allowed through the filter. Transmission will determine the amount of light that reaches the detector and is therefore important in selection of a filter, although not as important as deviation or cost. For this reason it was given a weight of 0.2.[7]
Optical Density	0.1	3.1	Optical density improves the accuracy of the instrument by decreasing the transmission of light outside the passband. Rejecting light outside the desired range is less important than maximizing the signal within the desired range. Thus, a weight of 0.1 is applied to the optical density.[7]

Table 73. Filter Trade Study Metrics and Weighting

The scoring system utilized for the filter trade study is outlined in Table 74. The further the CWL of the filter is from the target wavelength, the lower the trade score. The differences in cost are significantly large. Consequently, the cost intervals are fairly spread-out. The transmission trade scores are defined by increments of 10%, beginning at 50%. Lastly, greater optical densities are assigned higher trade scores.

Metric	1	2	3	4	5
Deviation from 1020 nm CWL	<60 nm	<45 nm	<30 nm	<15 nm	0 nm
Cost	C > \$1500	C > \$1200	C > \$600	C > \$300	C < \$300
Transmission	>50%	>60%	>70%	>80%	>90%
Optical Density	3		3.5		4

Table 74. Filter Metric Score Categorization

The results of the trade study for the filter selection are shown in Table 75. With a trade score of 4.1, the hard coating 1030 nm CWL filter is the the most practical design option. The low cost filter is near to the target wavelength and has a satisfactory transmission profile.

Metric	Weight	Linear Variable 1020 nm CWL	Traditional Coating 990 nm CWL	Traditional Coating 1064 nm CWL
Deviation from 1.02 μ m CWL	0.4	5	3	2
Cost	0.3	2	5	5
Transmission	0.2	5	1	1
Optical Density	0.1	3	5	1
Total	1	3.8	3.4	2.6

Metric	Weight	Hard Coating 980 nm CWL	Hard Coating 1030 nm CWL	Custom Coating 1020 nm CWL
Deviation from 1.02 μ m CLW	0.4	2	4	5
Cost	0.3	4	4	1
Transmission	0.2	4	4	3
Optical Density	0.1	5	5	3
Total	1	3.3	4.1	3.2

Table 75. Filter Trade Study Scoring

11.3. Metric Score Justification

11.3.1. Photodiode Selection

1. Si

I Bandwidth (3/5) The score was a 3 here because it does not meet the best bandwidth requirements that a 5 required. However, it has a small range of sensitivity on the upper bound of the nanometer spectrum, so the bandwidth is limiting in that respect. However, on the lower bound, it can detect wavelengths as small as 190 nm.

II Dark Current (4/5) Since the dark current is in the pico- to nano- Amperes range, it is scored the highest among the three photodiodes. Ideally, no dark current would be preferable since the data's sensitivity to pA levels of current – so it is not ranked a 5.

III Active Area (4/5) Since the average active area is significantly larger than InGaAs but slightly smaller than Ge, the score is placed at a 4 – close but not above Ge, and significantly higher than InGaAs

IV Responsivity @ 1020 nm (5/5) The responsivity is the the highest in Si compared to the other two types of photodiodes when it doesn't have a filter – at around 0.6 A/W.

V *Cost (5/5)* The cost of Si photodiodes are insanely inexpensive compared to the InGaAs and Ge photodiodes – averaging at around \$50/piece, and the range of price ranging from \$15- \$114. This is a price that is completely affordable in the \$5000 budget.

2. InGaAs

I *Bandwidth (3/5)* The score was a 3 here because it does not meet the best bandwidth requirements that a 5 required. However, it has a small range of sensitivity on the lower of the nanometer spectrum, so the bandwidth is limiting in that respect. However, on the upper bound, it can detect wavelengths as large as 2600 nm which far exceeds the maximum range of wavelengths the photo

II *Dark Current (3/5)* Since the max dark current is in the nano- to micro- Amperes range, while it is still relatively small, it is significantly larger than the Si photodiodes. However, since the current on average is smaller than Ge's dark current, it is scored higher than it.

III *Active Area (2/5)* The average active area for InGaAs is two orders of magnitude smaller than both Si and Ge. Since the active area is also measured in mm^2 , this area is significantly smaller than ideal.

IV *Responsivity @ 1020 nm (4/5)* The responsivity is the highest in InGaAs compared to the other two types of photodiodes. However, it is not placed at a 5 since it is unsure how much sensitivity a photodiode can have that it is considered large.

V *Cost (3/5)* The cost of InGaAs photodiodes are reasonable for the given budget – around \$150/piece with a range of prices from \$58-\$240. Since the average price is more than Si and less than Ge, the score is around that middle – a 3.

3. Ge

I *Bandwidth (5/5)* The score was given a 5 since according to our source[17], it states that the wavelength sensitivity is around 800-1700 – which is really close to our ideal wavelength.

II *Dark Current (2/5)* Since the max dark current is in the micro Amperes range, while it is still relatively small, it is significantly larger current flow than the other photodiodes

III *Active Area (5/5)* Ge photodiodes have the largest average active area than any of the other photodiodes we are trade studying – around 36 mm^2 ! This is big for a tiny photodiode, and therefore, placed at a 5.

IV *Responsivity @ 1020 nm (3/5)* The responsivity in Ge is between the InGaAs and the Si photodiodes.

V *Cost (1/5)* The cost of Ge photodiodes are quite expensive – as they average to around \$300/piece with a range of prices from \$150-\$500! This is by far more expensive than the Si and InGaAs photodiodes, and far more unreasonable in the given budget.

11.3.2. ADC Selection

1. Flash

I *Resolution (1/5)* - The resolution of the flash ADC is the lowest compared to the other ADC types, typically less than 8 bits.

II *SNR (2/5)* - The SNR of the flash ADC is typically lower than other ADC types however it is not crippling to the accuracy of the signal output, therefore it deserves a 2/5 score.

III *Dynamic Range (3/5)* - The dynamic range for most flash ADC's varies depending on the certain model, therefore it deserves a mid-tier 3/5 score.

IV *Sampling Rate (5/5)* - Flash ADC types have the greatest sampling rates when compared to other ADC types. They typically have sampling rates upwards of hundreds of MSPS (mega-samples per second).

V *Power Consumption (1/5)* - Flash ADC types typically consume the most power compared to other ADC types. This is due to the high power demand of the comparator and internal circuitry.

VI Latency (5/5) - The latency time of flash ADC types is the shortest amongst our ADC selection. Their internal circuitry is designed to rapidly convert analog to digital signals, and offers the most time efficient choice, with conversion times typically less than 1 nano-second.

2. Successive Approximation

I Resolution (3/5) - The resolution of the successive approximation ADC is mid-tier compared to the other ADC types, typically 8 - 16 bits.

II SNR (3/5) - The SNR of the successive approximation ADC is mid-tier compared to other ADC types, therefore it deserves a 3/5 score.

III Dynamic Range (3/5) - The dynamic range of successive approximation ADC types varies greatly and depends on the model of the specific ADC, therefore a mid-tier 3/5 shall suffice.

IV Sampling Rate (3/5) - Successive Approximation ADC types generally have mid-tier sampling rates when compared to other ADC types. They typically have sampling rates greater than 1 MSPS (mega-samples per second).

V Power Consumption (4/5) - Successive Approximation ADC types typically require low power, and are the default ADC types for low power mission design.

VI Latency (3/5) - The latency time of successive approximation ADC types is mid-tier compared to other ADC's. They typically convert the analog signal to digital in less than 1 micro-second.

3. Sigma-Delta

I Resolution (5/5) - The output resolution of the sigma-delta ADC is the greatest compared to the other ADC types, typically greater than 16 bits. Although the delta-sigma ADC uses a single bit comparator, the output resolution is much greater due to digital filtering.

II SNR (5/5) - The SNR of the delta-sigma ADC is unparalleled when compared to the other ADC types due to oversampling and noise shaping of its internal digital filter.

III Dynamic Range (3/5) - The dynamic range of sigma-delta ADC types also varies with the specific model of the ADC, therefore it deserves a mid-tier 3/5 score. This metric will need to be taken into account when purchasing the final ADC selected for our project.

IV Sampling Rate (1/5) - Sigma-delta ADC types have the lowest sampling rates when compared to other ADC types. They typically have sampling rates of 0.001 to 1 MSPS (mega-samples per second).

V Power Consumption (4/5) - Sigma-delta ADC types also require low power due to its internal digital circuitry.

VI Latency (1/5) - The latency time of sigma-delta ADC types is the greatest compared to other ADC types. The settling time of the sigma-delta ADC is the greatest malefactor to its conversion rate and typically takes time near the magnitude of a milliseconds to convert the analog to digital signal.

11.3.3. On-Board Controller Selection

1. FPGA

I Size & Weight (4/5) FPGAs are available as either single chips or as small breakout modules. Either of these options have relatively low mass. Using a single chip requires supporting circuitry already present on a breakout module. FPGA modules can be directly integrated with custom PCBs containing other necessary electronic components. This minimizes the volume used by the FPGA in the CubeSat electronics.

II Hardware Interface (3/5) An FPGA can implement almost any hardware interface in firmware, making this the most versatile option when it comes to interfacing with hardware. However, writing that firmware is not trivial, and requires significant development time. This is what decreases the hardware interface score to 3/5.

- III Ease of Programming (1/5)* An FPGA is by far the most difficult to controller to program of the options considered. Verilog or VHDL has an extremely steep learning curve. This is somewhat mitigated by the existence of available software solutions, especially for systems such as Xilinx FPGAs.
- IV Processing Power (5/5)* The access to low level logic fabric in FPGAs allows for extremely quick digital processing. Instead of waiting for instructions to be completed on subsequent clock cycles, as on a traditional processor, an FPGA allows for many tasks to be completed in parallel with dedicated circuits for each one.
- V Power Draw (1/5)* FPGAs can draw a large ammount of power, especially during start up and during complex operations.
- VI Available Software Solutions (2/5)* FPGAs have a decent library of available software solutions, especially for the Xilinx family of devices, where large IP catalogs are available, including implementations of microprocessors, block memory, and hardware interfaces. However, using these software solutions is more complex than with other design options

2. Micro-controller

- I Size & Weight (5/5)* Micro-controllers are available as single chips and as breakout modules. The single chips require fewer supporting electronics than FPGAs, meaning a single chip implementation is more feasible. This makes them the smallest option available
- II Hardware interfacing (3/5)* While interfacing with hardware is more limited on a micro-controller than an FPGA, and generally these limits cannot be overcome in firmware, implementation of the interface is much simpler, making it more feasible for this team than on an FPGA.
- III Ease of programming (3/5)* Micro-controllers are much easier to program than FPGAs, often running on compiled C or C++ code. Writing code to achieve the mission objectives would be relatively simple.
- IV Processing Power (3/5)* Many micro-controllers have very limited processing power, with extremely limited clock speeds and memory, while others can have extremely capable ARM processors with speeds up to 600MHz and large amounts of RAM (Teensy 4.0).
- V Power Draw (5/5)* Micro-controllers draw the least ammount of power of the options considered.
- VI Available Software Solutions (3/5)* Many open-source libraries exist for micro-controllers, implementing solutions for interfacing with a wide variety of hardware.

VII Single Board Computer

- I Size & Weight (1/5)* Single board computers generally occupy a large volume and have a considerable mass. They are only available as discrete circuit boards, and interfacing with other circuit boards generally requires cables. This is a large concern for this CubeSat.
- II Hardware Interfaces (4/5)* Like micro-controllers, single board computers have limited hardware interfaces, and these limits cannot be overcome in firmware or software. However, there are generally more hardware interfaces on an SBC than on a micro-controller. When it comes to storage with a single board computer, some have sufficient on-board flash that external storage is unnecessary, while others do not, and require the use of potentially undesirable storage, such as SC cards, to function at all (Raspberry Pi).
- III Ease of Programming (4/5)* Single board computers are much easier to program than FPGAs or micro-controllers once the single board computer system is up and running. However, to get to that state, flashing an operating system to either on-board memory, or an SD card is necessary to start using the system. Any user code would run on top of this operating system. This means high level languages such as MATLAB can be used. However, running mission critical code on top of an operating system could be considered an overly complex solution that's more difficult to debug and find all potentially mission ending issues.

- IV Processing Power (4/5)* Single board computers generally have more processing power than micro-controllers, but less than FPGAs.
- V Power Draw (3/5)* Single board computers generally draw more power than microcontrollers but less than FPGAs.
- VI Available Software Solutions (4/5)* Single board computers have a wide array of software solutions available, but again, the large amount of underlying systems for these solutions present a mission risk.

11.3.4. External Memory Selection

1. SSD

- I Complexity of Use (2/5)* A lot of SSD cards require SATA connections, which would be very difficult to interface with our micro-controller. Other external SSDs can be connected using a microUSB connection which would be easy to interface with, however, this would cost read/write speed.
- II Storage Capacity (5/5)* Out of all of the external memory options, SSDs have the highest storage capacity, typically on the range of hundreds of GB to a few TB.
- III Read/Write Speed (5/5)* The read/write speed is on the order of hundreds of MB/s, making SSDs one of the fastest external storage options offered.
- IV Reliability (4/5)* The SSDs are very reliable as they are heavily used in many tablets, laptops, etc. However, on a mission like NanoSAM, where it will eventually be exposed to the harsh conditions of space, SSDs may lose reliability. Thus, SSDs were not scored the highest on reliability.
- V Size/Weight (1/5)* SSDs are far too large to fit in a CubeSat of NanoSAM's scale. Some smaller SSD options would even take up much of the area/volume of a 1U CubeSat. The weight of an SSD is also much heavier than the other external storage option considered.
- VI Cost (1/5)* The cost of SSDs is large and could take up a decent chunk of our limited budget. SSDs for less than \$30 are not common and other external memory options are far cheaper. Therefore, the cost metric received the lowest possible score.

2. Micro-SD Card

- I Complexity of Use (5/5)* A microSD card is very trivial to use as it only takes a microSD card slot on a micro-controller, thus is received the highest score in this metric.
- II Storage Capacity (5/5)* MicroSD cards have high capacities and could easily cover the storage necessary for this mission so it received a very high score in this area.
- III Read/Write Speed (1/5)* The read speed was found to be about a maximum of 100 MB/s upon research in the subject. The maximum write speeds were found to be less than about 60 MB/s, so the microSD received a low score in this metric.
- IV Reliability (3/5)* MicroSD cards are fairly reliable because they are so simple and small and can stay locked into a microSD slot pretty well. However, many CubeSat missions (including a few at LASP) have failed due purely to SD card failures. They are prone to charged particle strikes that could cause them to fail. For these reasons, the microSD cards received an average score in this area.
- V Size/Weight (4/5)* MicroSDs are very tiny and would normally be considered negligible in size/weight, however, relative to our other option considered (specifically the NAND Flash chip), the microSD is not the smallest in size/weight. Therefore, the microSD did not score the highest in this metric.
- VI Cost (3/5)* The microSD card is fairly cheap but finding one for less than \$10 is not common as they are usually in the \$10-\$20 range so it scored an average score in this metric.

3. USB

- I Complexity of Use (5/5)* The USB stick is probably one of most trivial external storage devices as it just involved a USB drive on the micro-controller so it received the highest score in this category.
- II Storage Capacity (5/5)* The storage capacity of USB sticks is more than enough for this mission, so it received the highest score in this metric.
- III Read/Write Speed (1/5)* The read/write speed of a USB stick is among the lowest of the options considered. The read/write speeds are typically much less than 100 MB/s, so it received the lowest score in this area.
- IV Reliability (4/5)* The reliability of a USB stick has few concerns other than the connection between the drive and the USB stick can be prone to thermal contraction/expansion and can be faulty in this manner. Therefore, it did not receive the highest score in this area.
- V Size/Weight (3/5)* The size and weight of a USB stick is about average as it would not take up much mass/volume in a CubeSat compared to an SSD, but it would take up more space than a NAND Flash chip and a microSD card, so it received an average score in this area.
- VI Cost (3/5)* The cost of many typical USB sticks are on the scale of \$10-\$20 for the storage necessary for this mission, therefore it received an average score in this metric.

4. NAND Flash

- I Complexity of Use (4/5)* NAND Flash is available in packages designed to interface over an SPI bus. This allows them to easily connect to all of the on-board controller options.
- II Storage Capacity (4/5)* NAND Flash has the least storage per chip of the available options, however, it is trivial to include multiple chips on a circuit board, allowing for large amounts of data storage.
- III Read/Write Speed (2/5)* NAND Flash uses SPI, same as microSD. The difference is that SD cards generally use a file access table to allocate memory, which adds some overhead to transfer speeds compared to NAND Flash.
- IV Reliability (5/5)* NAND Flash forms the basis of all the other storage options considered. The microcontroller that handles the transfer of data for the other options considered is susceptible to radiation damage in the space environment. By bypassing this and interfacing directly with the NAND flash, this risk is removed. Additionally, thermal expansion and contraction can cause failure of the contacts on an SD card, SSD, or USB drive. Directly soldering a flash chip eliminates this risk
- V Size/Weight (5/5)* NAND Flash is the smallest of the considered options.
- VI Cost (5/5)* NAND Flash is the cheapest of the considered options.

11.3.5. Optics System

11.3.6. Reflector Telescope Type Selection

The telescope type cost trade-off score was computed using a weighted scheme. The cost of each reflector design is primarily a function of the number of optics and the shape of optics. Curved mirrors are assigned a weight of 2.5, flat mirrors are assigned a weight of 1, and spider vane mounts are assigned of weight of 0.5. The following is based on research conducted through the Edmund Optics website. Mirror cost is influenced by the substrate composition, surface coating, surface accuracy, and size. 51 mm and 25.4 mm diameter spherical and flat mirrors composed of Floated Borosilicate (highest trade score), coated with Protected Aluminum (highest trade score), and having surface accuracy ratings of $\lambda/4$ were compared. These parameters are not meant to represent the final requirements of NanoSAM. Rather, they provide a consistent metric for cost comparison similar to the substrate and surface coating studies. The smaller spherical mirror costs \$103.00, while the larger spherical mirror costs \$139.00. The corresponding flat mirrors cost \$32.00 and \$52.50. The ratio of mirror costs are 3.22 and 2.65, or 2.93 on average. Curved mirrors are assumed to be roughly 2.5 times more expensive than their flat mirror counterparts, resulting in the weights described above. The functional form of the weighted scheme is as follows: $\text{Cost Rating} = (2.5) \times \text{Number of Curved Mirrors} + \text{Number of}$

Flat Mirrors + (0.5) x Number of Mounts. Trade scores, in descending order correspond to cost ratings on the intervals: [0,2), [2,3), [3,4), [4,5), [5,∞). Cost is a critical project element to consider. The price of COTS optics components can extend into the hundreds to thousands of dollars. Working within a \$5000 project budget, the cost of the reflector telescope requires proper attention. The weight of the cost factor is chosen to be 0.3 (highest individual weight).

In a similar manner, the reflector manufacturing complexity trade study was scored using a weighted scheme. The manufacturing complexity was evaluated based on the required number of optic alignments, optic mounts (excluding the primary mirror mount), and custom manufacturing specifications (e.g. a hole in the primary mirror). The hierarchy of these factors, in order of most complex to least complex, was chosen as: optic alignment, optic mounting, then custom manufacturing specification. Assigning the weights 3, 2, and 1 to these factors, respectively provides a quantitative measure of the relative complexities associated with each reflector. An individual reflector type is assigned a trade score of 5, 4, 3, 2, or 1 for a sum of complexities on the interval [1,2], [3,4], [5,6], [7,8], or [9,10], respectively. The manufacturing complexity will directly expend time, equipment, and labor resources. There is little flexibility in the project schedule and appropriate equipment may be difficult to access. Therefore, a weight of 0.2 is assigned to the manufacturing complexity.

The EFL is an important metric used to define the relative sizes of the mirrors as well as their curvatures. The EFL also affects the location and size of the sensor making irradiance measurements. Moreover, manipulating the EFL can alter the effects of certain aberrations, namely comatic aberrations associated with curved mirrors. Due to its extensive impact on the overall design and indirect influence over the performance of the sensor, the EFL metric is given a weight of 0.25. Optical aberrations are the least significant metric. Aberrations are usually mitigated through the use of different mirror shapes and corrective lenses. Furthermore, the precision manufacturing of mirrors decreases the probability of aberrations caused by surface defects. In the end, a weight of 0.1 is assigned to the optical aberrations metric. Lastly, the obstruction metric is considered. The efficiency of the photodiode is dependent upon the number of photons impacting the contact surface. Restricting the number of incident photons limits the photodiode output. A sufficient photon stream is necessary for the photodiode to operate effectively. With that said, the obstruction metric is not as important as the cost or manufacturing complexity metrics and is assigned a weight equal to 0.15.

1. Cassegrain

I Cost (1/5) The Cassegrain reflector is composed of two curved mirrors and one secondary mirror mount. The cost rating is 5.5, which falls into the High cost trade score category.

II Manufacturing Complexity (1/5) For a Cassegrain reflector, the two mirrors require two alignments, a single interior mirror mount, and a precisely dimensioned hole through the primary mirror. According to the simple weighted scheme, the Cassegrain reflector has a complexity rating of 9, corresponding to the High trade score.

III Optical Aberrations (3/5) Cassegrain telescopes will have comatic, spherical, and astigmatism aberrations. Assuming the spherical aberration can be diminished by using parabolic mirrors, the comatic and astigmatism aberrations are more likely. Both result from a slight misalignment of the mirrors relative to the optical axis. There is moderate risk of producing these two aberrations.

IV Effective Focal Length (5/5) The telescope length is constrained by the size constraint of the payload. For a given telescope length, Cassegrain reflectors are capable of achieving large effective focal lengths. As a result, the Cassegrain reflector was assigned the highest trade score of 5.

V Obstruction (3/5) The secondary mirror will cause an obstruction of the optical tube. The decrease in the effective aperture is typical for a reflector telescope with a secondary mirror located between the light source and the primary mirror. Thus, the trade score assigned for the obstruction is the average.

2. Newtonian

I Cost (2/5) The Newtonian reflector utilizes one curved mirror, one flat mirror, and one secondary mirror mount. The cost rating of 4 is considered Medium/High.

- II Manufacturing Complexity (2/5)* Newtonian reflectors require two optic alignments and a single secondary mirror mount. Newtonian reflectors receive a complexity rating of 8, corresponding to a trade score of Medium/High.
- III Optical Aberrations (3/5)* Newtonian telescopes are at risk of generating comatic, spherical, and tilt aberrations. Again, assuming the spherical aberration can be addressed, the comatic and tilt aberrations dominate. Although the effects are minimal, the intermediate risk of inducing these aberrations is similar to the Cassegrain telescope.
- IV Effective Focal Length (3/5)* The EFL of a Newtonian telescope is less than the EFL of the Cassegrain configuration. The EFL can be larger than the length of the optical tube. Placing the focal point of the secondary mirror away from the optical axis allows for an EFL larger than both the OAP Reflector and Prime Focus telescopes. Thus, the Newtonian telescope is assigned a trade score corresponding to Medium EFL.
- V Obstruction (3/5)* For a given primary mirror with a specific focal length, the Newtonian secondary mirror is slightly smaller than the Cassegrain secondary mirror due to the tilt angle. However, for the scale of the NanoSAM telescope, this disparity is very small. The Newtonian configuration produces an obstruction similar in size to the Cassegrain telescope. The obstruction size is typical for a reflector telescope with a secondary mirror located between the light source and the primary mirror.

3. OAP Reflector

- I Cost (4/5)* The OAP reflector telescope design employs a single curved mirror. The cost rating of 2.5 is the lowest of the four design options. OAP reflectors are assigned a Low/Med trade score.
- II Manufacturing Complexity (4/5)* OAP telescopes require a single mirror alignment, corresponding to a complexity rating of 3 according to the simple weighted scheme. Ultimately, the manufacturing complexity of the OAP reflector is given a trade score of Low/Medium.
- III Optical Aberrations (1/5)* The primary mirror for the OAP reflector is at a relatively high risk for developing comatic aberration. The risk for developing aberrations is slightly greater than Newtonian and Cassegrain reflectors.
- IV Effective Focal Length (1/5)* For small diameter mirrors, the EFL of a single reflector telescope is limited. In general, the OAP telescope type will have smaller EFLs than Newtonian telescopes. Due to their relatively short EFLs, the OAP reflector configuration is awarded a trade score of 1.
- V Obstruction (5/5)* The OAP telescope eliminates the secondary mirror and is capable of focusing light to a point outside of the optical tube. Consequently, an ideal OAP configuration will have no obstruction, and therefore, no decrease in effective aperture. The obstruction trade score is the highest possible.

4. Prime Focus (On-Axis)

- I Cost (3/5)* Prime Focus telescopes require an optical mount in addition to a single curved mirror. Applying the weighted scheme produces a cost rating of 3, corresponding to a trade score of 3 (Medium).
- II Manufacturing Complexity (3/5)* The Prime Focus reflector manufacturing complexity is a function of the primary mirror alignment and the optical mount needed to install the sensor and supporting electronic components. The complexity rating of 5 coincides with a trade score of Medium.
- III Optical Aberrations (5/5)* The Prime Focus reflector is at risk of producing comatic aberrations and spherical aberrations. Ignoring the spherical aberrations, the Prime Focus telescope is at a relatively low risk for developing aberrations compared to the other telescope types.
- IV Effective Focal Length (1/5)* The EFLs of Prime Focus telescopes are severely limited. The focal point lies along the optical axis. For a constant sensor size and image size at the sensor location, the EFL of the Prime Focus telescope is typically less than the multi-mirror reflectors. Compared to the OAP configuration, the EFLs are similar.

V Obstruction (1/5) The Prime Focus telescope design requires that the sensor is placed between the light source and the primary mirror. In addition to the photodiode, any wires or other components required to measure and record the solar irradiance will obstruct the telescope. At smaller scales, this obstruction is more significant. The worst-case trade score is assigned due to the increased risk of high obstruction.

11.3.7. Mirror Substrate Selection

1. Aluminum 6061-T6

I CTE (1/5) Aluminum 6061-T6 has a CTE of $\alpha_{20-300K} = 2.36 * 10^{-5} K^{-1}$. This is the highest CTE seen with the substrates considered.

II Consistent CTE (5/5) Aluminum 6061-T6 is a viable surface coating thus a consistent CTE optic is possible.

III Density (1/5) Aluminum 6061-T6 has a density of $\rho = 2.7 \frac{g}{cm^3}$. This is the highest density of all substrates considered.

IV Cost (1/5) An un-coated 50 mm dia. off-axis parabolic mirror with a 100mm EFL costs \approx \$330

2. Floated Borosilicate

I CTE (5/5) Floated Borosilicate has a CTE of $\alpha_{20-300K} = 3.25 * 10^{-6} K^{-1}$. This is the lowest CTE seen with the substrates considered.

II Consistent CTE (1/5) Floated Borosilicate is not a viable surface coating thus a consistent CTE optic is not possible.

III Density (5/5) Floated Borosilicate has a density of $\rho = 2.2 \frac{g}{cm^3}$. This is tied for the lowest density of all substrates considered.

IV Cost (5/5) An un-coated 50 mm dia. parabolic mirror with a 100mm EFL costs \approx \$112

3. Borosilicate

I CTE (2/5) Borofloat Borosilicate has a CTE of $\alpha_{20-300K} = 8.3 * 10^{-6} K^{-1}$.

II Consistent CTE (1/5) Borosilicate is not a viable surface coating thus a consistent CTE optic is not possible.

III Density (2/5) Floated Borosilicate has a density of $\rho = 2.5 \frac{g}{cm^3}$.

IV Cost (5/5) An un-coated 50 mm dia. spherical mirror with a 100mm EFL costs \approx \$58

4. Fused Silica

I CTE (4/5) has a CTE of $\alpha_{20-300K} = 5.84 * 10^{-6} K^{-1}$.

II Consistent CTE (1/5) Fused silica is not a viable surface coating thus a consistent CTE optic is not possible.

III Density (5/5) Fused silica has a density of $\rho = 2.2 \frac{g}{cm^3}$. This is tied for the lowest density of all substrates considered.

IV Cost (3/5) An un-coated 50 mm dia. spherical mirror with a 100mm EFL costs \approx \$197

11.3.8. Mirror Surface Coating Type Selection

1. Protected Aluminum

I Cost (5/5) A protected aluminum coated 50 mm dia. spherical mirror with a 100 mm EFL costs approximately \$220.

II Reflection % @ 1020 nm (3/5) Protected aluminum has a reflection of approximately 88% @ 1020 nm.

III Surface Quality (3/5) Protected aluminum has a MIL surface quality rating of 60-40.

IV Durability (5/5) Protected aluminum is coated with a silicon monoxide layer which provides durability against abrasion, general handling, and cleaning.

2. Enhanced Aluminum

I Cost (3/5) A enhanced aluminum coated 50 mm dia. spherical mirror with a 100 mm EFL costs approximately \$260.

II Reflection % @ 1020 nm (4/5) Enhanced aluminum has a reflection of approximately 93% @ 1020 nm.

III Surface Quality (3/5) Enhanced aluminum has a MIL surface quality rating of 60-40.

IV Durability (5/5) Enhanced aluminum has a multi-layer dielectric coating that shares the same durability and handling characteristics of protected aluminum.

3. Protected Silver

I Cost (3/5) A protected silver coated 50 mm dia. spherical mirror with a 100 mm EFL costs approximately \$305.

II Reflection % @ 1020 nm (5/5) Protected silver has a reflection of approximately 95% @ 1020 nm.

III Surface Quality (3/5) Protected silver has a MIL surface quality rating of 60-40.

IV Durability (1/5) Protected silver has a tendency to tarnish when exposed to a high humidity environment. A protective coating is added as an overcoat to reduce the effects of tarnishing. However it is still recommended that silver mirror coatings be operated in a low humidity environment.

4. Protected Gold

I Cost (3/5) A protected gold coated 50 mm dia. spherical mirror with a 100 mm EFL costs approximately \$305.

II Reflection % @ 1020 nm (5/5) Protected gold has a reflection of approximately 96% @ 1020 nm.

III Surface Quality (3/5) Protected gold has a MIL surface quality rating of 60-40.

IV Durability (3/5) Gold as a surface mirror coating is very delicate and requires a protective overcoat for many applications to maintain its high reflectance.

11.3.9. Filter Selection

1. Linear Variable (1.020 μm CWL)[10]

I Deviation from 1.02 μm CLW (5/5) The CWL is exactly 1.02 micron as required. 0 nm deviation.

II Cost (2/5) Cost of the filter is \$2000.

III Transmission (5/5) These filters can transmit 90-95% of incident light in the passband.

IV Optical Density (3/5) The average optical density of this filter type is 3.5.

2. Traditional Coating (0.990 μm CWL)

I Deviation from 1.02 μm CLW (3/5) Deviation from required CWL is 30 nm.

II Cost (5/5) Cost of the filter is \$265.

III Transmission (1/5) Transmission is greater than or equal to 50%.

IV Optical Density (5/5) Minimum Optical Density is 4.

3. Traditional Coating (1.064 μm CWL)

I Deviation from 1.02 μm CLW (2/5) Deviation from required CWL is 44 nm.

II Cost (5/5) Cost of the filter is \$365.

III Transmission (1/5) Transmission is greater than or equal to 50%.

IV Optical Density (1/5) Minimum Optical Density is 3.

4. *Hard Coating (0.980 μm CWL)*

I Deviation from 1.02 μm CLW (2/5) Deviation from required CWL is 40 nm.

II Cost (4/5) Cost of the filter is \$495.

III Transmission (4/5) Transmission is greater than or equal to 85%.

IV Optical Density (5/5) Minimum Optical Density is 4.

5. *Hard Coating (1.030 μm CWL)*

I Deviation from 1.02 μm CLW (4/5) Deviation from required CWL is 10 nm.

II Cost (4/5) The cost of the filter is \$177.47.

III Transmission (4/5) Transmission is greater than or equal to 85%.

IV Optical Density (5/5) Minimum Optical Density is 4.

6. *Custom Coating (1.020 μm CWL)*

I Deviation from 1.02 μm CLW (5/5) CWL is exactly as required. 0 nm deviation.

II Cost (1/5) Cost of the filter is on a quote basis. Uncertain given that it varies based on aperture but generally very expensive.

III Transmission (3/5) Transmission is greater than or equal to 70%.

IV Optical Density (3/5) Minimum Optical Density 3.5.

12. Appendix B: Drawings

12.1. Optical Bench Part Drawings

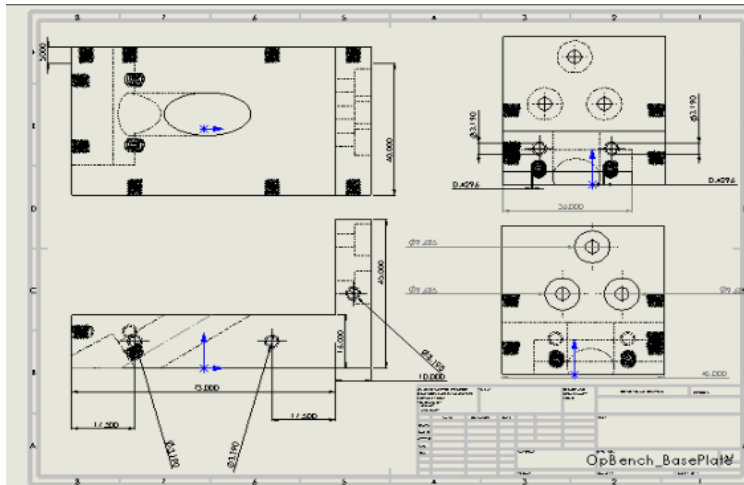


Figure 112. Optical Bench Drawing

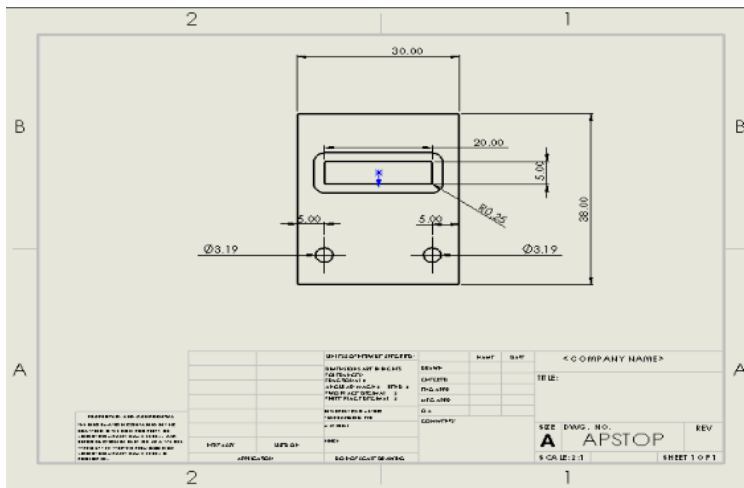


Figure 113. Aperture Stop Drawing

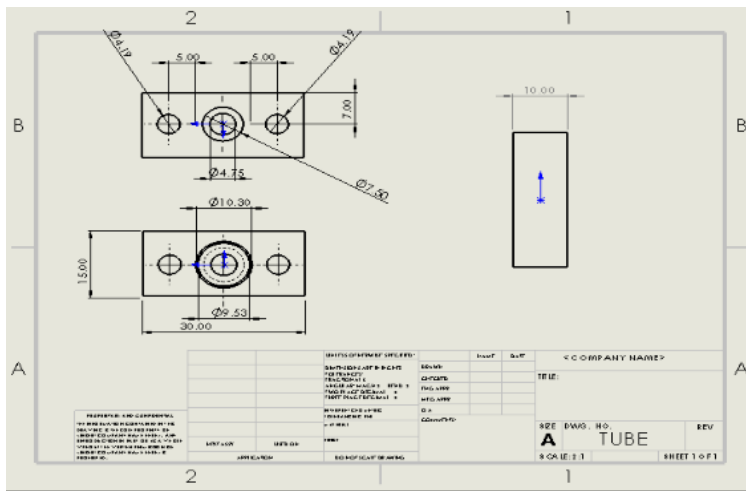


Figure 114. Diode Block Drawing

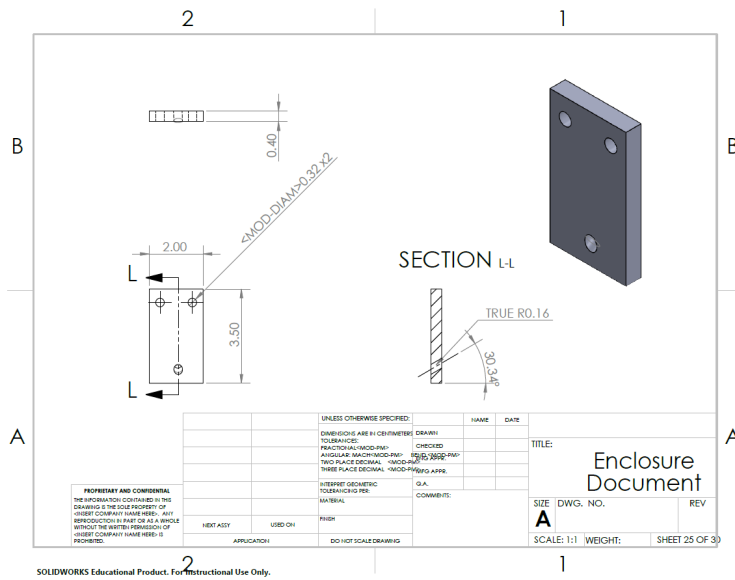


Figure 115. Tooling Plate Drawing

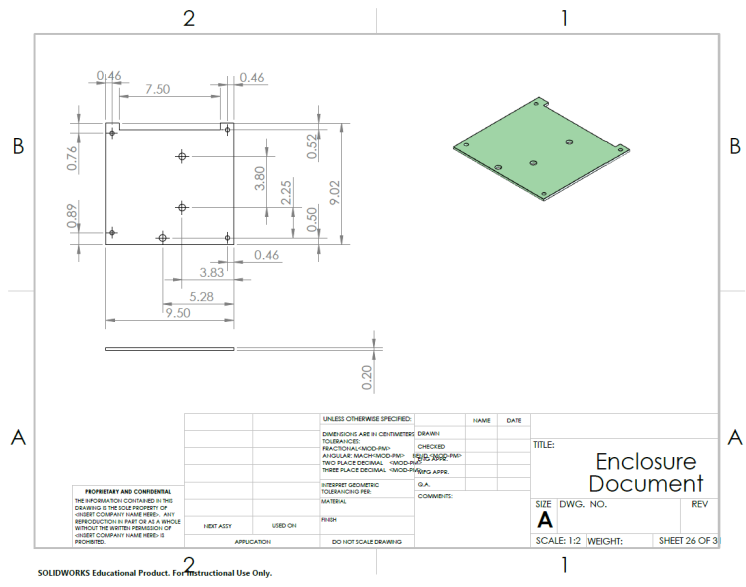


Figure 116. Tooling Plate Drawing

12.2. Enclosure Drawings

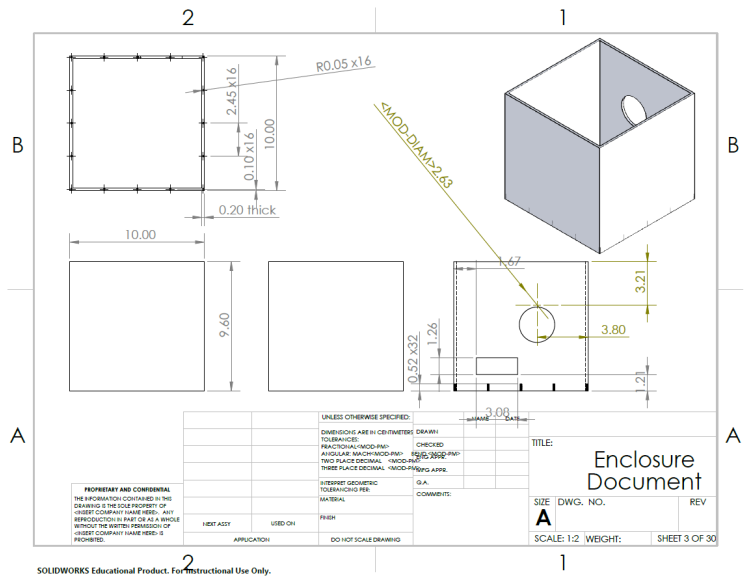


Figure 117. Enclosure Tube Drawing

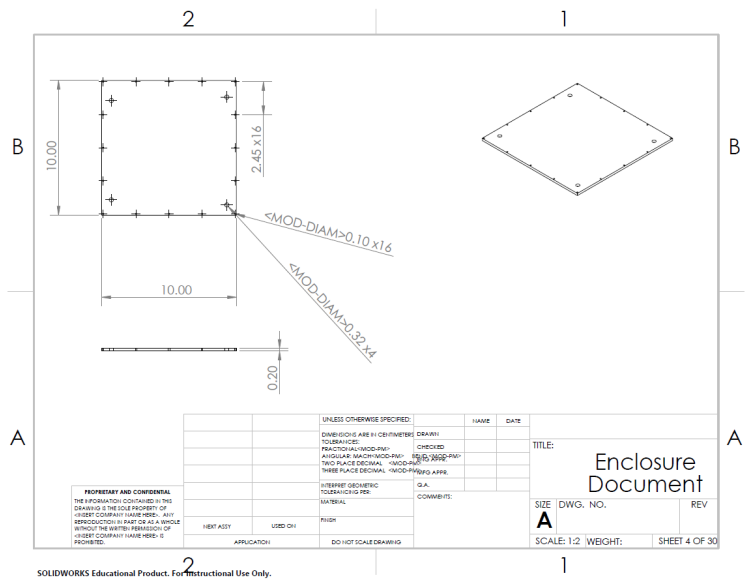


Figure 118. Enclosure Bottom Drawing

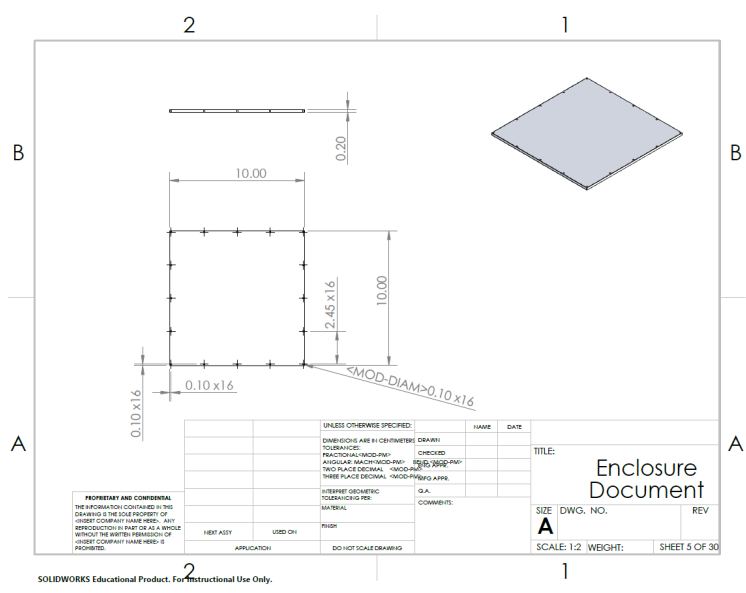


Figure 119. Enclosure Top Drawing

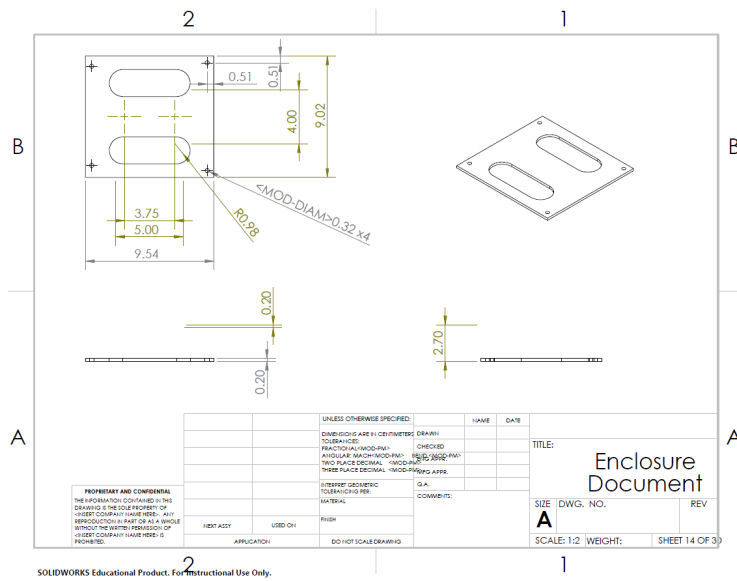
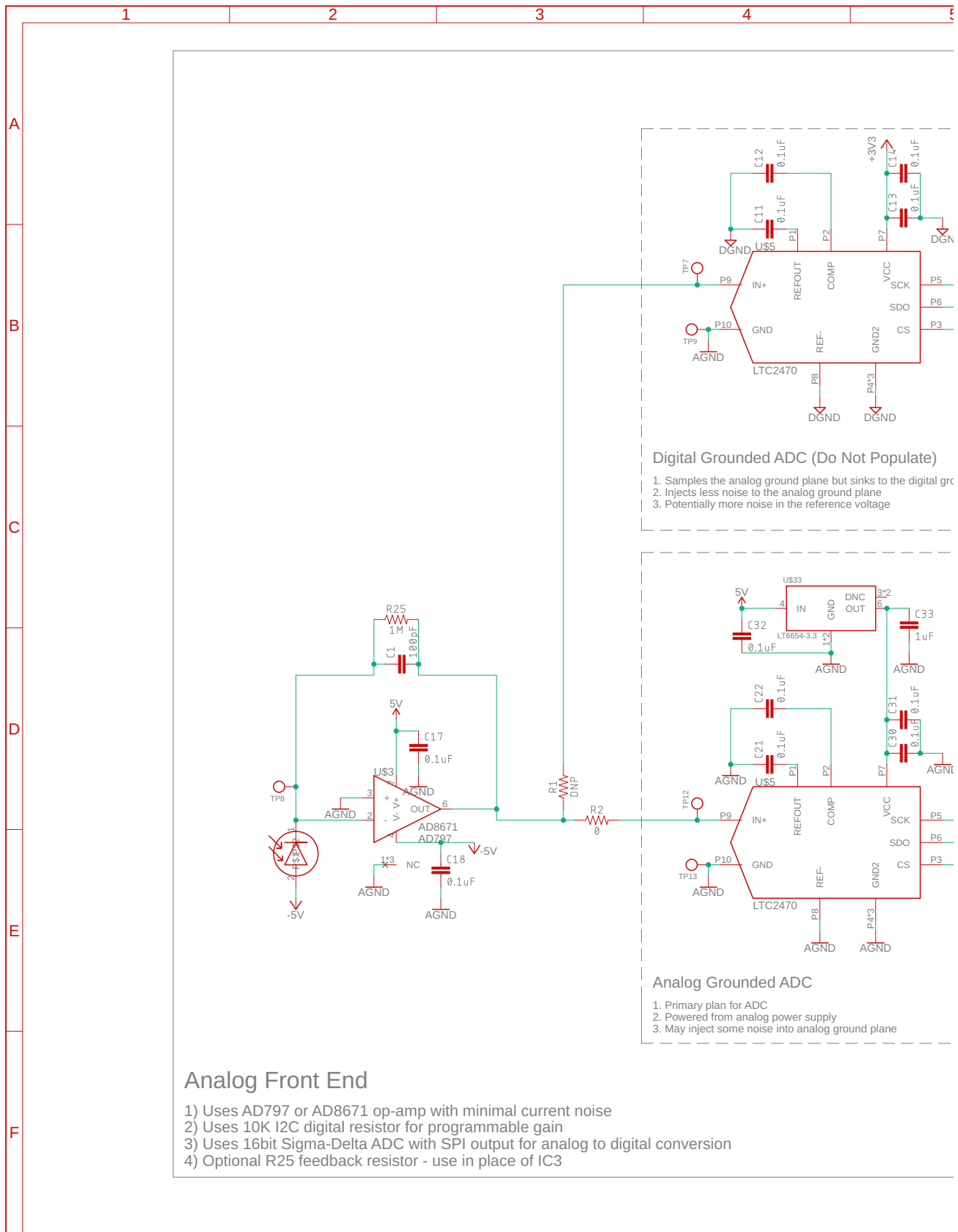


Figure 120. Enclosure Handle Drawing

12.3. Electronics

12.3.1. Schematic

See next page



Digital Grounded ADC (Do Not Populate)

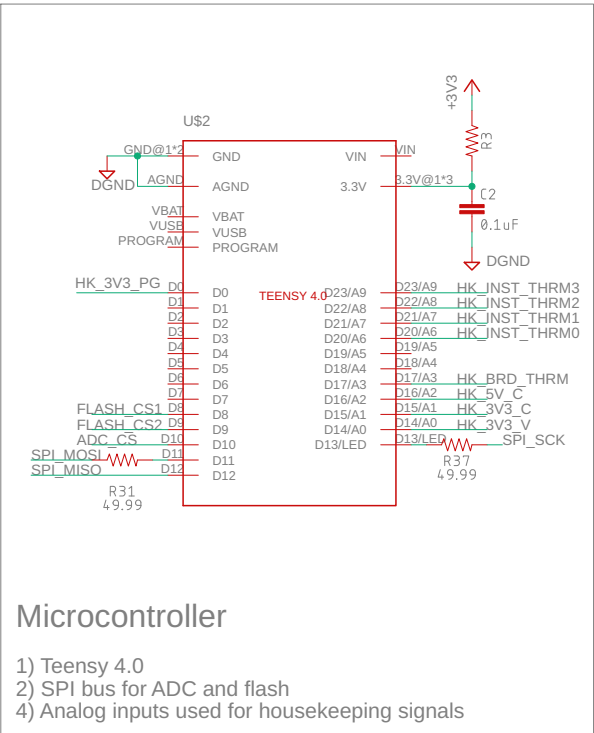
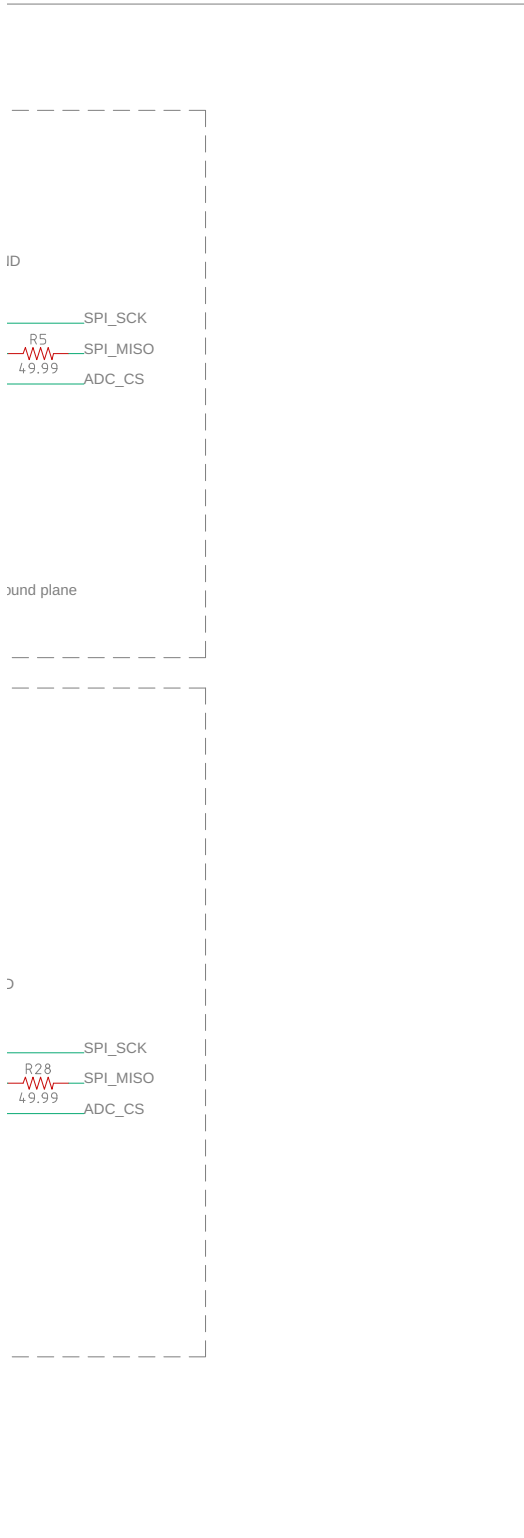
1. Samples the analog ground plane but sinks to the digital grc
2. Injects less noise to the analog ground plane
3. Potentially more noise in the reference voltage

Analog Grounded ADC

1. Primary plan for ADC
2. Powered from analog power supply
3. May inject some noise into analog ground plane

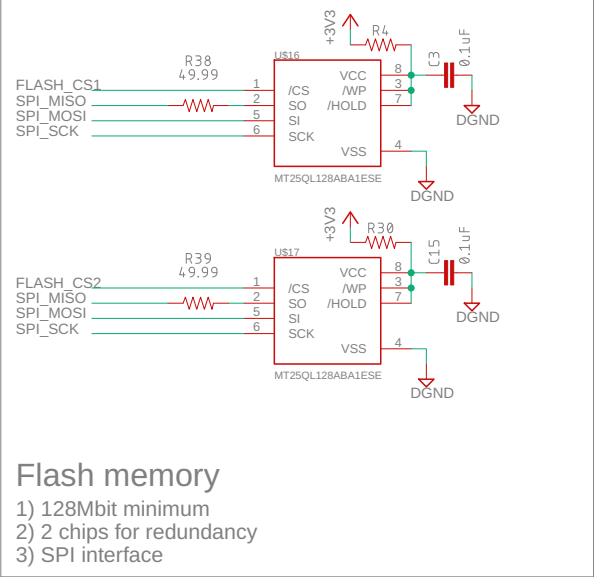
Analog Front End

- 1) Uses AD797 or AD8671 op-amp with minimal current noise
- 2) Uses 10K I2C digital resistor for programmable gain
- 3) Uses 16bit Sigma-Delta ADC with SPI output for analog to digital conversion
- 4) Optional R25 feedback resistor - use in place of IC3



Microcontroller

- 1) Teensy 4.0
- 2) SPI bus for ADC and flash
- 4) Analog inputs used for housekeeping signals



Flash memory

- 1) 128Mbit minimum
- 2) 2 chips for redundancy
- 3) SPI interface

NanoSAM Electronics Board	
TITLE: nanoSAM	
Document Number:	REV: A
Date: 12/14/19 5:52 PM	Sheet: 1/2

A

B

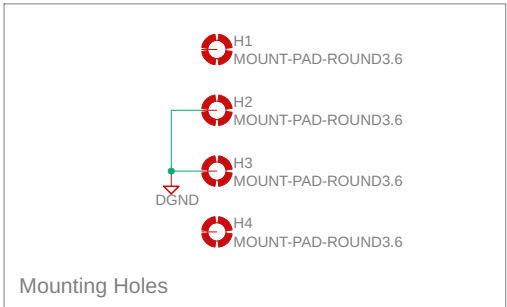
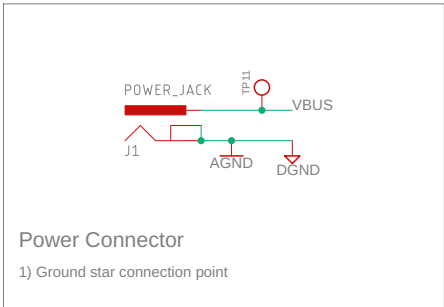
C

D

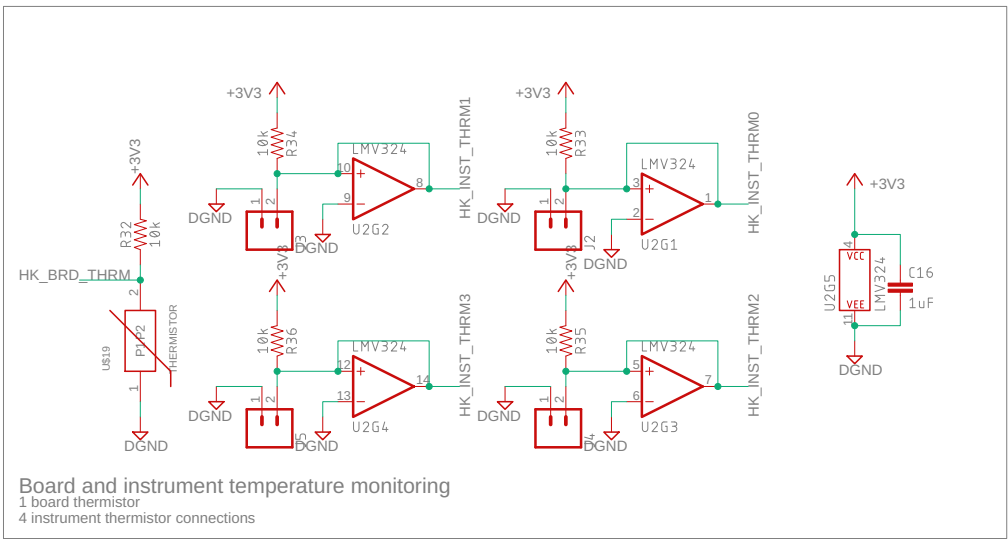
E

F

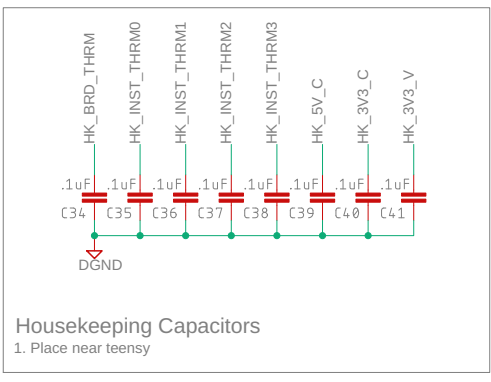
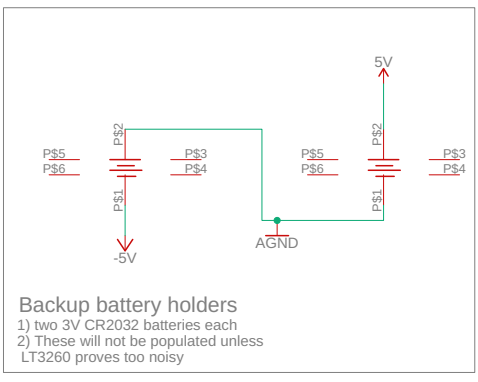
A
B
C
D
E
F



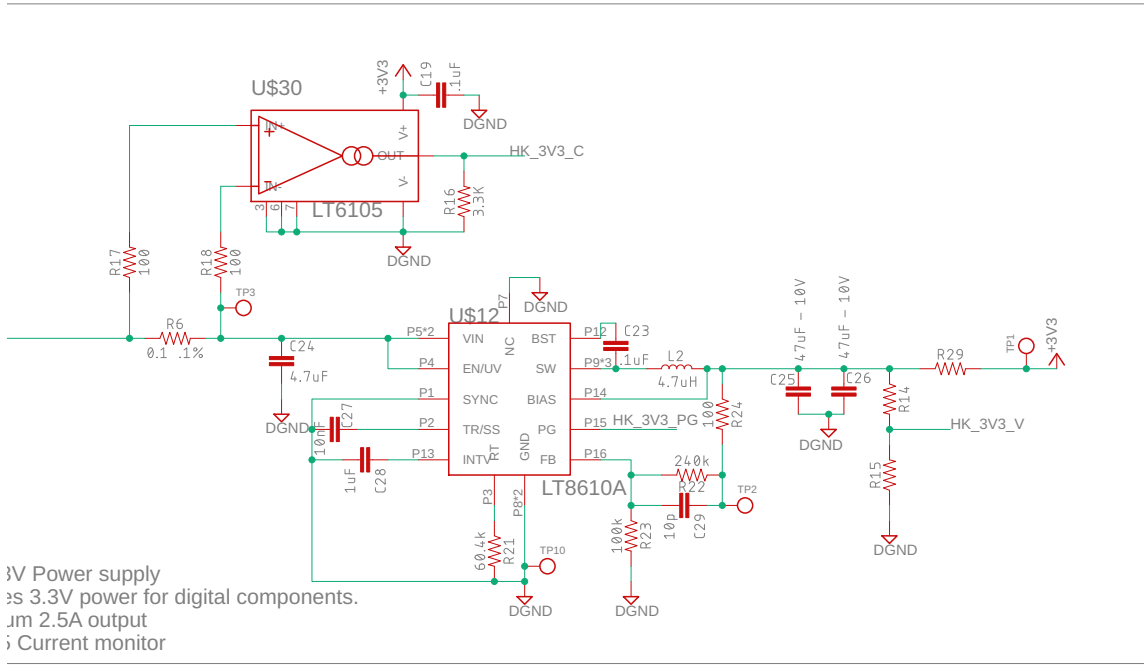
VBUS



Digital 3.3
1) Provide
2) Maxim
3) LT6105



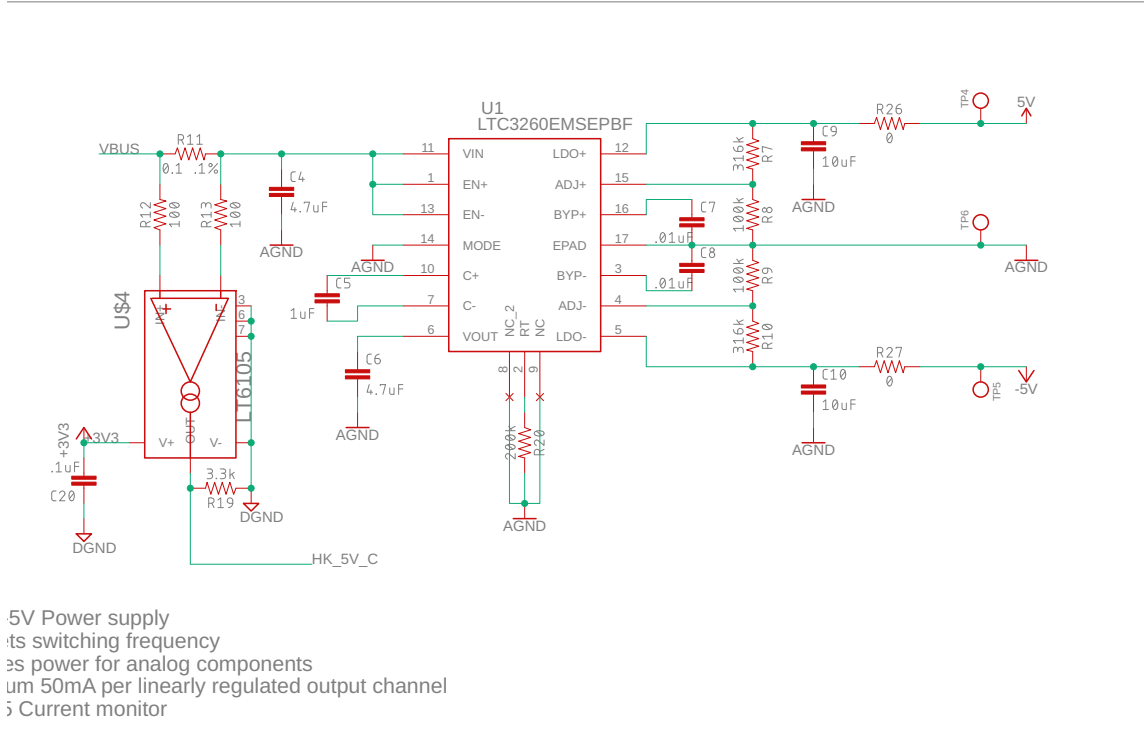
Analog +
1) R20 se
2) Provid
3) Maxim
4) LT1605



A

B

C



D

E

F

12.3.2. Layout

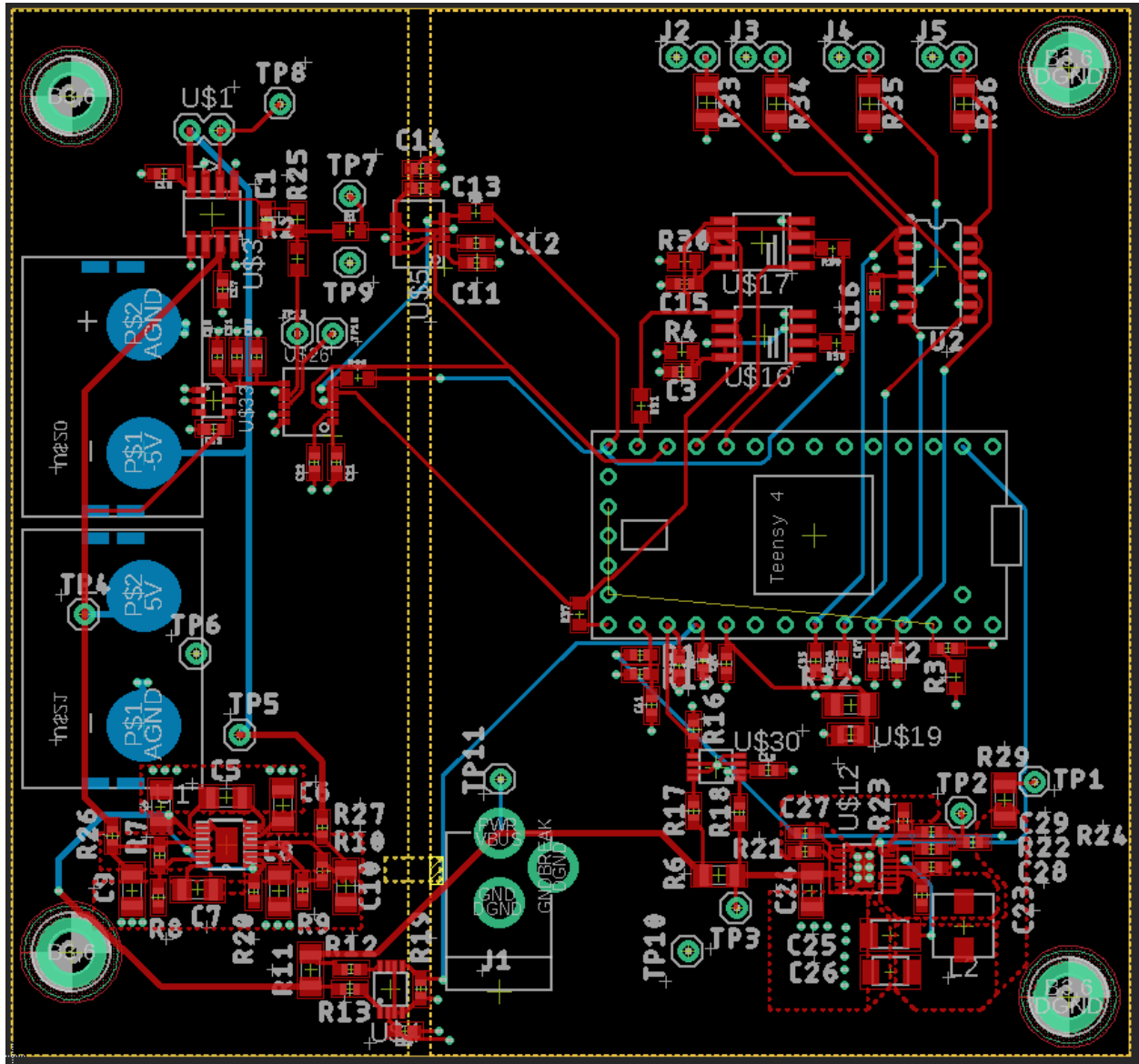


Figure 121. PCB Layout

12.4. Signal-to-Noise Ratio Calculation Code

```
% Signal to noise for nominal 1020 nm wavelength and testing 1030 nm
% wavelength
clear all; close all; clc

% Organize constants for computing signal and noise terms
h = 6.626e-34; % Planck's constant, kg-m^2/s
c = 2.99792458e8; % speed of light in vacuum, m/s
l = [1020,1030]; % wavelength vector, nm
Ep = h*c./(l/10^9); % energy per photon, J
ap_arcmin = 0.947; % aperture, arcmin
solardisk_avg_arcmin = 31.99; % solar disk diameter, arcmin
Phi = [709.75,698.00]*10^(-3); % solar spectral irradiance, W/(m^2*nm)
BW = 10; % bandwidth, nm
Aap = 1e-4; % Aperture area, m^2
Rmirror = 0.97; % mirror reflectivity in testing wavelength range, dimensionless
R = [0.398,0.3485]; % Responsivity, A/W
e = 1.60218e-19; % Elementary charge, C/electron
f = 208; % ADC Sampling rate, Hz
Ts = 1/f; % Sampling time for ADC, s
N = 3; % Number of samples to average for f_samp = 70 Hz
SNRreqt = 2^10*sqrt(12); % Ideal SAM-II SNR for 10 bit signal

% Calculate signal
fraction = (ap_arcmin/solardisk_avg_arcmin)^2;
Power = Phi*BW*Aap; % W/(m^2*nm)*nm*m^2=W
Power_a = fraction*Power; % power through aperture, W
photon_rate = Rmirror*Power_a./Ep; % photons/sec through aperture
QE = R.*Ep/e; % Quantum efficiency
signal = photon_rate.*QE; % Signal from photodiode, counts/s
photons = photon_rate*Ts; % number of photons for a sample time
photoelectrons = photons.*QE; % Signal from photodiode for a sample time, counts

% Calculate Shot Noise
Nshot = sqrt(photon_rate).*QE; % Shot noise

% Calculate Dark noise
Idark = 10e-12/e; % counts/s
Ndark = sqrt(Idark); % Dark current noise term

% Quantization Noise
bits = 16; % Test with both 12 and 16 bits
ADC_margin = 0.20; % 20% ADC margin
LSB = (1+ADC_margin).*(signal./2^bits); % least significant bit
Nquan = LSB/sqrt(12); % Quantization noise term

% Transimpedance noise
Inoise_imp = 27e-12; % A/sqrt(Hz)
fsig = 25; % Worst case DC signal 'frequency'
Inoise = Inoise_imp*sqrt(fsig)/e; % Transimpedance noise current, counts/s
Ntran = sqrt(Inoise); % Transimpedance noise term

% Power Supply Noise
VnoisePS = 100; % microV
ratio = 10^(-110/20); % rejection ratio from op amp (110dB)
Vnoise = ratio*VnoisePS*10^(-6); % voltage noise
Rfeed = 1./(signal.*e); % ohms (purpose is for a check)
InoisePS = Vnoise./Rfeed*(1/e); % counts/s
NPS = sqrt(InoisePS); % Power supply noise term
```

```

% Calculate Signal to Noise
SNR = sqrt(N)*signal./sqrt(Nquan.^2 + Ndark.^2 + Nshot.^2 + Ntran.^2 + NPS.^2);
Margin = (SNR(2)/SNRreq-1)*100; % SNR margin to requirement in percent

% Display relevant values
fprintf('Signal %1.3E \n', signal(2))
fprintf('SNR %1.3E \n', SNR(2))
fprintf('Nsignal %1.3E \n', signal(2))
fprintf('Nquant %1.3E \n', Nquan(2))
fprintf('Nshot %1.3E \n', Nshot(2))
fprintf('Ndark %1.3E \n', Ndark)
fprintf('Ntrans %1.3E \n', Ntran)
fprintf('Nps %1.3E \n', NPS(2))
fprintf('Bits %d \n', bits)
fprintf('SNR margin (%)%4.0f \n',Margin)

```

The signal-to-noise model was developed using the maximum transmission, bandwidth, and mirror reflectivity for a predicted signal and incorporating terms for the shot noise, dark noise, trans-impedance amplifier noise, and power supply noise. The predicted signal was calculated using the following process.

$$P = \left(\frac{FOV}{\theta_{sd}^2} \right) \Phi BWA_{ap} \quad (11)$$

First, the power coming through the aperture after the filter needed to be estimated. In order to quantify the power, the equation in eq. 11 was used. Equation 11 incorporates the solar spectral irradiance at the center wavelength (1030 nm) found from tabulated data [2]. This irradiance value is multiplied by the proportion of the instrument FOV to the square of the solar disk diameter to predict the irradiance seen by the instrument. Additionally, the irradiance should be multiplied by the filter system bandwidth and area of the aperture to determine what power is expected to reach the mirror.

$$E_{photon} = hf = \frac{hc}{\lambda} \quad (12)$$

The value for the power reaching the mirror can be used to find the rate of photons reflected off the mirror. This can be completed by first calculating the energy of a photon at the testing wavelength of 1030 nm using eq. 12.

$$\Psi = R_{mirror} \frac{P}{E_{photon}} \quad (13)$$

By dividing the power through the aperture by the energy of the photon, the rate of photons hitting the mirror is calculated. However, the mirror is not a perfect reflector, therefore the photons reflected off the mirror is slightly less than those reaching the mirror. Therefore, the rate of photons reflected by the mirror must also take the mirror reflectivity into account.

$$Q = \frac{RE_{photon}}{e} \quad (14)$$

The signal expected from the photodiode (photocurrent) will be determined using the rate of photons from the mirror. It is important to note that not every collision of an incoming photon with the photodiode active area releases an electron for current. Whether this occurs or not is dependent on the quantum efficiency of the photodiode at the incoming wavelength of the light. The photodiode quantum efficiency can be determined using the responsivity of the photodiode at the testing wavelength of 1030 nm and eq. 14.

$$S = Q\Psi \quad (15)$$

The photocurrent from the photodiode using the quantum efficiency and photon rate from the mirror can be calculated using eq. 15. The value from eq. 15 is used in the SNR model for the signal term. The units of the signal using

the set of equations in the forms as outlined above is counts per second.

Significant noise terms were identified by taking into account the shot noise from the input to the photodiode (light reflected from the mirror) and non-negligible noise sources from the electronics system. The noise terms from the electronics system that were determined to be significant are noise from the dark current, the quantization of the data in the ADC, the transimpedance amplifier, and the power supply. These terms are what will be included in the SNR model.

$$N_{shot} = Q\sqrt{\Psi} \quad (16)$$

The shot noise is a result of the counting of photons in order to read a signal from the photodiode. This noise term is calculated by taking the square root of the incoming photons to the photodiode and the multiplied by the quantum efficiency as shown in eq. 16. This gives the noise current from the photon counting that the photodiode is expected to output incorrectly as signal.

$$N_{dark} = \sqrt{\frac{I_{dark}}{e}} \quad (17)$$

Additionally the photodiode is will also output some dark current that contributes to the noise on the signal. The noise term for the dark current can be calculated using eq. 17.

$$LSB = \frac{(1 + M)}{2^n} S \quad (18)$$

$$N_{quan} = \frac{LSB}{\sqrt{12}} \quad (19)$$

The quantization noise calculation takes into account the number of bits used by the ADC and the ADC margin. In order to compute the quantization noise, the least significant bit must be for the incoming signal using eq. 18. The quantization noise term can then be computed using eq. 19. The $\sqrt{12}$ term in the denominator is a result of the uniform distribution of quantization noise and the root-mean-square of that noise distribution [32].

$$I_{tran} = I_{max,in} \sqrt{f_{DC}} \quad (20)$$

$$N_{tran} = \sqrt{\frac{I_{tran}}{e}} \quad (21)$$

The noise from the transimpedance amplifier is derived from a value from the data sheet. This is given as a maximum noise current from the transimpedance amplifier as a function of the signal frequency. At the point of the transimpedance amplifier, the signal should be DC. However, small signal fluctuations may be present that can be interpreted as a frequency and add significant noise. In order to account for this, a worst case “frequency” of the signal will be used in the SNR model. The expected maximum noise current is calculated using eq. 20 and the noise term is computed using eq. 21.

$$I_{PS} = \frac{V_{PS} PRR_{op-amp}}{R_{feedback}} \quad (22)$$

$$N_{PS} = \sqrt{\frac{I_{PS}}{e}} \quad (23)$$

The calculation of the noise term from the power supply incorporates the output from the op-amp connected to the power supply. The data sheet of the power supply gives a noise voltage. By taking into account the power rejection ratio of the op-amp the noise voltage drop across the feedback resistor can be estimated. By dividing that voltage by the feedback resistor value, the current noise output from the power supply can be calculated as in eq. 22. The power supply noise term can then be calculated using eq. 23.

$$SNR = \frac{\sqrt{NS}}{\sqrt{N_{quan}^2 + N_{shot}^2 + N_{dark}^2 + N_{tran}^2 + N_{PS}^2}} \quad (24)$$

The signal-to-noise ratio is calculated using the eq. 24. The noise terms are summed in quadrature in the denominator. In this case, the ADC samples at a rate of 208 Hz and every three samples are averaged for a reduced sampling rate of 70 Hz. Therefore, three samples are taken per measurement recorded, therefore the noise terms must be multiplied by the $\frac{1}{\sqrt{N}}$. The multiplier accounting for number of measurements per sample can then be moved as a multiplier in the numerator for clarity. [39]

13. Appendix C: Project Management

	Name	% Complete	Start	Finish	Predecessors
1	☐ Preliminary Design Phase	100%	09/16/2019	10/14/2019	
2	Project Definition Document (PDD)	100%	09/16/2019	09/16/2019	
3	Define Requirements	100%	09/16/2019	09/18/2019	
4	Conceptual Design Document (CDD)	100%	09/30/2019	09/30/2019	3
5	☐ Preliminary Design Review (PDR)	100%	10/06/2019	10/14/2019	
11	☐ Critical Design Phase	100%	10/13/2019	12/02/2019	
12	☐ Systems	100%	10/13/2019	12/01/2019	
13	Create Work Breakdown Structure (WBS)	100%	10/30/2019	11/04/2019	
14	Order Preliminary Components	100%	10/21/2019	10/23/2019	
15	Finalize CONOPS	100%	11/11/2019	11/11/2019	
16	FMEA	100%	11/13/2019	11/13/2019	
17	Budget	100%	11/15/2019	11/15/2019	
18	Risk Matrix	100%	11/17/2019	11/17/2019	
19	Bill of Materials	100%	11/21/2019	11/21/2019	
20	Implement PDR Feedback	100%	10/15/2019	12/01/2019	10
21	Create Organizational Chart	100%	10/13/2019	10/14/2019	
22	☐ Integration/Test	100%	11/18/2019	11/22/2019	
23	Test Plan Draft	100%	11/18/2019	11/18/2019	
24	ICD	100%	11/18/2019	11/18/2019	
25	Assembly Drawings	100%	11/20/2019	11/20/2019	
26	Testing Flowchart	100%	11/21/2019	11/22/2019	
27	☐ Electronics/ Software	100%	11/13/2019	11/20/2019	
28	All Electronics Schematics	100%	11/13/2019	11/13/2019	
29	Power Budget	100%	11/18/2019	11/18/2019	
30	Software Pseudocode	100%	11/15/2019	11/15/2019	
31	Radiometric Model	100%	11/20/2019	11/20/2019	
32	☐ Optics	100%	11/10/2019	11/15/2019	
33	Optical Bench Drawing	100%	11/10/2019	11/10/2019	
34	Filter Housing Drawing	100%	11/15/2019	11/15/2019	
35	Optical Mounts Drawing	100%	11/15/2019	11/15/2019	

Figure 122. Part 1 of 4 of task list

	Name	% Complete	Start	Finish	Predecessors
36	<input type="checkbox"/> Mechanical	100%	11/13/2019	11/15/2019	
37	Cubesat Enclosure Drawing	100%	11/15/2019	11/15/2019	32
38	Finalize Materials	100%	11/13/2019	11/13/2019	
39	<input type="checkbox"/> Critical Design Review (CDR)	100%	11/19/2019	12/02/2019	
40	CDR Draft	100%	11/19/2019	11/20/2019	
41	CDR Presentation Practice	100%	11/29/2019	12/01/2019	
42	CDR Due Date	100%	12/02/2019	12/02/2019	10
43	<input checked="" type="checkbox"/> Fall Final Report (FFR)	100%	12/08/2019	12/16/2019	
46	<input type="checkbox"/> Manufacturing Phase	100%	01/13/2020	02/21/2020	
47	<input type="checkbox"/> Systems/ PM	100%	01/13/2020	02/21/2020	
48	Risk Mitigation	100%	01/13/2020	02/21/2020	
49	Monitor/Track Requirements	100%	01/13/2020	02/21/2020	
50	Create Internal Deadlines	100%	01/13/2020	01/24/2020	
51	Update Schedule	100%	01/13/2020	01/17/2020	
52	Update Expenditure Plan	100%	01/13/2020	01/17/2020	
53	Update Bill of Materials	100%	01/13/2020	01/17/2020	
54	Purchasing & Procurement for Testing	100%	01/14/2020	01/17/2020	
55	<input type="checkbox"/> Optics	100%	01/14/2020	01/22/2020	
56	Purchasing	100%	01/14/2020	01/22/2020	
57	<input type="checkbox"/> Electronics	100%	01/14/2020	01/22/2020	
58	Purchasing & Ordering	100%	01/14/2020	01/22/2020	
59	<input type="checkbox"/> Mechanical	100%	01/15/2020	01/24/2020	
60	Purchasing & Procurement	100%	01/15/2020	01/22/2020	
61	Half-ball Lens Release Mechanism	100%	01/16/2020	01/24/2020	
62	<input type="checkbox"/> Manufacturing	100%	01/22/2020	02/14/2020	
63	Manufacturing Plan	100%	01/22/2020	01/29/2020	
64	Diode Tube	100%	01/29/2020	02/14/2020	
65	Stack Handle	100%	01/31/2020	02/05/2020	
66	Shims Stacks	100%	01/31/2020	02/05/2020	
67	Enclosure Plates	100%	01/31/2020	02/05/2020	

Figure 123. Part 2 of 4 of task list

	Name	% Complete	Start	Finish	Predecessors
68	Optical Bench Plate	100%	01/31/2020	02/05/2020	
69	Gold Coating	100%	02/03/2020	02/10/2020	
70	Rectangular Tube Enclosure	100%	02/03/2020	02/10/2020	
71	Optical Bench	100%	02/03/2020	02/13/2020	
72	Tooling Plate	100%	02/03/2020	02/14/2020	
73	Aperture Stop	100%	02/03/2020	02/14/2020	
74	<input type="checkbox"/> Software	99%	01/20/2020	02/17/2020	
75	Software Code	99%	01/20/2020	02/17/2020	
76	Manufacturing Slack	100%	02/14/2020	02/21/2020	
77	MSR Draft	100%	01/27/2020	01/27/2020	
78	MSR Practice Presentation	100%	01/29/2020	01/29/2020	
79	Manufacturing Status Review	100%	02/03/2020	02/03/2020	
80	AIAA Abstract Deadline	100%	02/15/2020	02/15/2020	
81	<input type="checkbox"/> Integration Phase	83%	02/03/2020	03/20/2020	
82	Assemble PCB to Stack	100%	02/03/2020	02/10/2020	
83	Assemble Stack Plates	100%	02/10/2020	02/17/2020	65
84	Integrate Electronics with Software	100%	02/17/2020	03/07/2020	74
85	MTF & Alignment Practice	100%	02/27/2020	03/06/2020	
86	Assemble Optics System on Bench	100%	02/27/2020	03/10/2020	68,64
87	Assemble NanoSAM	8%	03/09/2020	03/13/2020	79
88	Alignment & Integration Slack	0%	03/13/2020	03/20/2020	
89	<input type="checkbox"/> Testing Phase	34%	02/09/2020	04/15/2020	
90	<input type="checkbox"/> Logistics	0%	02/09/2020	02/21/2020	
94	Measure Power Consumption	100%	02/24/2020	03/02/2020	

Figure 124. Part 3 of 4 of task list

	Name	% Complete	Start	Finish	Predecessors
95	Bus Compatibility Verification	100%	02/26/2020	03/06/2020	
96	MTF Verification	100%	02/28/2020	03/10/2020	
97	TRR Draft	100%	02/27/2020	02/27/2020	
98	Software Testing	100%	03/02/2020	03/13/2020	
99	Test Readiness Review	100%	03/06/2020	03/07/2020	85
100	AIAA Paper Draft Deadline	100%	03/06/2020	03/06/2020	80
101	Electronics & Software Interaction Testing	100%	03/13/2020	03/24/2020	98
102	AIAA Paper Course Deadline	100%	03/13/2020	03/13/2020	100
103	Temperature Verification	0%	03/18/2020	03/22/2020	
104	Electronics Testing Slack	0%	03/21/2020	03/29/2020	
105	Stability Testing	0%	03/22/2020	04/03/2020	
106	Error Verification	0%	03/22/2020	04/03/2020	
107	Day-in-life	0%	03/30/2020	04/06/2020	
108	Data Verification	0%	04/03/2020	04/10/2020	
109	SNR Verification	0%	04/03/2020	04/10/2020	
110	Day-in-Life Slack	0%	04/06/2020	04/13/2020	
111	Verify All Requirements	0%	04/06/2020	04/13/2020	
112	General Slack	0%	04/10/2020	04/15/2020	
113	Project Closeout	25%	03/21/2020	05/04/2020	
114	AIAA Conference Paper Due	100%	03/21/2020	03/21/2020	
115	Report Requirements Compliance	0%	04/13/2020	04/13/2020	
116	Final Oral Review	0%	04/20/2020	04/20/2020	115
117	Project Final Report	0%	05/04/2020	05/04/2020	116

Figure 125. Part 4 of 4 of task list

14. References

References

- [1] Oleg Alexandrov. *Prime Focus Ray Diagram*, CC BY-SA 3.0. 2019. URL: https://upload.wikimedia.org/wikipedia/commons/b/b4/Prime_focus_telescope.svg (visited on 10/01/2010).
- [2] American Society for Testing and Materials. *Reference Air Mass 1.5 Spectra*. 2019. URL: <https://www.nrel.gov/grid/solar-resource/spectra-aml1.5.html> (visited on 12/15/2019).
- [3] Atmospheric Radiation Measurement User Facility. *Update to Langley VAP Dismisses Outliers*. 2019. URL: <https://www.arm.gov/news/data/post/19810> (visited on 12/15/2019).
- [4] Clayton B. Crail. *Ranking CubeSat Communication Systems Using a Value-centric Framework*. Report. Massachusetts Institute of Technology, 2013.
- [5] CU Boulder. *ASEN_ASTR_GEO 6050 Space Instrumentation: Lecture 16 Remote Sensing Instruments*. PDF. University of Colorado Boulder, 2019.
- [6] Edmund Optics. *5 Tips for Designing with Off-the-Shelf Optics*. 2019. URL: <https://www.edmundoptics.com/resources/application-notes/optics/5-tips-for-designing-with-off-the-shelf-optics/> (visited on 10/01/2010).
- [7] Edmund Optics. *Bandpass Interference Filter*. 2019. URL: <https://www.edmundoptics.com/f/bandpass-interference-filters/14371/> (visited on 10/01/2019).
- [8] Edmund Optics. *Comparison of Optical Aberrations*. 2019. URL: <https://www.edmundoptics.com/resources/application-notes/optics/comparison-of-optical-aberrations/> (visited on 10/01/2019).
- [9] Edmund Optics. *Considerations in Collimation*. 2019. URL: <https://www.edmundoptics.com/resources/application-notes/optics/considerations-in-collimation/> (visited on 10/01/2010).
- [10] Edmund Optics. *Linear Variable Bandpass Filter*. 2019. URL: <https://www.edmundoptics.com/f/linear-variable-bandpass-filters-5fd8f505/14865/> (visited on 11/01/2019).
- [11] Edmund Optics. *Metallic Mirror Coatings*. 2019. URL: <https://www.edmundoptics.com/resources/application-notes/optics/metallic-mirror-coatings/> (visited on 10/01/2019).
- [12] Edmund Optics. *Off-Axis Parabolic Mirror Selection Guide*. 2019. URL: <https://www.edmundoptics.com/resources/application-notes/optics/off-axis-parabolic-mirror-selection-guide/> (visited on 10/01/2019).
- [13] Edmund Optics. *Optical Filters*. 2019. URL: <https://www.edmundoptics.com/c/optical-filters/610/#> (visited on 10/01/2019).
- [14] Edmund Optics. *Optical Glass Specifications*. 2019. URL: <https://www.edmundoptics.com/resources/application-notes/optics/optical-glass/> (visited on 10/01/2010).
- [15] Edmund Optics. *SURFACE SPECIFICATIONS*. 2019. URL: <https://www.edmundoptics.com/resources/application-notes/optics/understanding-optical-specifications/> (visited on 10/01/2010).
- [16] Edmund Optics. *Ø25.4 X 54.45mm EFL 30° OAP PROTECTED ALUMINUM MIRROR 100Å*. 2019. URL: <https://www.edmundoptics.com/p/254-x-508mm-pfl-30-off-axis-parabolic-aluminum-mirror/33454/> (visited on 12/15/2019).
- [17] Electronic Notes. *Photodiode Structures*. 2019. URL: www.electronics-notes.com/articles/electronic_components/diode/photodiode-detector-structures-fabrication-materials.php (visited on 12/15/2019).

- [18] Epilog Laser. *Epilog Fusion M2 Laser Series*. 2019. URL: <https://www.epiloglaser.com/laser-machines/fusion-laser-series.htm> (visited on 12/15/2019).
- [19] S. Horne. “Concentrating Photovoltaic (CPV) Systems and Applications”. In: (2015).
- [20] Krishnavedala. *Cassegrain Telescope Rays - CC BY-SA 4.0*. 2019. URL: https://upload.wikimedia.org/wikipedia/commons/b/b1/Cassegrain_%5BTelescope.svg (visited on 10/01/2019).
- [21] Krishnavedala. *Newtonian Telescope Rays - CC BY-SA 4.0*. 2019. URL: https://upload.wikimedia.org/wikipedia/commons/8/86/Newtonian_%5Btelescope2.svg (visited on 10/01/2019).
- [22] John M. Kusterer. “SAGE III-ISS Data and Information”. In: NASA (2019).
- [23] Anatoly A. Maslov et al. “Mach 6 Boundary-Layer Stability Experiments on Sharp and Blunted Cones”. In: *Journal of Spacecraft and Rockets* (2006).
- [24] MatWeb. *Aluminum 6061-T6 Data Sheet*. 2019. URL: http://amet-me.mnsu.edu/UserFilesShared/DATA_ACQUISITION/mts/met277/9_13-12/MaterialData_9391_Al-6061.pdf (visited on 12/15/2010).
- [25] Mouser Electronics - Electronic Components Distributor. *SAR Analog to Digital Converters - ADC*. 2019. URL: www.mouser.com/Semiconductors/Data-Converter-ICs/Analog-to-Digital-Converters-ADC/-/N-4c43g?P=1z0t3by (visited on 10/01/2010).
- [26] Mouser Electronics - Electronic Components Distributor. *Sigma-Delta ADCs*. 2019. URL: www.maximintegrated.com/en/design/technical-documents/tutorials/1/1870.html (visited on 10/01/2010).
- [27] Myers, Matthew G. and Piszczor, Michael F. *High Altitude Solar Cell Calibration Flights*. 2019. URL: <https://ntrs.nasa.gov/archive/nasa/casi.ntrs.nasa.gov/20160005276.pdf> (visited on 12/15/2019).
- [28] National Renewable Energy Laboratory. *2000 ASTM Standard Extraterrestrial Spectrum Reference E-490-00*. 2000. URL: <https://www.nrel.gov/grid/solar-resource/spectra-astm-e490.html> (visited on 10/28/2010).
- [29] *Parabolic shape eliminates spherical aberration in telescope mirrors*. 2019. URL: <https://amazing-space.stsci.edu/resources/explorations/groundup/lesson/basics/gl2/> (visited on 10/01/2019).
- [30] M. R. Rampino and S. Self. “Sulphur-rich volcanic eruptions and stratospheric aerosols”. In: *Nature* 310 (1984), pp. 677–679.
- [31] Cora E. Randall et al. “POAM III retrieval algorithm and error analysis”. In: *Journal of Geological Research* 102.D21 (2002). DOI: [10.1029/2002JD002137](https://doi.org/10.1029/2002JD002137).
- [32] RP Photonics Encyclopedia. *Quantization Noise and Signal-Noise Ratio (SNR)*. 2019. URL: <http://www.onmyphd.com/?p=quantization.noise.snr> (visited on 12/15/2019).
- [33] RP Photonics Encyclopedia. *Responsivity*. 2019. URL: https://www.rp-photonics.com/quantum_efficiency.html (visited on 12/15/2019).
- [34] Schott. *Schott Borofloat 33 Data Sheet*. 2019. URL: https://psec.uchicago.edu/glass/borofloat_33_e.pdf (visited on 12/15/2019).
- [35] Schott. *Schott N-BK7 Data Sheet*. 2019. URL: https://www.us.schott.com/d/advanced/_optics/31255521-bf27-46f1-ab3b-f35290482499/schott-datasheet-nbk7-english.pdf (visited on 10/01/2010).
- [36] Daniel J. Schroeder. “Astronomical Optics”. In: Second. Academic Press, 2000. Chap. Chapter 11 Transfer Functions; Hubble Space Telescope.
- [37] Katie M. Schwertz and James H. Burge. *Optomechanical Design and Analysis*. Vol. FG26. SPIE, 2012.

- [38] Warren J. Smith. "Modern Optical Engineering 4th Edition". In: 2007 (2007).
- [39] John R. Taylor. "An Introduction to Error Analysis". In: *University Science Books* (1997).
- [40] ThorLabs. *FELH1000 - Ø25.0 mm Premium Longpass Filter, Cut-On Wavelength: 1000 nm*. 2019. URL: <https://www.thorlabs.com/thorproduct.cfm?partnumber=FELH1000> (visited on 12/15/2019).
- [41] ThorLabs. *FLH1030-10 - Premium Bandpass Filter, Ø25 mm, CWL = 1030 nm, FWHM = 10 nm*. 2019. URL: <https://www.thorlabs.com/thorproduct.cfm?partnumber=FLH1030-10> (visited on 12/15/2019).
- [42] ThorLabs. *Photodiodes*. 2019. URL: www.thorlabs.com/newgrouppage9.cfm?objectgroup_id=285 (visited on 12/15/2019).
- [43] Armen Toorian. *CubeSat Design Specification*. 9th ed. The CubeSat Program.
- [44] TOSOH. *Fused Silica Glass Data Sheet*. 2019. URL: <http://www.gmassoc.com/pdf/Tosoh\%20SGM\%20-\%20Fused\%20Silica\%20Glass.pdf> (visited on 10/01/2010).
- [45] User:Eudjinnius. *Herschelian Ray Diagram*, CC BY-SA 3.0. 2019. URL: https://upload.wikimedia.org/wikipedia/commons/e/e8/Herschel-Lomonosov_reflecting_telescope.svg (visited on 10/01/2010).
- [46] Wyant, J; Kreath, K. *Basic Wavefront Aberration Theory for Optical Metrology*. 1992. URL: https://wp.optics.arizona.edu/jcwyant/wp-content/uploads/sites/13/2016/08/03-BasicAberrations_and_Optical_Testing.pdf (visited on 05/03/2020).